UNIVERSITY OF LIEGE

FACULTY OF APPLIED SCIENCES

AEROSPACE AND MECHANICAL
ENGINEERING DEPARTMENT

THERMODYNAMIC LABORATORY

Design, optimization and modeling of an organic Rankine cycle for waste heat recovery

Sébastien Declaye

Thesis Submitted in Partial Fulfillment of the
Requirements for the Degree of

ElectroMechanical Engineer

June 2009

Remerciements

Je tiens à remercier les professeurs Lebrun et Ngendakumana pour la confiance qu'ils m'ont témoignée en diverses occasions ces deux dernières années.

Je remercie également Sylvain Quoilin et Vincent Lemort pour leur disponibilité et leurs conseils tout au long de ce travail.

J'adresse mes remerciements à José Concha et Richard Labenda, pour les nombreuses heures qu'ils ont consacrées au montage du banc d'essai.

De nombreux membres du laboratoire de thermodynamique m'ont fait profiter de leur inestimable expérience : B. Georges, J. Hannay, C. Cuevas, B. Loly, JM Ralet, Que par ces lignes ils en soient remerciés.

Enfin, je remercie Nathalie Dumont pour son soutien ces deux dernières années ainsi que pour la relecture de ce travail.

Sommaire

1 Introduction

This section describes the working principle of an Organic Rankine Cycle (ORC), gives the most important criteria used to the select the fluid and summarizes the key points in waste heat recovery by means of ORC.

1.1 Working principle of organic Rankine cycle

The goal of an Organic Rankine Cycle is to convert thermal power into mechanical power. The cycle can be decomposed into four (or five) consecutive steps:

- An organic fluid in liquid state at low pressure is pressurized by a pump.
- This pressurized flow is then vaporized by means of a heat source.
- The superheated vapour is expanded trough a turbine, producing mechanical power.
- An optional regenerator can be added between expander exhaust and condenser supply.
- The fluid is condensed and flows back to the pump supply.

The working principle of an organic Rankine cycle is thus identical to the one of traditional Rankine cycle for which the working fluid is water.

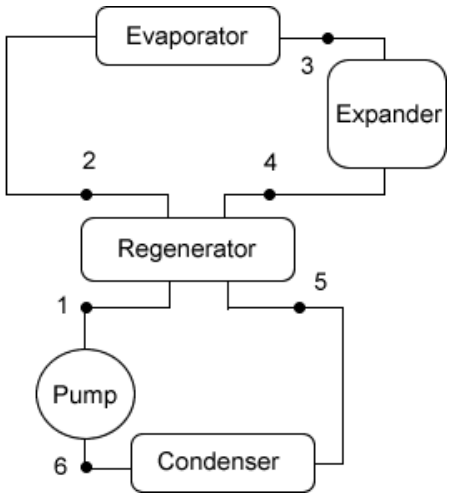

Figure 1 : components of an organic Rankine cycle

Organic Rankine cycles are particularly well-adapted to low temperature heat sources which include geothermal source, waste heat from industrial process and solar power.

1.2 Fluid selection

The fluid selection is of key importance while designing an ORC system.

1.2.1 Chemical and physical properties

Firstly, according to X.D. Wang [1], the ORC fluid should satisfy a few general criteria: chemical stability, non-fouling, non corrosiveness.

The slope of the vapour saturation curve on the T-S diagram is another important characteristic to take into account. Organic fluids can be divided into three categories:

- Wet fluids such as R152a which have a positive slope (see Figure 2)
- Dry fluids such as n-pentane which have a negative slope (see Figure 3)
- Isentropic fluids such as R11 which has infinitely large slopes (see Figure 4)

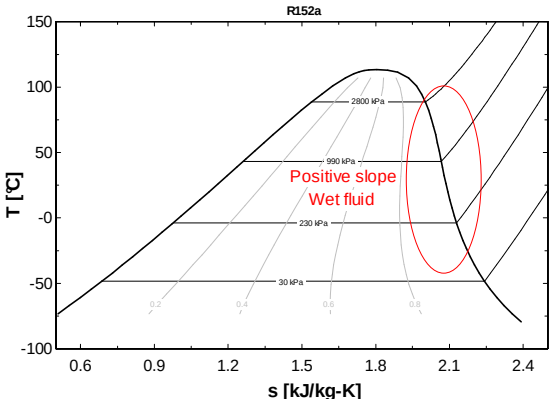

Figure 2: R152a T-S diagram

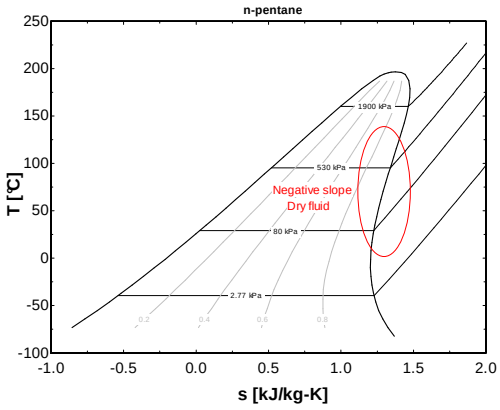

Figure 3: n-pentane T-S diagram

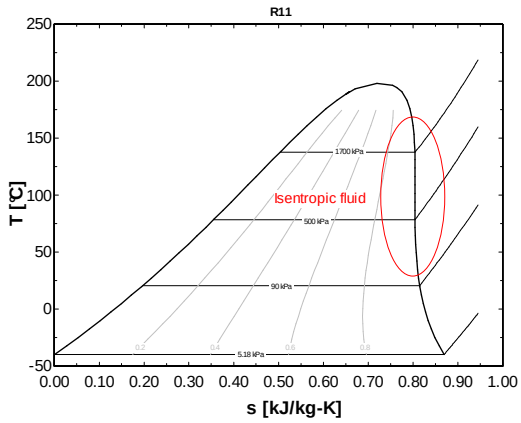

Figure 4 : R11 T-S diagram

According to Mago et al. [2], dry and isentropic fluids show better thermal efficiencies because they do not condense during the expansion process. This behaviour also allows the use of turbo expanders, for which liquid droplets are a

source of damage. Saleh et al. [3] showed that dry fluids can reach efficiencies almost as great as isentropic fluids if a regenerator is added to the cycle.

Since organic Rankine cycles are usually coupled to low temperature heat sources, the working fluid should also have a relatively low boiling point. Finally, in order to lower the mass flow rate of fluid for a given output power, high heat of vaporization and density are preferable.

1.2.2 Environmental impact and safety

During the past few years environmental impact of organic fluids turned out to be a primordial issue. Fluids with a very high ozone depletion potential (ODP) were phased out by Montréal protocol (1996) while fluids with a lower (but non-null) ODP will be phased out in 2030. Figure 5 and Figure 6 shows ODP and GWP (Global warming potential) for some organic fluids.

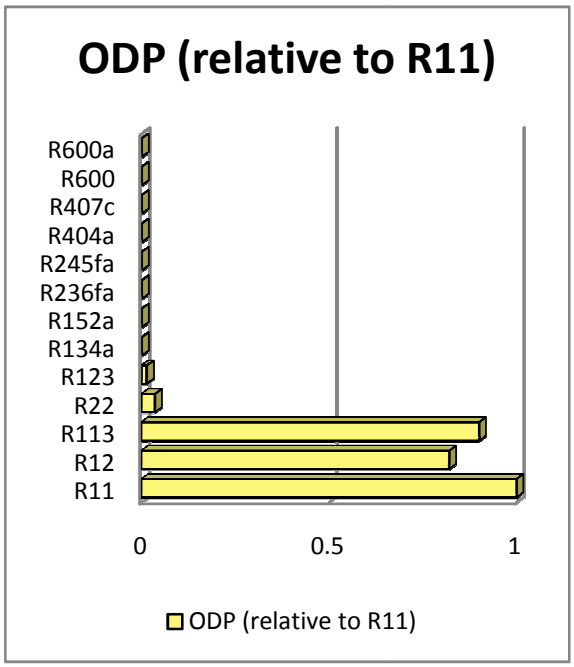

Figure 5 : ODP of some organic fluids

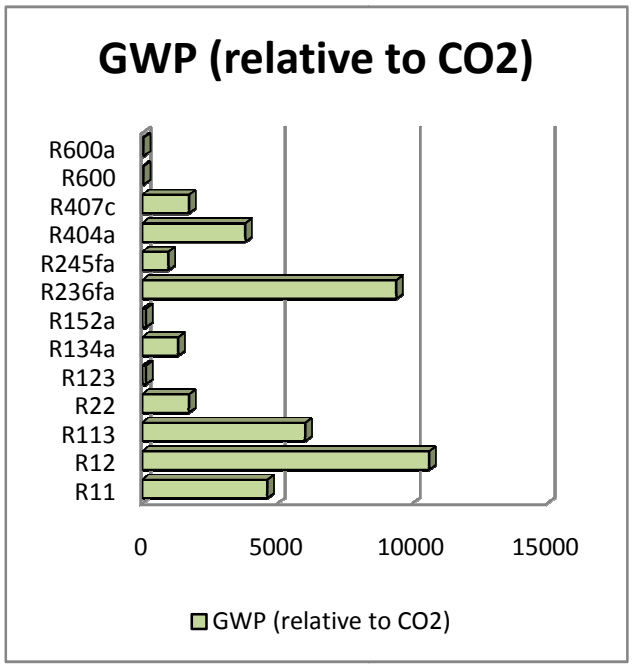

Figure 6 : GWP of some organic fluids

Non-toxic and non-flammable fluids are usually preferred over high-risk fluids such as ammonia or pentane. The use of these fluids requires appropriate safety measures but according to G. Kosmadakis et al. [4], excellent performance can be achieved.

1.2.3 Cost

The cost of the fluid can have a non-negligible impact on the global cost of the system. Some fluids like pentane are very inexpensive while some others are very costly.

1.3 Waste heat recovery

Since this work focuses on the application of ORC to waste heat recovery, this section summarizes the main features of this kind of application.

1.3.1 Power vs cycle efficiency

In fuelled Rankine system, an increase of the cycle efficiency leads to reduce fuel consumption and therefore fuel cost. Obtaining highest cycle efficiency as possible therefore remains the main preoccupation in this kind of installation. By contrast, in organic Rankine cycle adapted to waste heat recovery the main goal is to produce the maximum power using the available heat source (this is now considered as "free").

Joost J. Brasz [5] illustrated this by an example with a hot water source (see Figure 7). In the first case (see Figure 7 left), hot water enters the system at 105°C and leaves it at 95°C. The heat power transmitted to the Rankine cycle is thus relatively low but a cycle efficiency of 10.1% is achieved. In the second case (Figure 7 right), hot water enters the system at 105°C and leaves it at 60°C. The heat power transmitted is therefore 4.5 times higher than in the first case while cycle efficiency only falls to 7.1%. The mechanical power produced in the second case remains thus more than 3 times higher than is the first case.

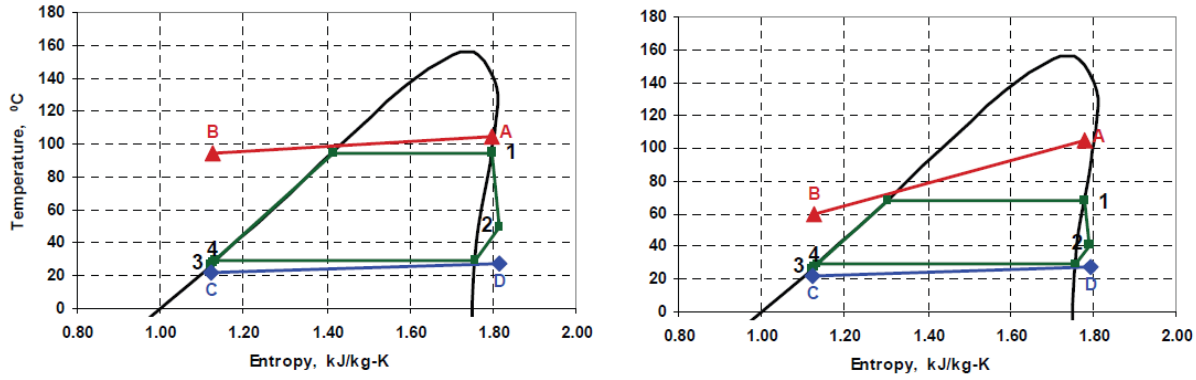

Figure 7: difference between cycle efficiency and power output [5]

1.3.2 Possible use of zeotropic fluids

In order to reduce irreversibility of heat transfer in the evaporator when sensible heat sources (such as hot gases) are used, zeotropic fluids can be selected. Indeed,

since the evaporation temperature of zeotropic mixture increases with the vapour quality, the mean temperature difference between the hot source and the working fluid is reduced (see Figure 9).

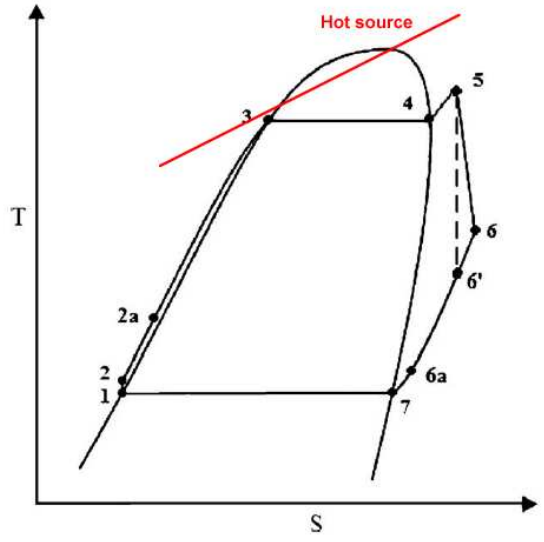

Figure 8: Schematic of the Rankine cycle for pure drying working fluids [1]

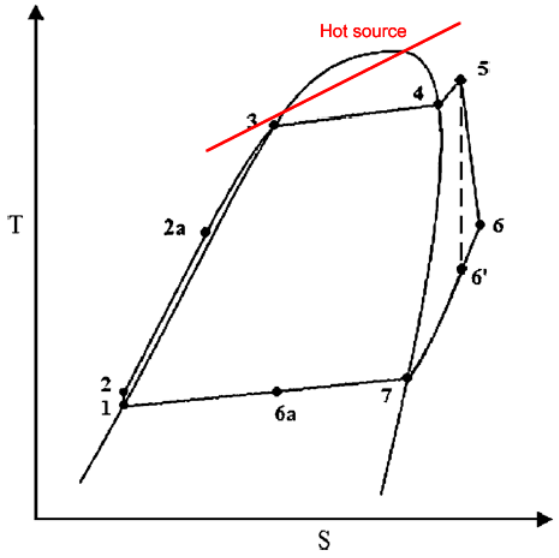

Figure 9: Schematic of the Rankine cycle for mixed drying working fluids [1]

For instance, X.D. Wang [1] compared the performances obtained with pure R245fa and three mixtures of R245fa/R152a and obtained the higher output power for a mixture 0.45/0.55 (mass fraction)

2 Scope of the work

2.1 Brief description

In 2006-2007, a first ORC test bench was built at the thermodynamics laboratory by Lemort et al. [6] and improved by Quoilin [7]. The heat source was constituted of two hot air streams characterized by the same mass flow rate but slightly different temperatures. The temperature of the first hot air stream was about 185°C while the one of the second hot air stream was about 160°C. This hot source was used to vaporize a flow of pressurised R-123 which was then expanded through a scroll machine coupled with an asynchronous machine producing electric power. Figure 10 shows a scheme of the test bench built in 2007.

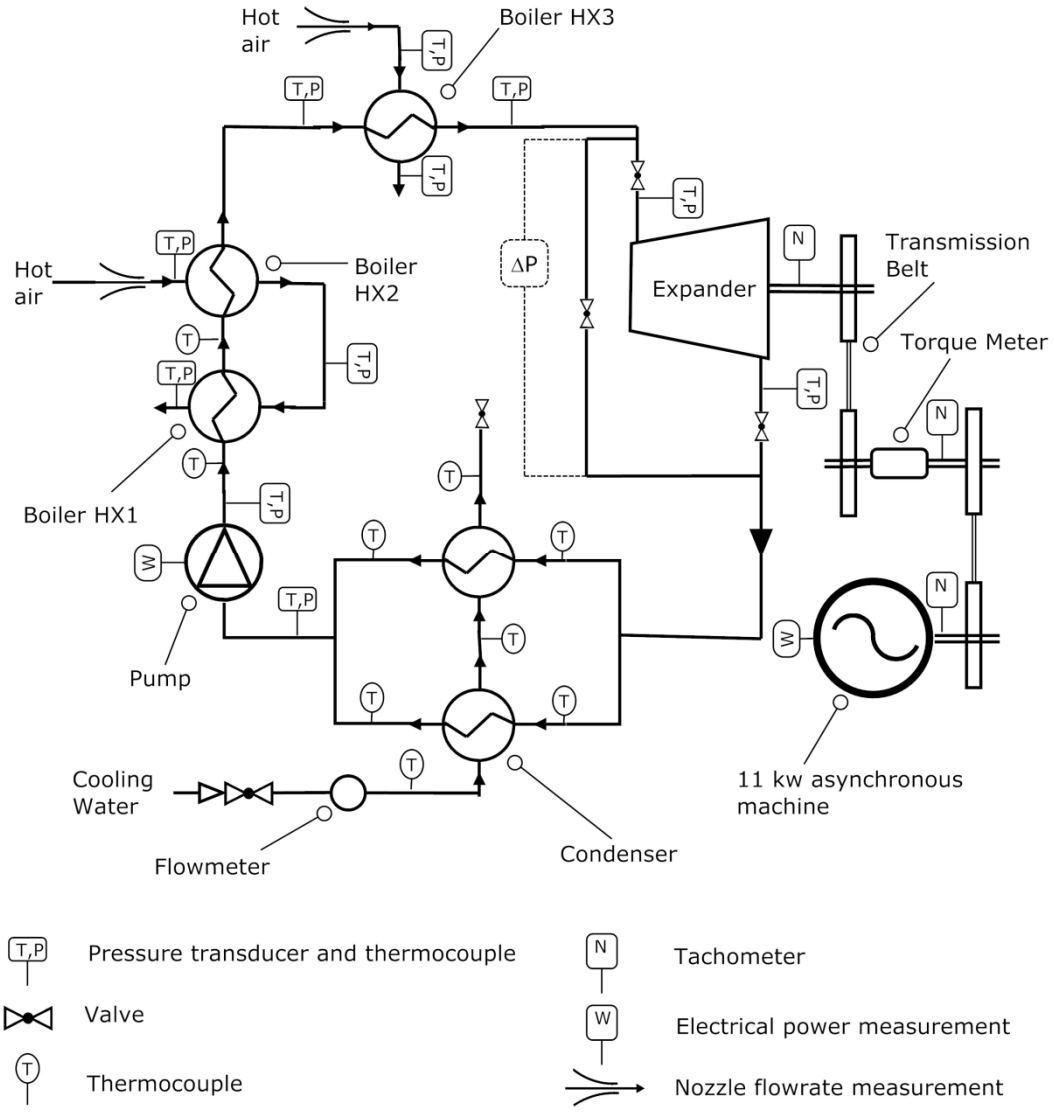

Figure 10 : scheme of the ORC test bench built in 2007

As the heat source of this ORC is not fuel but waste heat of an industrial process, the main goal is not to obtain the maximum cycle efficiency but rather to produce the maximum power.

2.2 Results

The main results obtained in 2007 are displayed in Table 1:

	Minimum value	Maximum value
Pressure ratio over the expander	2.7	5.4
Refrigerant flow rate	45 g/s	86 g/s
Output shaft power	0.38 kW	1.82 kW
Cycle efficiency	2,6 %	7,4 %
Expander isentropic effectiveness	43 %	68 %

Table 1 : main results obtained in 2007

2.3 Potential improvements

In 2007, S. QUOILIN [7] drew up a list of the most important achievable improvements of the test bench. This list has been used as guidelines during the design of the new test bench. The main elements are detailed hereunder.

2.3.1 Evaporator

A typical temperature profile obtained during the test in 2007 is shown in Figure 11. On this T-S diagram, it appears that the heat power transmitted to the refrigerant by the second heat source (green curve) is relatively low. In some tests, the second heat source was even heated up by the refrigerant. A first potential improvement therefore consists in finding a better suited heat exchangers configuration for the evaporator.

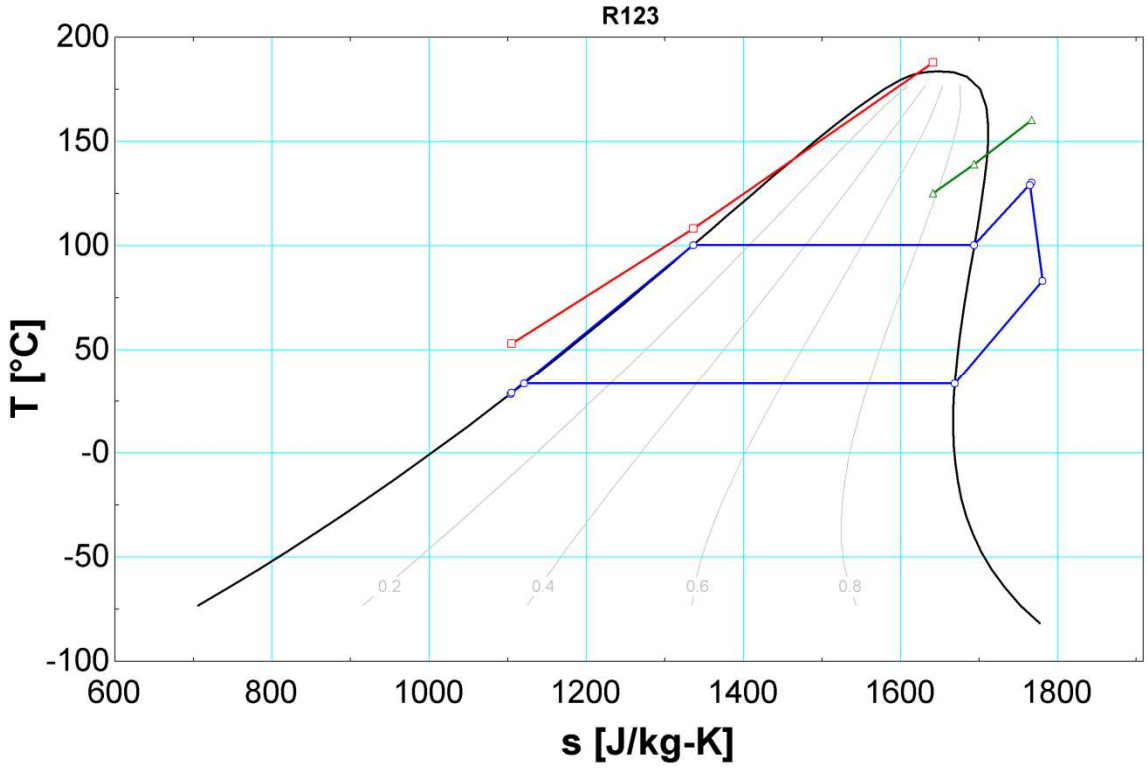

Figure 11 : typical temperature profile obtained during the test in 2007

2.3.2 Condenser

In 2007, the asymmetric configuration of the condenser (parallel on the refrigerant side and series on the water side) led to a non uniform power distribution over the heat exchangers. It was proposed to switch to a parallel configuration on both sides.

2.3.3 Torque measurement

As shown in Figure 12, the torque meter was connected to expander and asynchronous machine through transmission belts. The unknown efficiency of the expander-torque meter transmission belt (an efficiency of 95% was assumed) led to an increased uncertainty on the expander shaft power measurement.

Figure 12 : expander, torque meter and asynchronous machine [7]

In order to improve the accuracy of the power measurement, a better solution consists in connecting the torque meter directly on the expander shaft.

2.3.4 Expander

Three possible improvements of the expander were mentioned:

- Reduction of the friction torque
- Reduction of the internal leakages.
- Reduction of the external leakages on order to decrease refrigerant losses.

3 Description of the improved test bench

This section describes the new ORC test bench set up at the thermodynamics laboratory. The main goal is to improve the performances obtained in 2007.

3.1 Fluid

In 2007, a first selection was achieved among the usual working fluids used in ORC systems. Four potential candidates were identified: R123, R245fa, n-pentane and isooctane. A few thermodynamics and environmental properties of these four fluids are displayed in Table 2 and Table 3.

Working Fluid	Slope of the saturation vapor line	Critical Point	Vaporization heat at 1 atm (kJ/kg)	Boiling temperature at 1 atm	Safety
R123	Isentropic	184°C - 36,7 bars	171.5	27.7 °C	Non-flammable
R245fa	Isentropic	154°C - 36,4 bars	197.5	14.6 °C	Non-flammable
isopentane	Dry	187°C - 33,7 bars	342.8	27.5°C	Flammable
n-pentane	Dry	196°C - 33,6 bars	358.7	35.5°C	Flammable

Table 2 : thermodynamics properties of a four ORC working fluids

Working Fluid	Atmospheric lifetime	ASHRAE Level of safety	ODP	Net GWP 100 years (2102)	Phase out year
R123	1.3	B1	0.012	53	2030
R245fa	7.6	B1	0	1020	
isopentane			0	20	
n-pentane			0	20	

Table 3 : environmental properties of four ORC working fluids

N-pentane and isopentane were eliminated because of their flammability and R123 was finally selected regarding to its higher potential efficiency.

However, R123 has a non-null ODP and will be phased out in 2030. For this reason, the fluid selected for the new ORC test bench is R245fa despite of its very high GWP.

3.2 Evaporator

3.2.1 Configuration

Using the primary model developed under EES [Quoilin, 2007], four possible heat exchangers configurations (see Figure 13, Figure 14, Figure 15 and Figure 16) were

compared in terms of net output power and cycle efficiency. The results of these simulations are shown in Table 4.

	Net Power	Cycle efficiency
	W	%
Series	1899	9.3
Parallel	2026	9.44
Modular	1217	8.3
Asymmetric	2035	9.46

Table 4 : net power and cycle efficiency for several configurations

Regarding to these results, the asymmetric configuration is chosen.

Series configuration

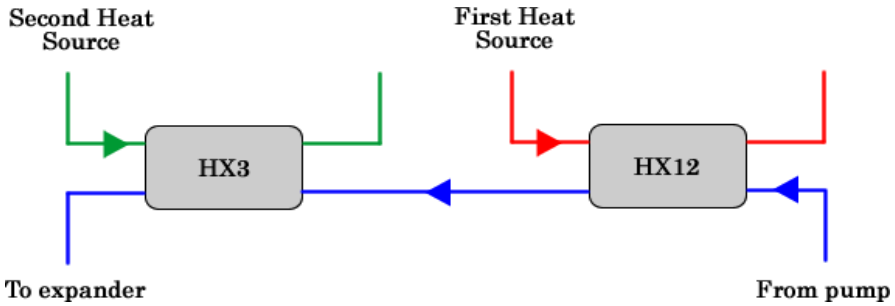

Figure 13 : series configuration

Modular configuration

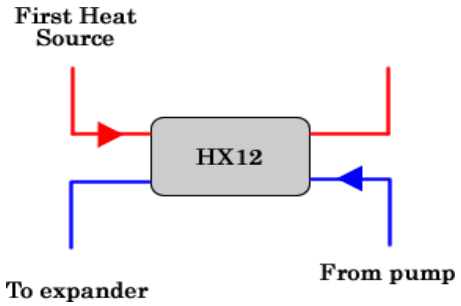

Figure 14 : modular configuration

Parallel configuration

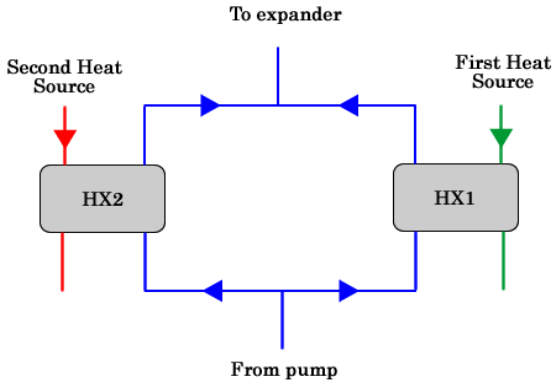

Figure 15 : parallel configuration

Asymmetric configuration

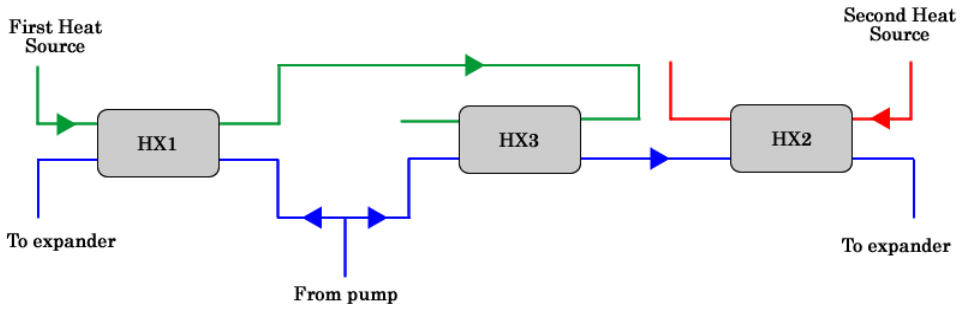

Figure 16 : asymmetric configuration

3.2.2 Components

The evaporator is composed of three plate heat exchangers (see Figure 17) whose characteristics are given in Table 5.

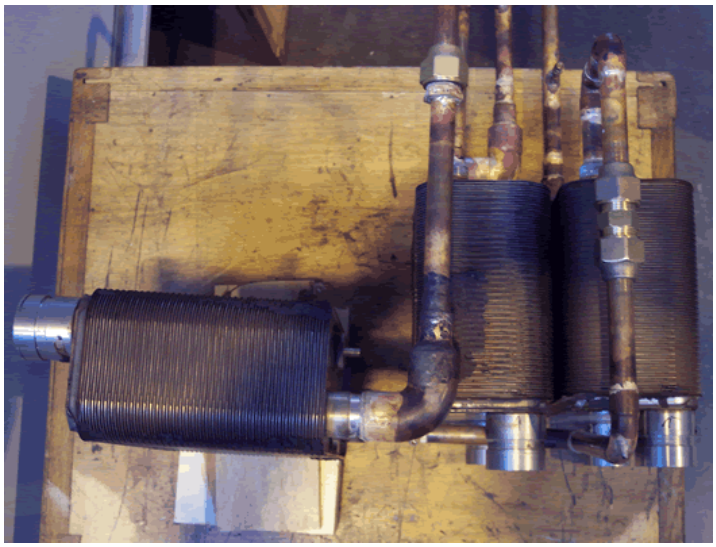

Figure 17 : evaporator

Number of plate	75
Total volume [l]	3,75
Dimension [mm]	250x112x189
Chevron angle [°]	60
Working temperature [°C]	-160 to 175
Working pressure [bar]	0 to 32

Table 5 : characteristics of evaporator plate heat exchangers

3.3 Pump

In order to accurately control the flow rate in both refrigerant lines of the evaporator, two diaphragm metering pumps are selected (See Figure 18). Diaphragm pumps are positive displacement machines that transmit the power by the intermediary of a flexible membrane (See Figure 19). One side of the membrane is filled up with the fluid to be pumped while the other side is filled up with oil. The piston is only in contact with the oil side.

The pump flow rate can be adjusted by modifying the stroke length of the piston from 0 to 100%.

Figure 18 : diaphragm pumps

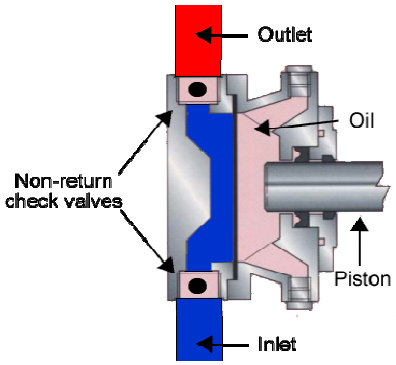

Figure 19 : diaphragm pump

The main characteristics of the pumps are displayed in Table 6.

Pump	A	B
Stroke frequency	112 strokes/min (50 Hz)	96 strokes/min (50 Hz)
Maximum flow rate	210 l/h	180 l/h
Maximum pressure	12 bar	12 bar
Motor	0.55 kW (1400 rpm)	0.55 kW (1400 rpm)
Piston diameter	40 mm	40 mm
Diaphragm diameter	120 mm	120 mm
Stroke length	25 mm	25 mm
Net Weight	26 kg	26 kg

Table 6 : main characteristics of the pumps

3.4 Condenser

3.4.1 Configuration

The condenser is composed of two heat exchangers, connected by a set of valves, as described in Figure 20. These valves allow the selection between a parallel and a series configuration on the refrigerant side. If valves 1, 2 are open and valve 3 is closed, the parallel configuration is chosen; if valves 1, 2 are closed and valve 3 is open, the series configuration is chosen.

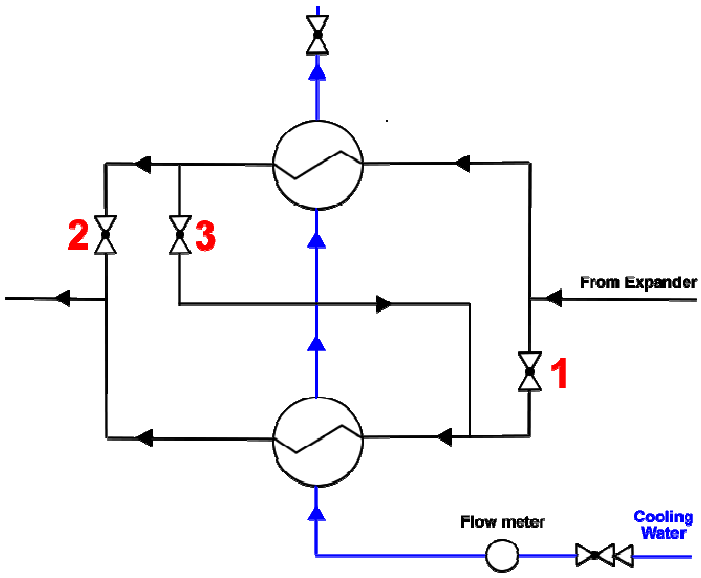

Figure 20 : configuration of the condenser

This will allow a comparison between both configurations in terms of pressure drops and heat transfer efficiency.

3.4.2 Components

The condenser is composed of two plate heat exchangers (see Figure 21) identical to those used for the evaporator (see Table 5). Both heat exchangers are fed with cold water.

Figure 21 : condenser

3.5 Liquid receiver and subcooler

3.5.1 Configuration

In order to control accurately the subcooling at the condenser exhaust, a liquid receiver and an additional heat exchanger (the subcooler) are added between the condenser and the pumps as shown on Figure 22. This additional heat exchanger is fed with cold water whose flow rate is adjustable.

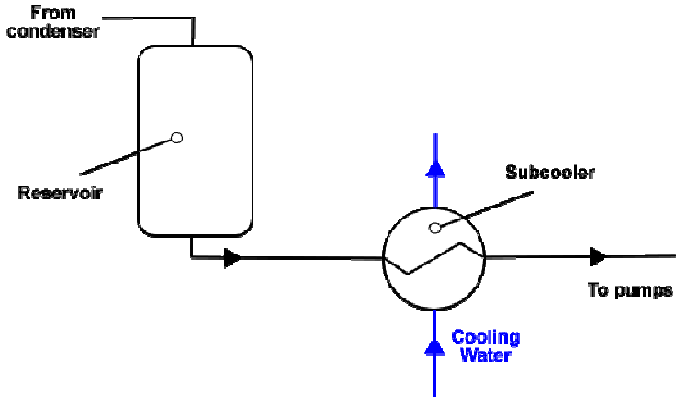

Figure 22 : reservoir and subcooler

In practice, the subcooler take place under the liquid receiver in order to ensure that only liquid will flow in it.

3.5.2 Components

The subcooler is a plate heat exchanger (see Figure 23)

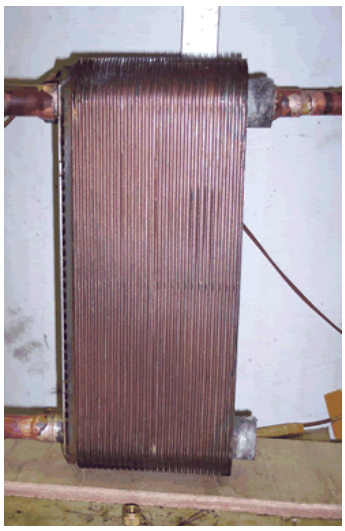

Figure 23 : the subcooler

The volume of the reservoir is 8 litres and its maximum acceptable pressure is 30 bars (see Figure 24)

Figure 24 : the reservoir

3.6 Expander

3.6.1 Scroll

The expander selected for the test bench is an oil-free open drive air scroll compressor. This machine is converted to an expander without the need of any modification except the removal of the cooling fan. Some arguments in favour of a scroll machine are:

- Its nominal rotational speed is 3000 RPM which is convenient since the expander is connected to an asynchronous machine.

- Its capacity to handle liquid without any damage which is essential since a two-phase medium will be expanded during some tests.
- Its high maximum acceptable pressure ratio (around 10) which allows a one stage expansion.
- Its ability to run without lubricant.

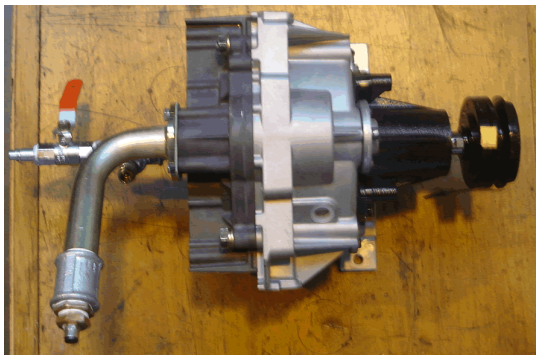

Figure 25 : air free scroll compressor

3.6.2 Sizing

Table 7 shows the characteristics of five machines proposed by the constructor.

	Swept volume in compressor mode [l/rev]	Built-in volume ratio
Size 1	0.225	3,9
Size 2	0.148	3.94
Size 3	0.136	3.94
Size 4	0.122	3.94
Size 5	0.100	3.24

Table 7 : characteristics of scroll machines proposed by the constructor

The swept volume of the first scroll is obviously too high while the built-in volume ratio of the fifth one is obviously too low. Indeed, the optimum volumetric ratio corresponding to a typical pressure ratio of 5 can be estimated by

$$r_v = r_p^{\frac{1}{\gamma}} \approx 4.2$$

The three remaining candidates were compared using the model developed under EES by S.QUOILIN [7] where the non-dimensional sizing relations suggested by V.LEMORT [8] were applied to the parameters of the expander:

$$d_{thr,su,exp} = d_{thr,su,exp,n} * \left(\frac{V_s}{V_{s,n}}\right)^{1/3}$$

Diameter of the fictitious nozzle modelling the supply pressure drop.

$$A_{leak} = A_{leak,n} * \left(\frac{V_s}{V_{s,n}}\right)^{2/3}$$

Fictitious internal leakage area.

$$T_m = T_{m,n} * \left(\frac{V_s}{V_{s,n}}\right)^{2/3}$$

Friction torque of the expander.

$$AU_{amb,exp} = AU_{amb,exp,n} * \left(\frac{V_s}{V_{s,n}}\right)^{2/3}$$

Heat transfer coefficient for the ambient losses.

$V_{s,n}$ is the nominal swept volume and V_s is the swept volume

For each machine, simulations were performed using a wide range of expander rotational speeds and refrigerant mass flow rates while air side conditions were kept constant (see Figure 26).

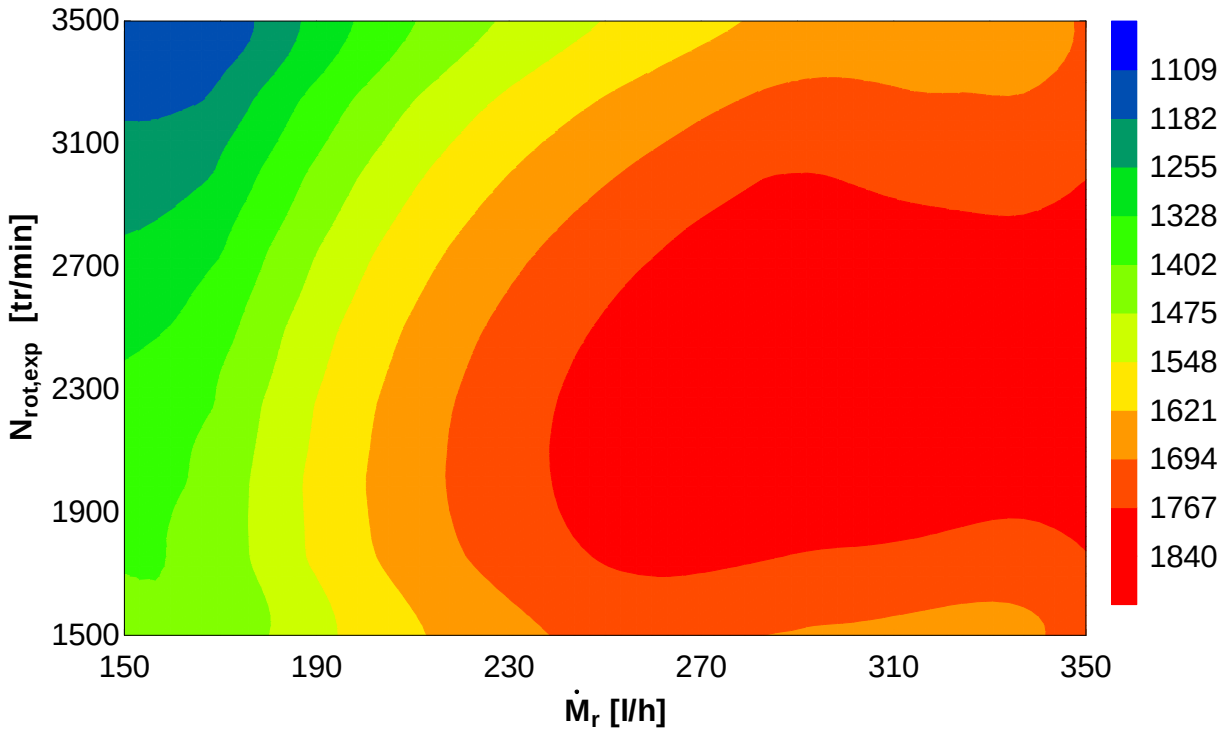

Figure 26 : expander sizing simulation result (122cc)

Figure 26 shows the shaft power produced as a function of the expander rotational speed and the refrigerant mass flow rate for 122cc machine. The optimum zone characterised by high mass flow rate and average rotational speed is clearly identified.

The same calculations were performed for 136 and 148 cc machines. The main results of these simulations are displayed in Table 8

Swept volume (l/rev)	Max net output power (kW)	Max efficiency (%)
122	1.84	8.0
136	1.81	7.93
148	1.79	7.87

Table 8: main results of expander sizing simulations

Regarding to these results, the scroll compressor with a swept volume of 0.122 l/rev is selected.

3.6.3 Static pressure test

In consequence of the high GWP and cost of R245fa, the amount of refrigerant released to the atmosphere during tests should be kept as low as possible. This is an issue with the expander selected for this test bench, because it is originally an air compressor, which is not air tight. The ideal configuration regarding the tightness would be a hermetic expander.

A static pressure test is performed on the expander. A tank of 54 litres is filled up with air at 5 bar (absolute pressure). The reservoir is then connected to the outlet of the expander and the pressure is measured every 15 seconds. During the first test, the circumferential sealing is ensured by a tube and a dust seal (see Figure 27 right). For the second test, the tube is replaced by an O-ring (see Figure 27 left).

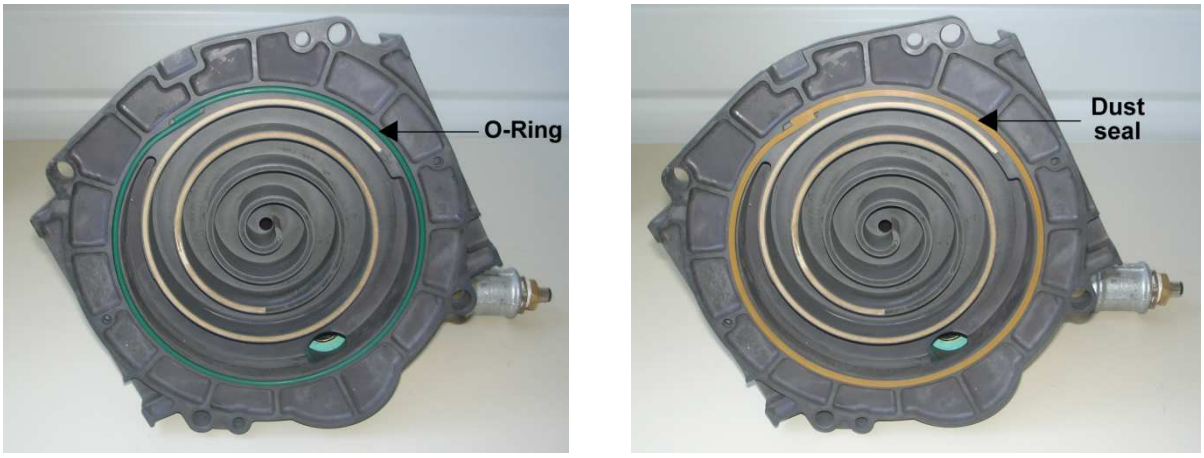

Figure 27 : circumferential sealing of the expander

Figure 28 shows that the decrease of the pressure is quick for both sealing solutions even if a slight improvement is noticed with the O-ring. The external leakage is therefore too high to use this expander as such.

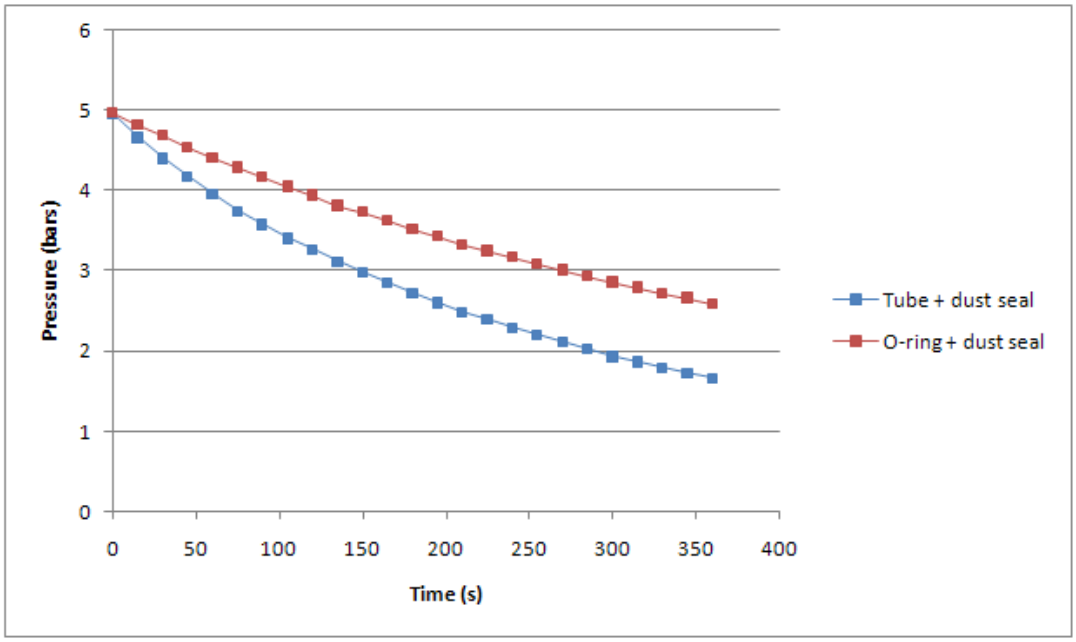

Figure 28 : results of the static pressure test on the expander

3.6.4 Modifications

In order to decrease the external leakages, the expander is enclosed inside a hermetic container (see Figure 29).

Figure 29 : hermetic container

The shaft sealing is ensured by a shaft seal which can handle a pressure difference of 9 bar and a rotational speed of 3500 RPM.

The container is filled up with air at 5 bar and the pressure is measured every 15 seconds. Figure 30 shows that no pressure decrease is noticed when the expander is enclosed inside the box.

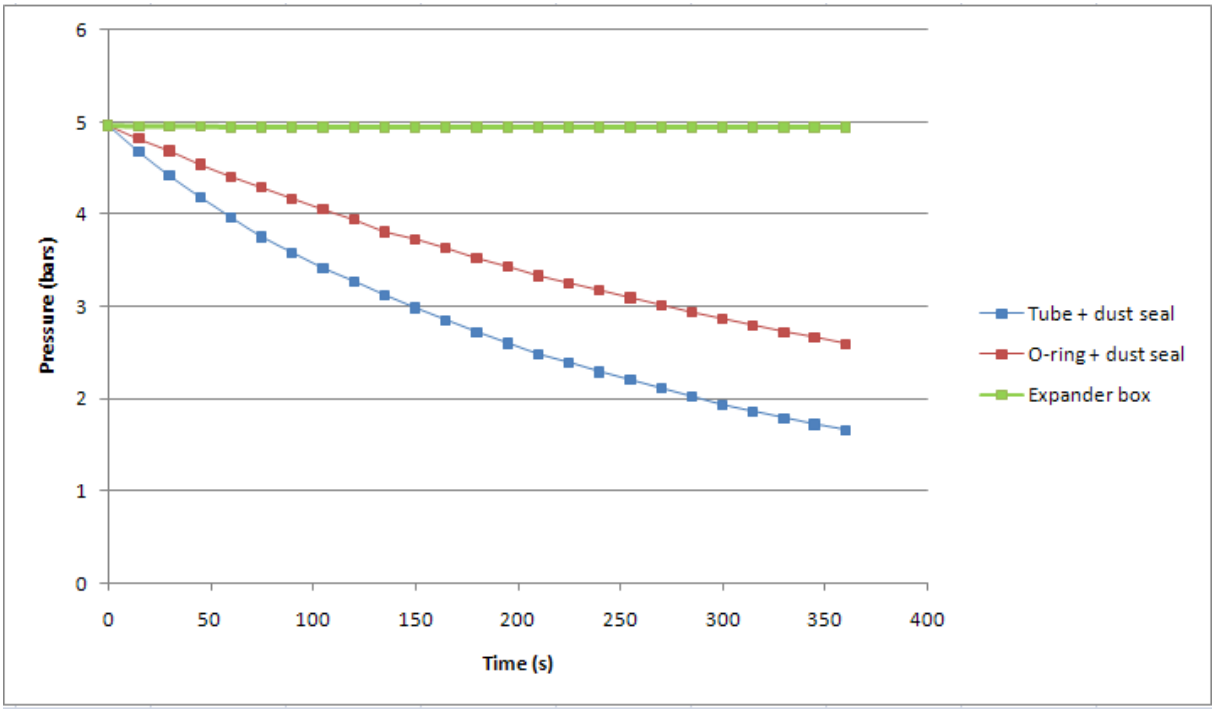

Figure 30 : results of the static pressure test on the expander

3.7 Asynchronous machine and inverter

The expander is connected to a 5kW asynchronous machine by the intermediary of a torque meter (see Figure 31)

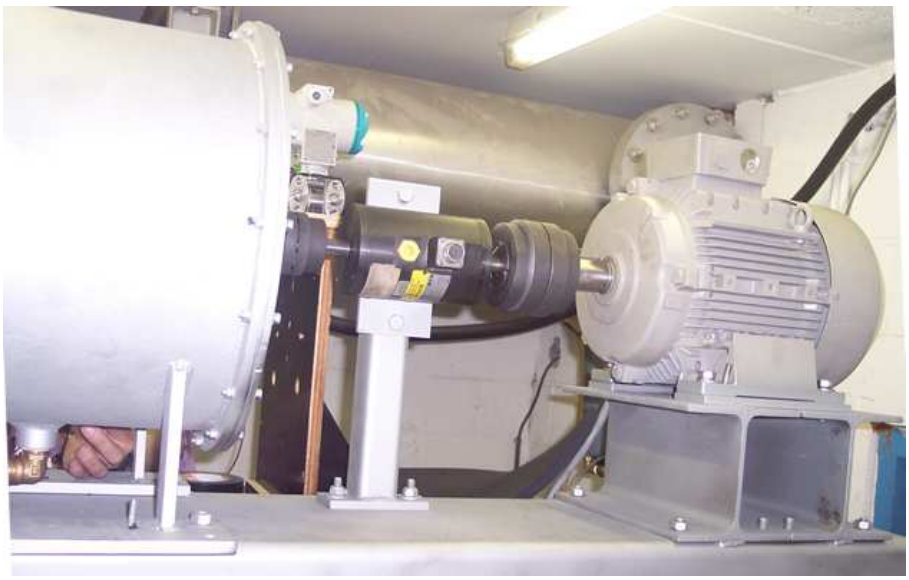

Figure 31 : connection between expander and asynchronous machine

The asynchronous machine is connected to an inverter in order to control its rotational speed by changing the frequency. The inverter range of frequency is 0 to 104Hz. Since the nominal rotational speed of the asynchronous machine is 1500

RPM, the frequency range allows setting the expander rotational speed from 0 to 3120 RPM.

3.8 Measurements

3.8.1 Temperatures

All temperatures are measured with Class 1 Type T thermocouples (copper-constantan) which are suited for measurements in -200 to 350°C range. Cold-junctions are kept in an ice bath.

3.8.2 Pressures

Eight pressure sensors are installed on the test bench. Their location, range and accuracy are displayed in Table 9 for the refrigerant side and in Table 10 for the air side.

	Range	Accuracy
Pumps supply	0-5 bar	+/- 25mbar
Expander supply	0-20 bar	+/- 100mbar
Condenser supply	0-5 bar	+/- 25mbar

Table 9 : pressure sensors on refrigerant side

	Range	Accuracy
Hot air source 1 supply	0-10 bar	+/- 50mbar
Hot air source 1 exhaust	0-10 bar	+/- 50mbar
Hot air source 2 supply	0-10 bar	+/- 50mbar
Hot air source 2 exhaust	0-10 bar	+/- 50mbar

Table 10 : pressure sensors on air side

3.8.3 Differential pressures

Four differential pressure sensors are installed on the test bench (see Figure 32). Their location, type, range and accuracy are displayed in Table 11.

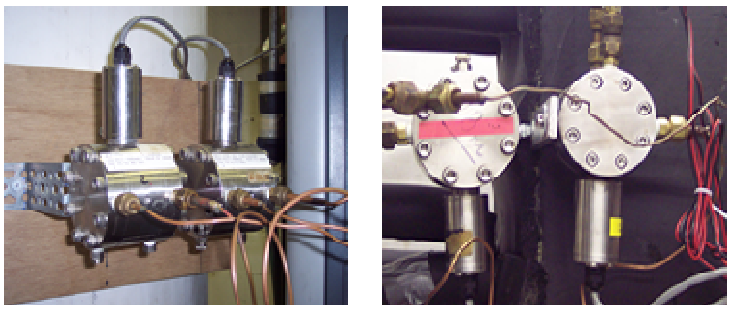

Figure 32 : differential pressure sensors

	Type	Range	Accuracy
Pressure drop over the evaporator (1 and 2)	Sensotec	0-500 mbar	+/- 2.5mbar
Pressure drop over the evaporator (3)	Sensotec	0-500 mbar	+/- 2.5mbar
Pressure drop over the condenser	Sensotec	0-1 bar	+/- 5mbar
Pressure drop over the expander	Sensotec	0-20 bar	+/- 100mbar

Table 11 : differential pressure sensors

3.8.4 Flow rates

The refrigerant flow rate is measured by means of a Coriolis flow meter (see Figure 33) whose characteristics are displayed in Table 12.

Figure 33 : Coriolis flow meter [7]

Range	0 to 0.6 kg/s
Accuracy liquid	Up to +/- 0.1 % of rate
Repeatability liquid	Up to +/- 0.05 % of rate
Process temperature	-240 up to 204°C
Maximum operating pressure	100 bar

Table 12 : characteristics of the Coriolis flow meter

Since the pumps are volumetric pumps with stroke frequency of 96 and 112 strokes/min, the flow rate delivered (and thus measured) is not constant (see Figure 34).

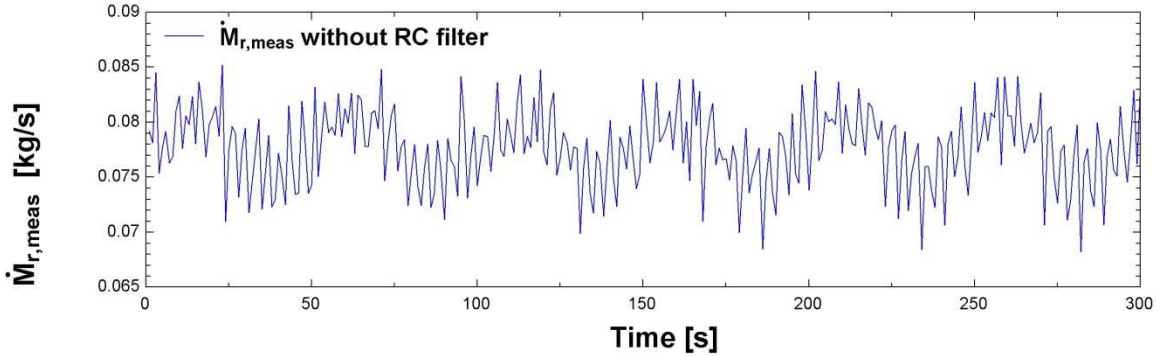

Figure 34 : measured flow rate vs time without RC integrator

In order to average the signal, a RC integrator is added between Coriolis transducer output and acquisition card output as shown in Figure 35.

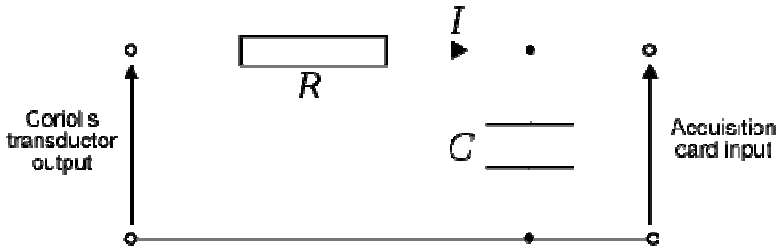

Figure 35 : RC integrator

The accuracy of this method will be discussed in section 4.2.5.2

3.8.5 Power

An electricity counter is installed on the test bench in order to measure the pump consumption.

Figure 36 : electricity counter

3.8.6 Rotational speed

The expander rotational speed is measured by means of a hand-tachymeter.

3.8.7 Torque

The torque is measured directly on the expander shaft by means of a torque meter (see Figure 31). Its full-scale is 20 N.m and its accuracy is 0.1% of full-scale.

3.8.8 Vapour quality

In order to study the behaviour of the expander if a fraction of liquid is supplied to it, an additional measurement device is needed. Indeed, if the fluid is in two phase state, pressure and temperature measurements are not sufficient to determine the enthalpy of the fluid.

A possible way to measure this enthalpy is to perform an isenthalpic expansion as shown on Figure 37. A pressure and a temperature measurement at the point B are sufficient to determine the enthalpy h_B that is equal to h_A as the expansion is isenthalpic. h_A is thus known.

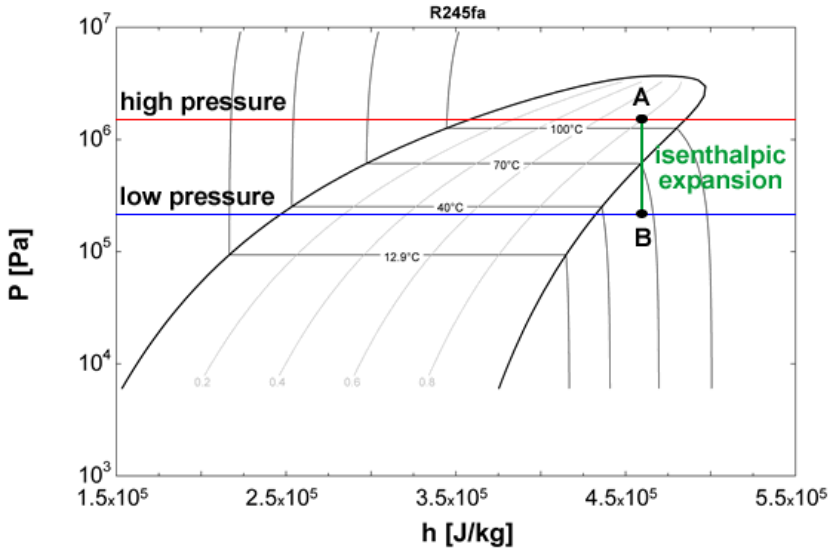

Figure 37 : isenthalpic expansion

In practice, a small by-pass is added between evaporator exhaust and condenser supply as shown on Figure 38. This by-pass is constituted of a 1.5 meter long copper capillary.

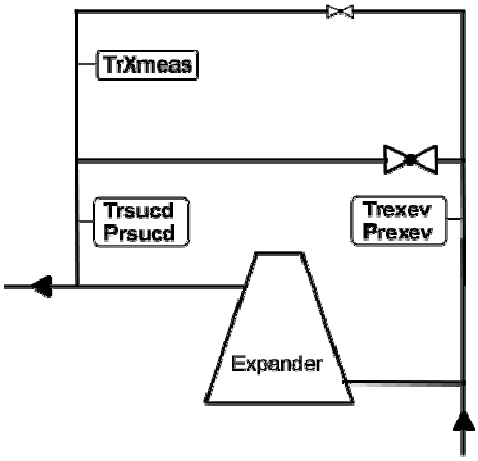

Figure 38 : by-pass to measure quality

At the exhaust of this by-pass, enthalpy is given by

$$h_{r,X,meas} = Enthalpy(R245fa, T = T_{r,X,meas}, P = P_{r,su,cd})$$

The first law of thermodynamics for a steady flow process written for the by-pass is

$$\dot{M}_{r,bypass} * \left(h_{r,ex,ev} - h_{r,X,meas}\right) = \dot{Q}_{bypass} + \dot{W}_{bypass}$$

As the by-pass is constituted of a valve and a small copper tube, it is obvious that no mechanical power can be produced and $\dot{W}_{bypass}$ is thus equal to zero.

The measurement error is then finally given by

$$\left(h_{r,ex,ev} - h_{r,X,meas}\right) = \dot{Q}_{bypass}/\dot{M}_{r,bypass}$$

In order to decrease $\dot{Q}_{bypass}$, the by-pass is strongly insulated as shown on Figure 39.

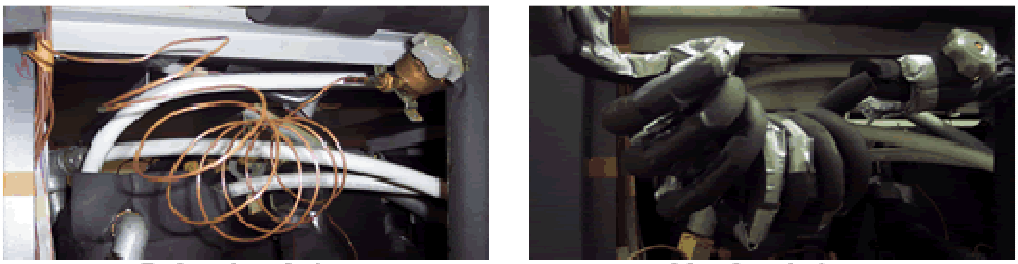

Figure 39 : insulation of the quality measurement device

Finally, the vapour quality at the evaporator exhaust is given by

$$X_{r,ex,ev} = Quality(R245fa, h = h_{r,X,meas}, P = P_{r,ex,ev})$$

3.9 Diagram of the test bench

Figure 40 shows a global diagram of the test bench.

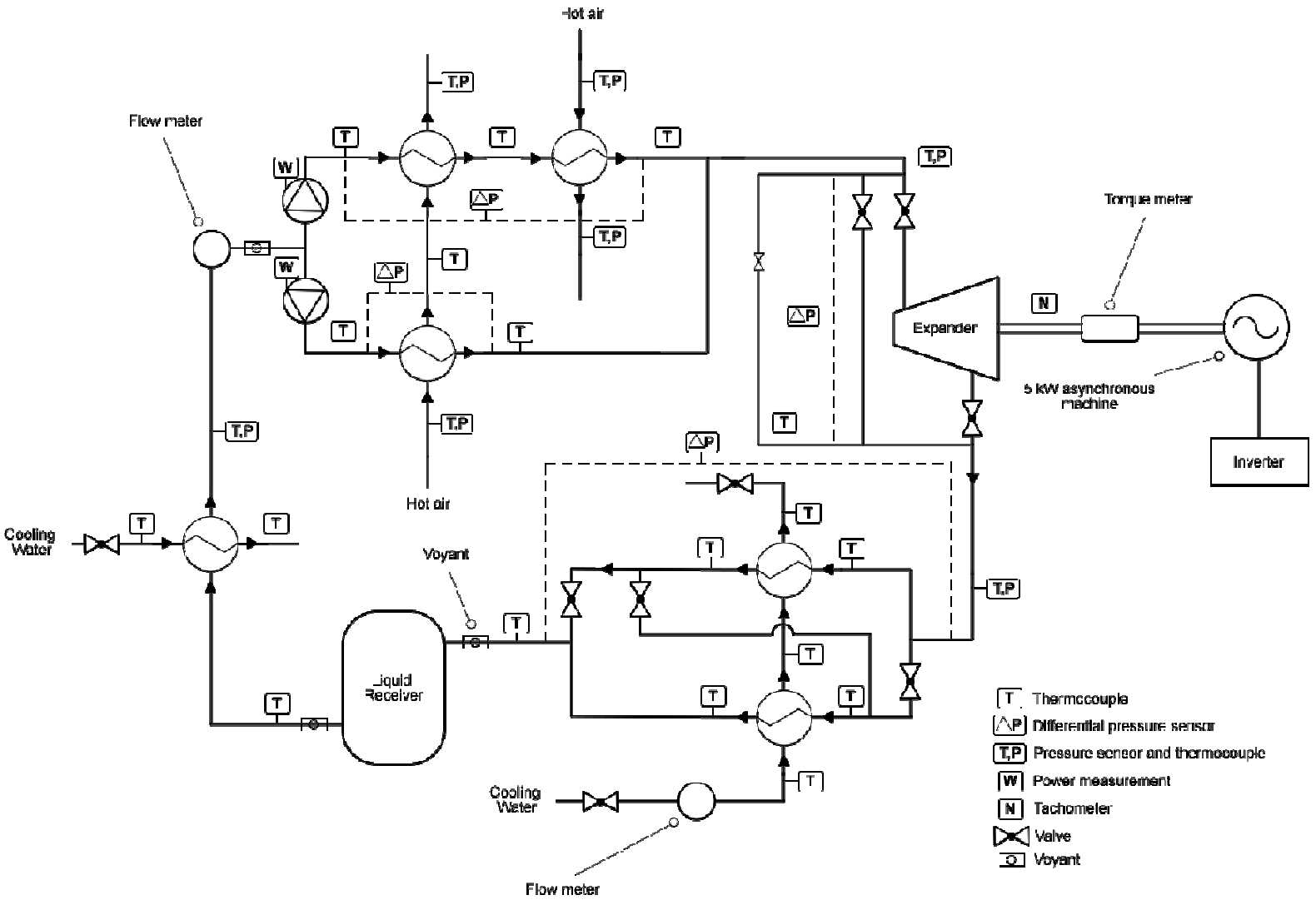

Figure 40 : diagram of the test bench

4 First set of tests

4.1 Cavitation test

4.1.1 Phenomenon

Cavitation is defined as the formation of vapour bubbles of a flowing liquid in a region where the pressure of the liquid falls below its vapour pressure. As a consequence, cavitation appears where the pressure is the lowest i.e. at the pump supply (see Figure 41).

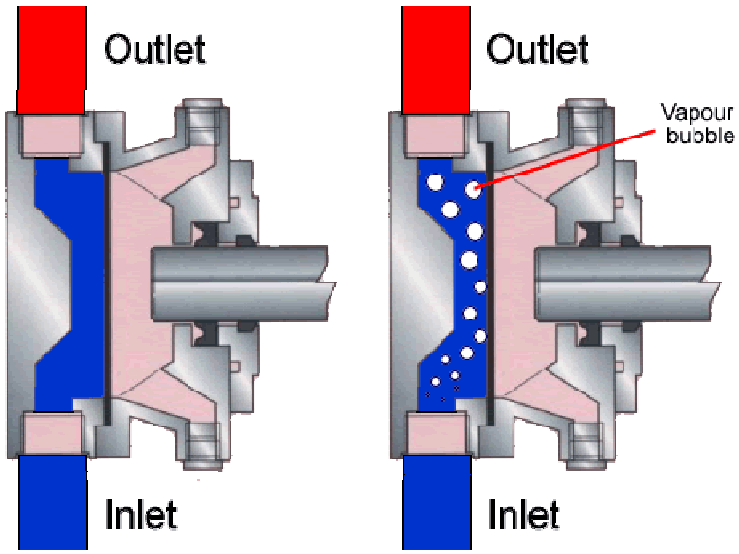

Figure 41 : formation of vapour bubbles in the pump itself

The first obvious consequence of cavitation in diaphragm pumps is the significant reduction of the mass flow rate delivered by the pump. Indeed, the specific volume of vapour being much higher than the one of liquid, the formation of a small fraction of vapour reduces dramatically the mass trapped in the pump.

Cavitation tests are carried out by decreasing progressively the difference between the fluid pressure and its vapour pressure. This difference is called available NPSH ($NPSH_a$). The pump NPSH ($NPSH_p$) is defined as the value of the NPSH available just before cavitation appears. It gives the minimum difference between the fluid pressure and its vapour pressure that must be maintained at the pump supply in order to avoid cavitation.

4.1.2 Testing description

The test ring is shown in Figure 42. The heat exchanger is fed with cold water whose the flow rate can be adjusted using a valve in order to control the temperature of R245fa at the pump supply.

Neglecting pressure drops in the line between the reservoir and the pump, the $NPSH_a$ is given by:

$$NPSH_a = \frac{P_0}{\rho g} + H - \frac{P_v}{\rho g}$$

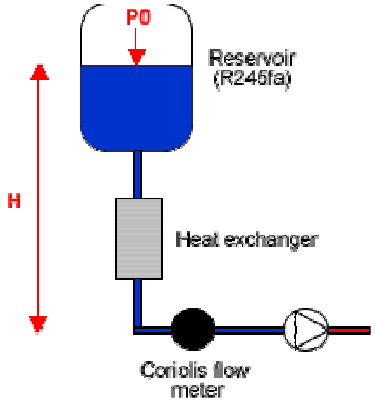

Figure 42

P_0 and H are kept constant all along the test and P_v is progressively increased by increasing the temperature of the fluid. Figure 43 shows NPSHa as a function of the temperature of the fluid.

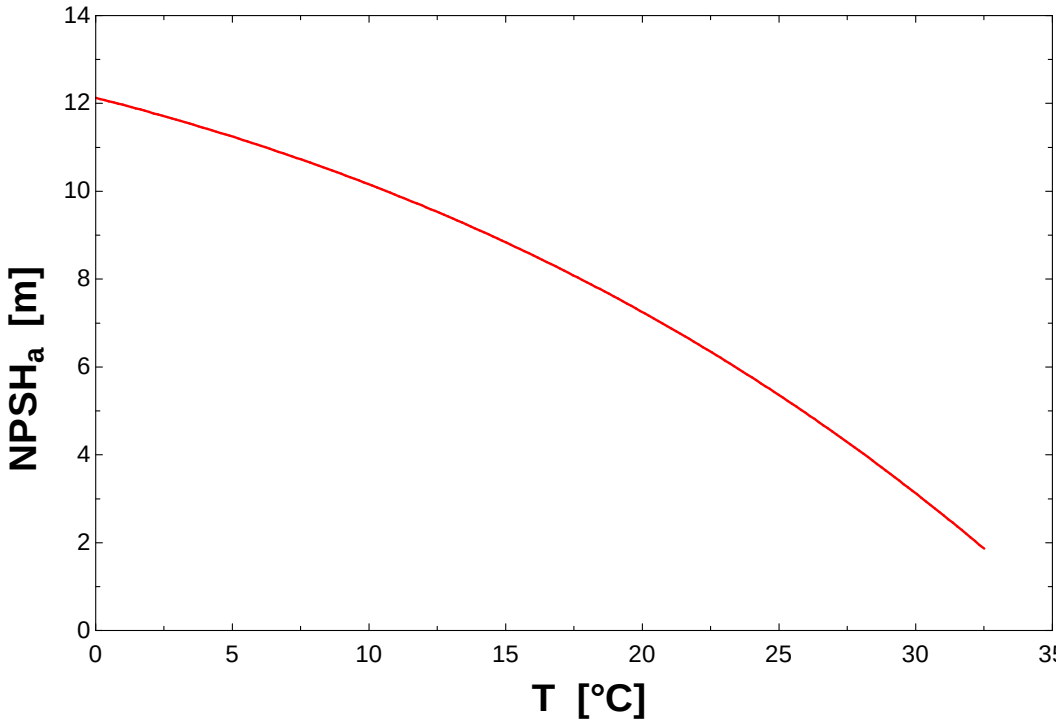

Figure 43 : NPSHa as a function of the temperature of the fluid

Cavitation is detected by a decrease of the measured pump flow rate compared to theoretical flow rate in the absence of cavitation. This theoretical flow rate is given by:

$$\dot{M}_{pp,theo} = X_{pp} * \dot{V}_{max,pp} * \rho_{su,pp}$$

Where X_{pp} is the pump capacity setting (between 0 and 1), $\dot{V}_{max,pp}$ is volumetric flow rate at full capacity in m^3/s and $\rho_{su,pp}$ is the fluid density at the pump supply in kg/m^3. The same procedure is repeated for two pump capacity settings.

4.1.3 Results and analysis

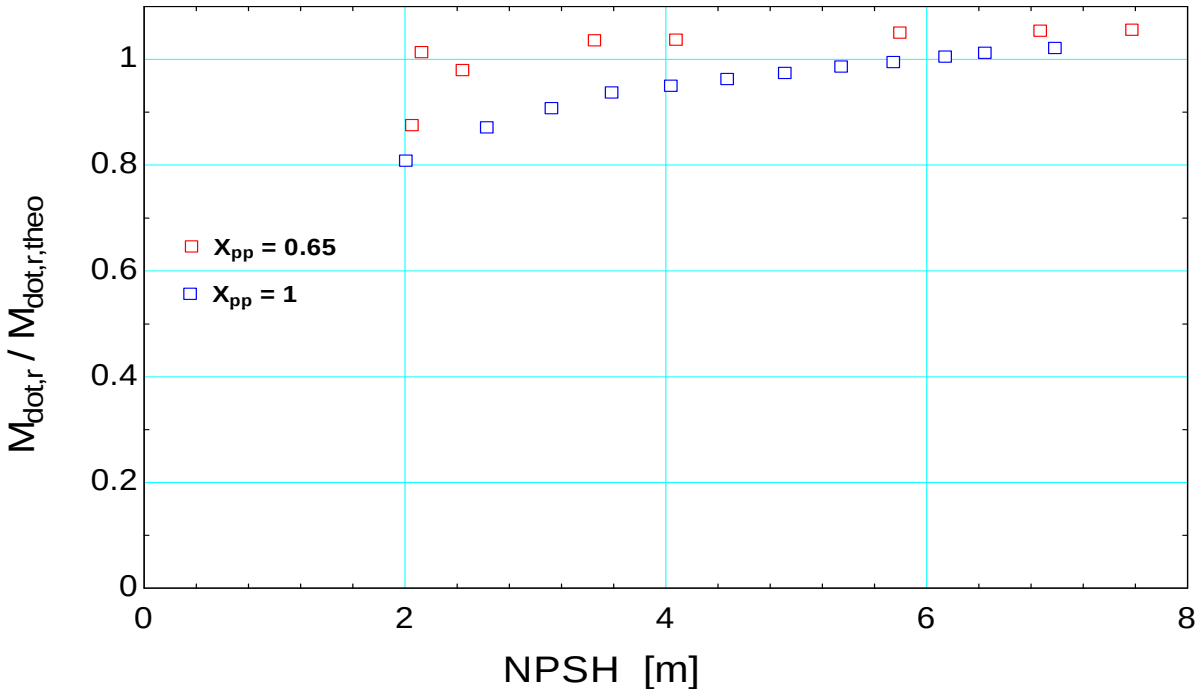

Figure 44 : mass flow rate ratio vs NPSH

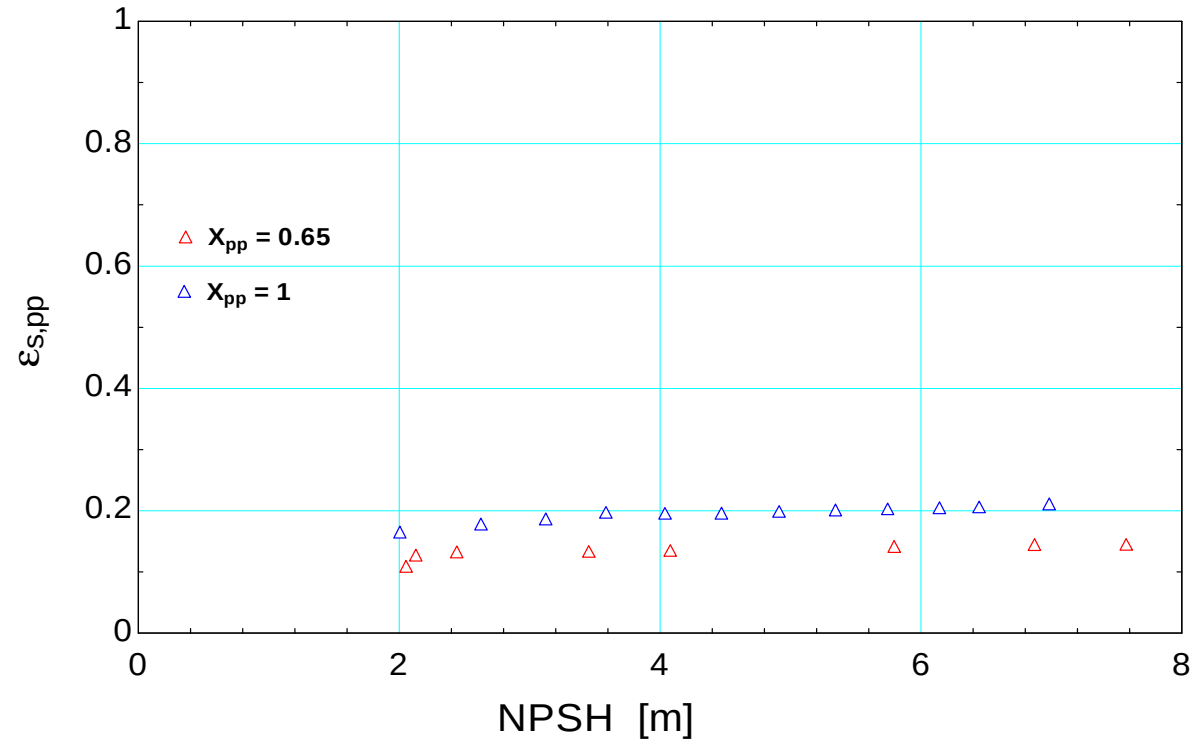

Figure 45 : pump efficiency vs NPSH

Cavitation phenomenon is clearly highlighted on Figure 44.

However, the behaviour of the pump seems to be linked to pump capacity setting. Indeed, when the capacity setting is set to 0.65, the ratio $\dot{M}_r/\dot{M}_{r,theo}$ remains

constant for a large NPSH range before a sharp decrease. When capacity setting is set to 1.00, the ratio $\dot{M}_r/\dot{M}_{r,theo}$ shows a more progressive decline. This could be explained by the fact that vapour bubbles are present in the pump even for high NPSH. This vapour fraction would increase progressively while the NPSH is decreased.

Figure 45 shows that the pump efficiency reaches a maximum value of 20% when capacity setting is 1.00 and that it falls around 15% when capacity setting is 0.65. In both case, the efficiency seems to be constant in a large range of NPSH even if a slight decrease is noticed for the lowest NPSH.

4.1.4 Conclusion

A NPSH of 4 meters is recommended in order to avoid pump cavitation. As the liquid receiver is situated only 1.2 meters higher than the pumps, the static pressure is not sufficient to ensure a normal functioning of the pumps. For a typical condensing pressure (2 bar), the required subcooling to increase NPSH up to 4 meters is around 6K.

4.2 Tests without the expander

A first set of 12 tests was performed without the expander in April 2009 in order to highlight possible issues on the test bench and to solve them. For this first set of tests, the expander is replaced by a valve which is fully open at the beginning of the test and then progressively closed in order to increase the pressure ratio.

All along these tests, the air flow rate is kept constant around a value of 0.126 g/s and four parameters of the cycle are modified:

- The evaporator pressure by opening or closing the by-pass valve.
- The condensing pressure by changing the water flow rate in the condenser.
- The overheating at the evaporator exhaust by modifying the refrigerant mass flow rate.
- The subcooling at the condenser exhaust by modifying the water flow rate in the subcooler.

Table 13 displays the extreme values taken by these parameters during the first set of test.

	Minimum value	Maximum value
Evaporator pressure (bars)	8.29	11.77
Condensing pressure (bars)	1.5	2.35
Overheating (K)	0	37.54
Subcooling (K)	9.81	20.23

Table 13 : extreme values taken by 4 parameters during the first set of tests

Table 14 displays the main results of this first set of tests.

	Minimum value	Maximum value
Pressure ratio over the by-pass valve	4.71	7.31
Refrigerant mass flow rate	73 g/s	110 g/s
Heat power recovered in the evaporator	24.1 kW	26.34 kW

Table 14 : main results of the first set of tests

4.2.1 Heat balances

4.2.1.1 Evaporator

Figure 46 shows the heat balance over the evaporator.

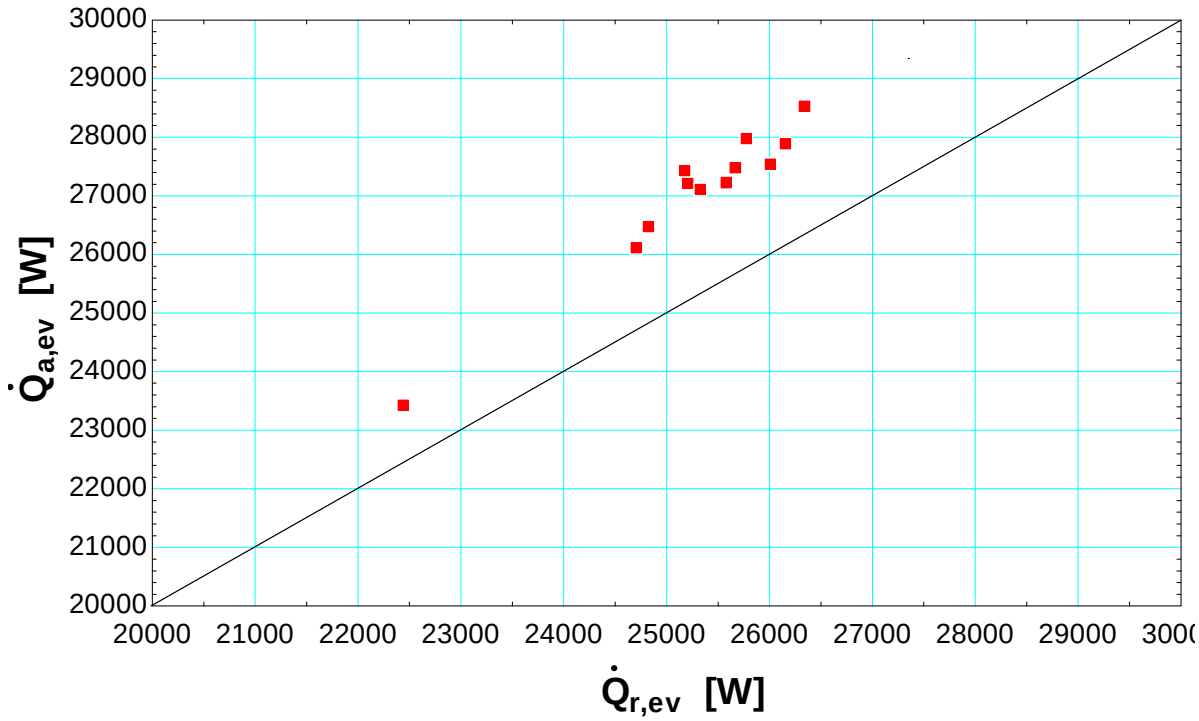

Figure 46 : heat balances over the evaporator

The heat power on the air side ($\dot{Q}_{a,ev}$) is higher than the heat power on refrigerant side ($\dot{Q}_{r,ev}$) for all points and the maximum difference is 7.8%.

This divergence can be explained by ambient losses on air side and measurement uncertainties. In order to reduce these measurement uncertainties during the second set of tests, a special attention will be paid to both flow rates measurements (see section 4.2.5.1).

4.2.1.2 Condenser

The heat balance over the condenser (see Figure 47) shows a good agreement with a maximum error of 4.7%.

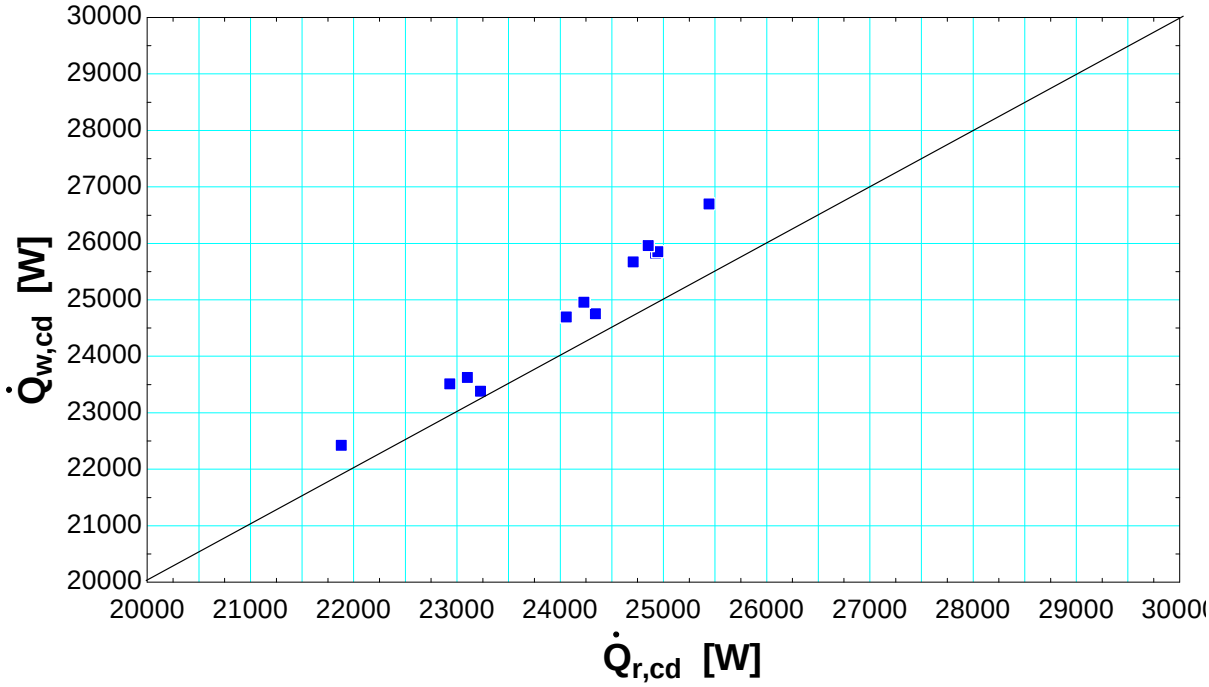

Figure 47 : heat balance over the condenser

4.2.2 Refrigerant flow rate splitting

The total mass flow rate ($\dot{M}_{r,total}$) is measured at the pumps supply but $\dot{M}_{r,pump1}$ and $\dot{M}_{r,pump2}$ are not measured (see Figure 48). These two values have to be determined by calculation.

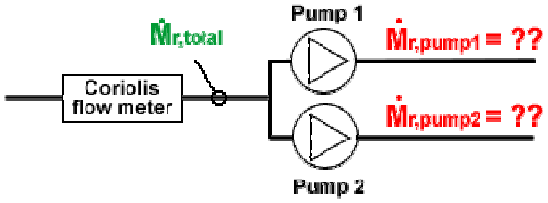

Figure 48

A first possible method to compute $\dot{M}_{r,pump1}$ and $\dot{M}_{r,pump2}$ is to use a simple rule of three with pumps capacity settings:

$$\dot{M}_{r,pump1} = \dot{M}_{r,total} * \left(\frac{X_{pump1} * 180}{X_{pump1} * 180 + X_{pump2} * 210} \right)$$

$$\dot{M}_{r,pump2} = \dot{M}_{r,total} * \left(\frac{X_{pump2} * 210}{X_{pump1} * 180 + X_{pump2} * 210} \right)$$

Where X_{pump1} and X_{pump2} are the capacity settings of pumps 1 and 2 respectively.

Figure 49 shows the heat balances over the three heat exchangers composing the evaporator if this rule of three method is used.

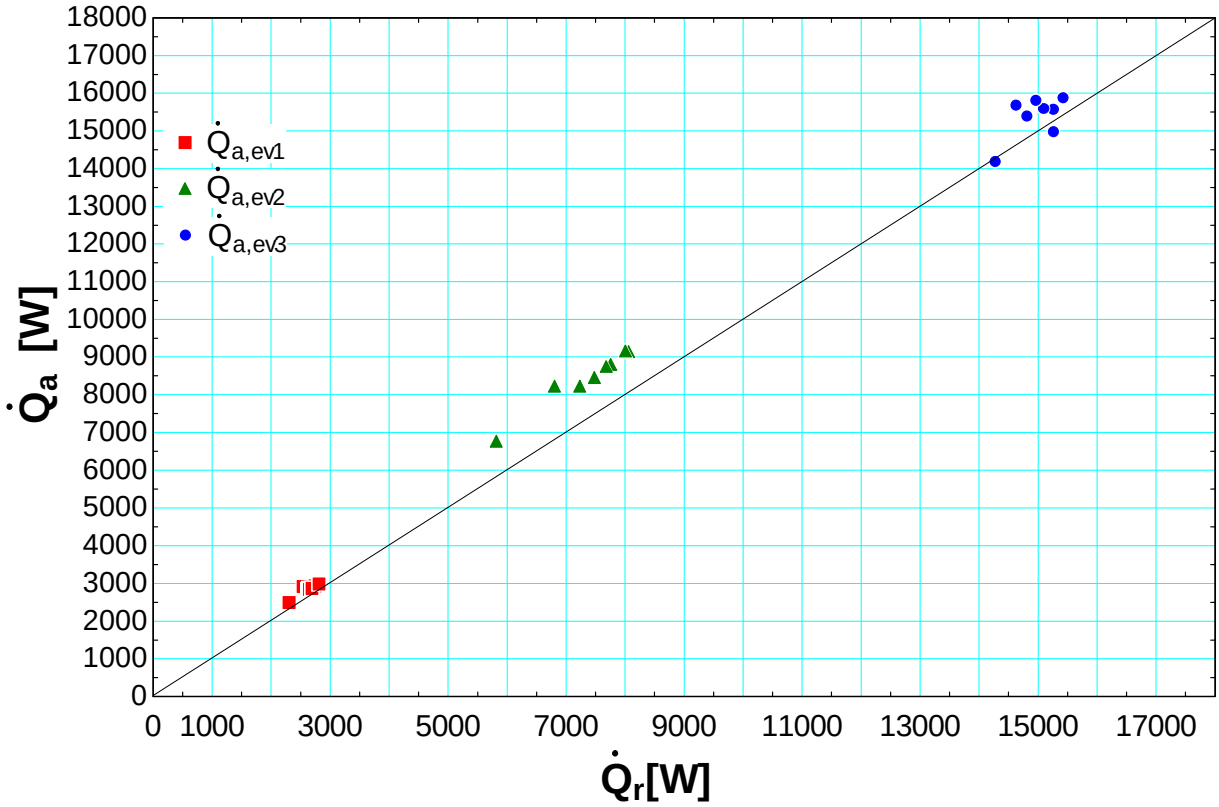

Figure 49 : heat balance over the evaporator using the rule of three method

Another possible way to compute $\dot{M}_{r,pump1}$ and $\dot{M}_{r,pump2}$ is to minimize the sum of errors ($\Delta\dot{Q}_{sum}$) on heat balances over the three heat exchangers composing the evaporator.

$$\Delta\dot{Q}_{sum} = \left(\Delta\dot{Q}_{ev1}\right)^2 + \left(\Delta\dot{Q}_{ev2}\right)^2 + \left(\Delta\dot{Q}_{ev3}\right)^2$$

$$\Delta\dot{Q}_{ev1} = \dot{Q}_{a,ev1} - \dot{Q}_{r,ev1}$$

$$\Delta\dot{Q}_{ev2} = \dot{Q}_{a,ev2} - \dot{Q}_{r,ev2}$$

$$\Delta\dot{Q}_{ev3} = \dot{Q}_{a,ev3} - \dot{Q}_{r,ev3}$$

Figure 50 shows the heat balances over the three heat exchangers composing the evaporator if this minimizing errors method is used.

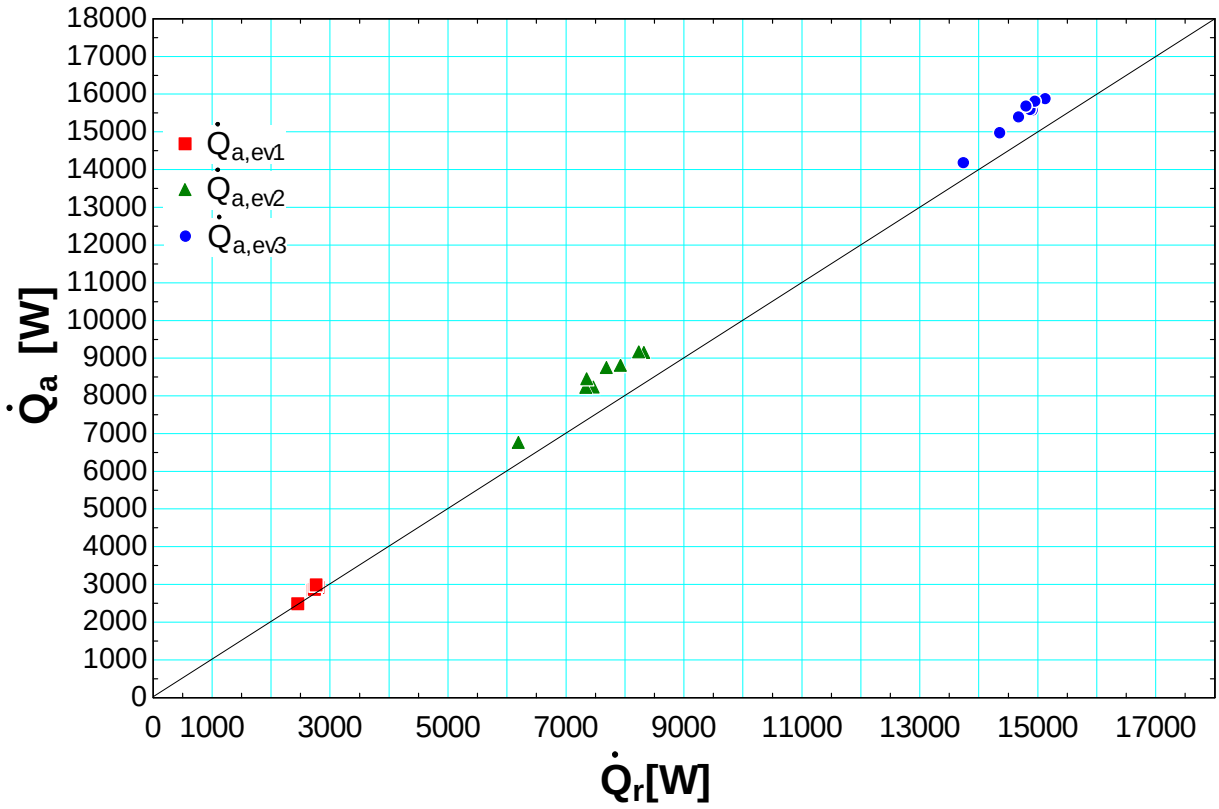

Figure 50 : heat balance over the evaporator using the minimizing error method

The temperatures of both air and refrigerant being very similar in second and third evaporators, there is no reason to have more ambient losses in the second evaporator than in the third one. The minimizing error method seems more in agreement with this consideration. This method will thus be used to split the refrigerant mass flow rate during all set of tests.

4.2.3 Pressure drop over the condenser

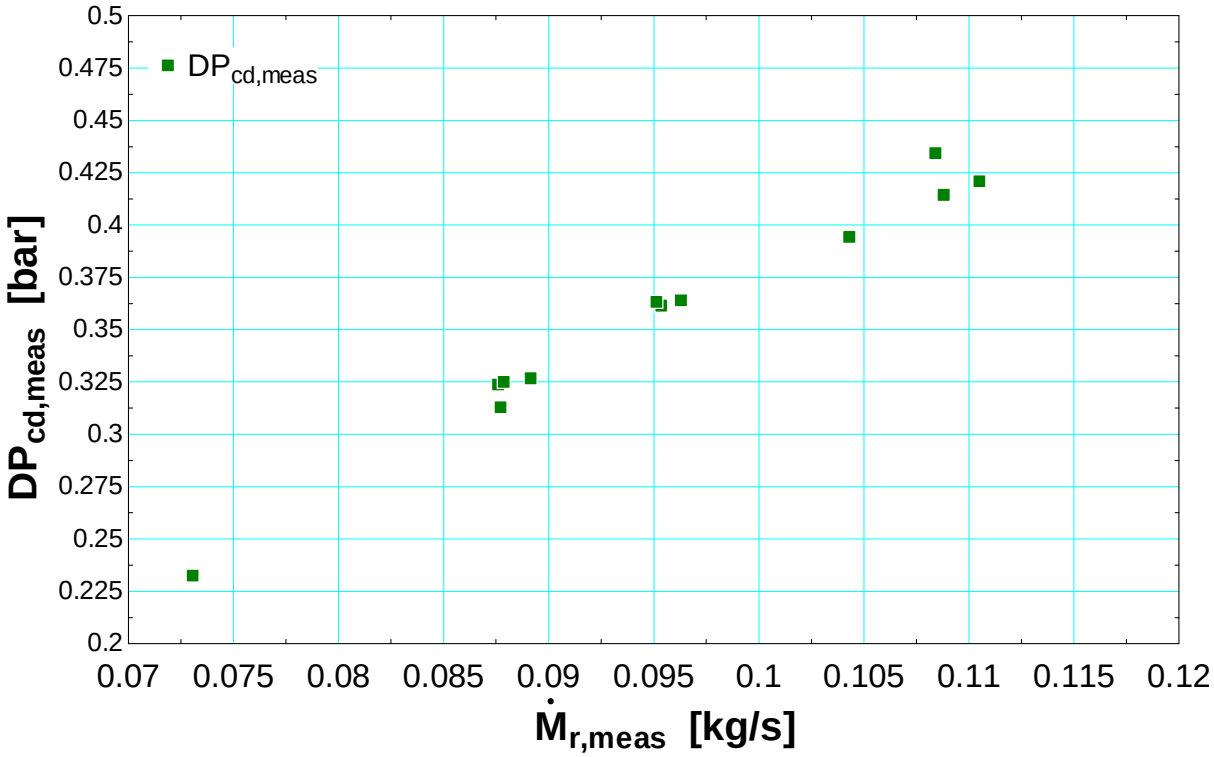

Figure 51 : pressure drop over the condenser as a function of the refrigerant mass flow rate

For these 12 first tests, series configuration was used for the refrigerant side. As shown in Figure 51, the pressure drop over the condenser is pretty high in this configuration.

4.2.4 Quality measurement

During tests 1, 2, 4, 5, 7, 8, 10, 11, a super heated vapour is produced by the evaporator. Enthalpy at the evaporator exhaust ($h_{r,ex,ev}$) is thus known using pressure and temperature measurements and can be compared to the enthalpy measured by the quality measurement device in order to evaluate the accuracy of this measurement device. If the expansion was perfectly isenthalpic in the by-pass used to measure quality, $h_{r,X,meas}$ would be equal to $h_{r,ex,ev}$. Figure 52 shows $h_{r,X,meas}$ vs $h_{r,ex,ev}$.

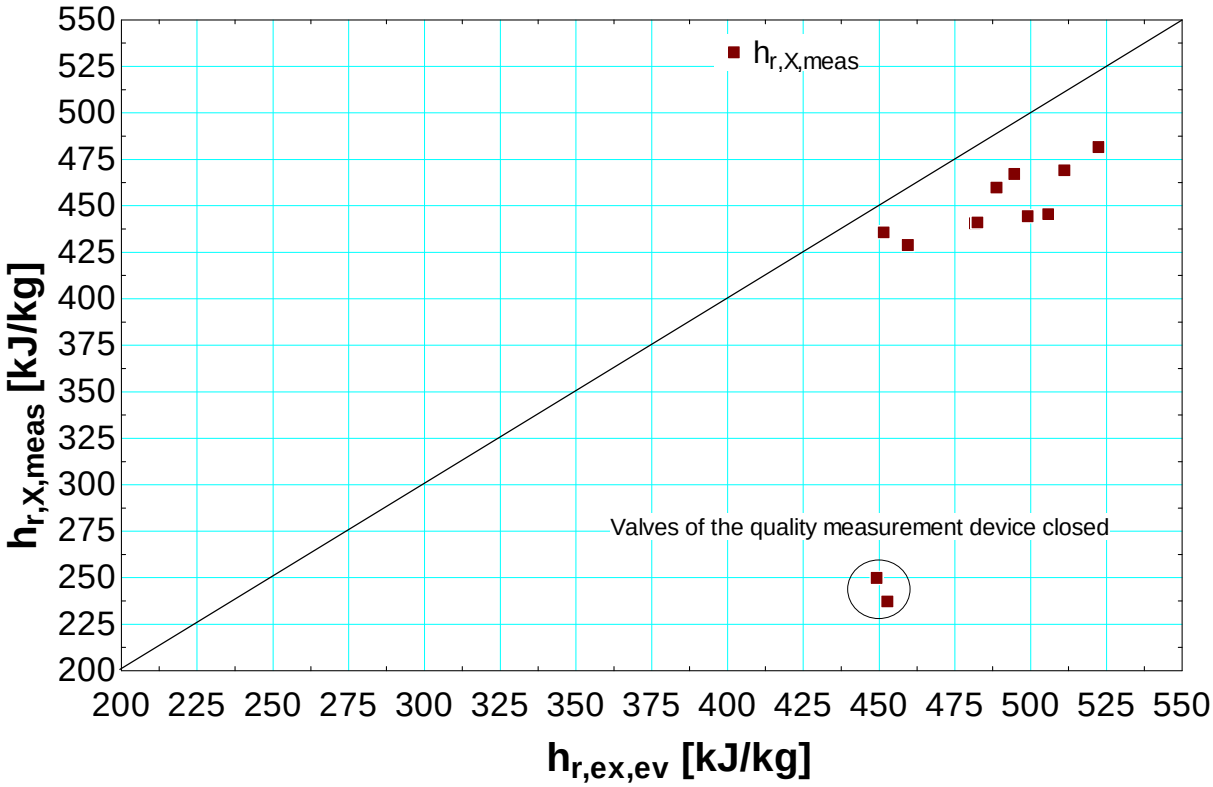

Figure 52 : enthalpy measured by the quality measurement device vs enthalpy measured at the expander supply.

The maximum error is 10.9 % which is pretty high for a measurement device.

4.2.5 Modifications of the test bench

4.2.5.1 Air flow rate measurement

During the first set of tests, air mass flow rate was not measured but a correlation given by the hot air generator was used. For the next sets of test, a diaphragm is added on the air side. Its internal diameter is 18 mm and its external diameter is 50mm. Both absolute pressure and pressure drop are measured and the air flow rate is calculated according to the ISO5167 standard.

4.2.5.2 Refrigerant flow rate measurement

In order to determine if a measurement error is introduced by the RC filter placed on the Coriolis output signal, three situations are compared:

- In the first situation, the RC filter is taken out. The blue curve on Figure 53 shows that the measured flow rate varies greatly in this case.
- In the second one, a RC filter with a 50kΩ resistance and a 150 μF capacitor is used. The red curve on Figure 53 shows much smaller variation on the measured flow rate.

- In the third one, a RC filter with a 300kΩ resistance and a 150μF capacitor is used. The green curve on Figure 53 shows an almost constant measured flow rate.

The temporal evolution of the output signal is thus different for the three cases. However, its mean value remains almost constant (77.69, 77.64 and 77.74 for situation 1, 2 and 3 respectively). The use of an RC filter therefore seems to be a reliable way to average the refrigerant flow rate measurement.

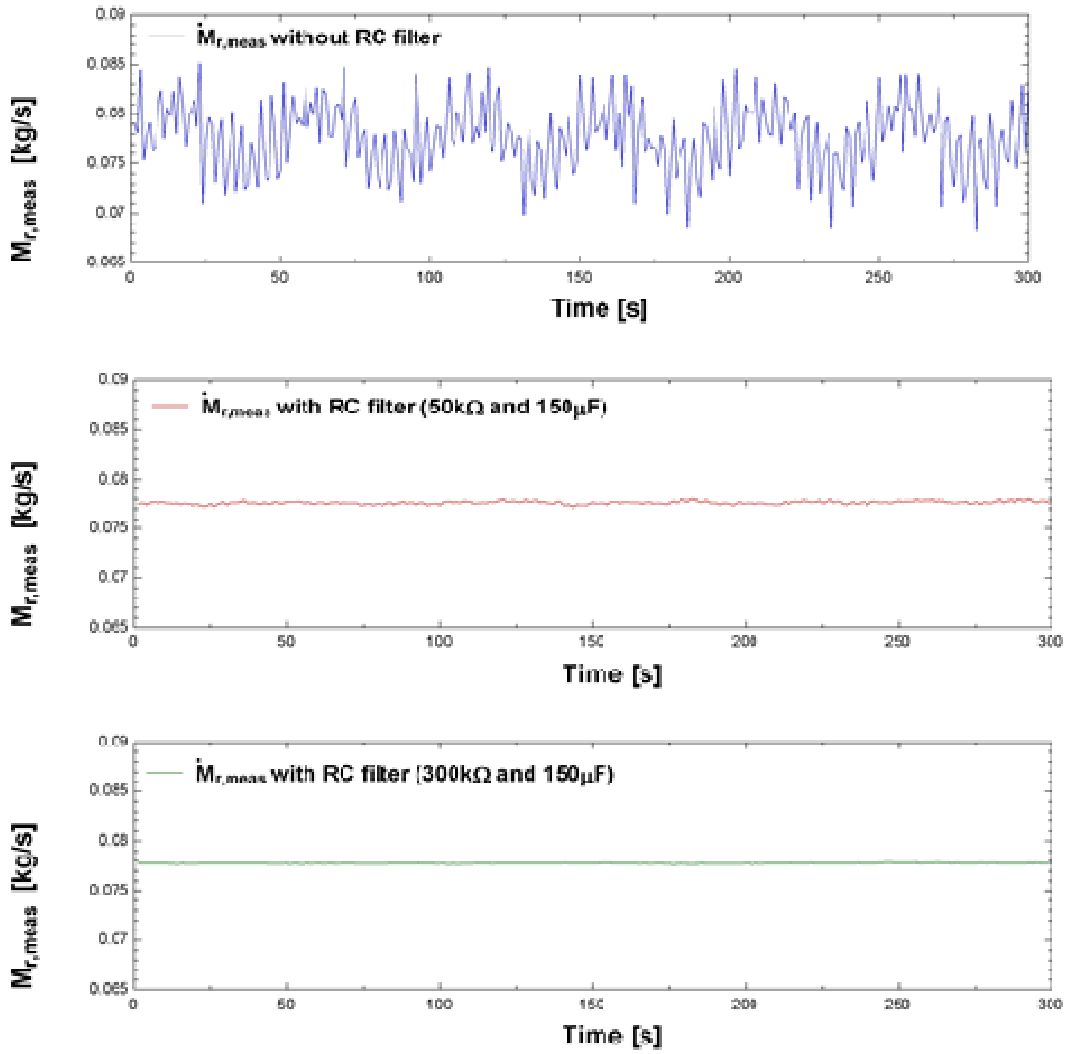

Figure 53 : output signal of the Coriolis flow meter for several R and C value.

4.2.5.3 Condenser configuration

For the next tests, in order to reduce the pressure drop over the condenser, the parallel configuration will be used on the refrigerant side. Since the use of an asymmetric configuration (parallel on refrigerant side and series on water side)

would lead to a non-uniform power distribution over the heat exchangers, the configuration on the water side is thus also changed to parallel one.

4.2.5.4 Quality measurement device

In order to increase the accuracy of the quality measurement device, ambient losses should be reduced by improving the insulation. The small copper tube is thus enclosed inside a wood box filled up with vermiculite.

5 Second set of tests

A second set of 21 tests was performed in May 2009. In this section, the test procedure is described, main results are showed and a critical analysis of both results and measurements is proposed. Finally, an exergetic analysis is performed in order to identify potential improvement.

5.1 Description of the tests

During this second set of tests, four parameters of the cycle are modified:

- The evaporator pressure by increasing or decreasing the expander rotational speed.
- The condensing pressure by changing the water flow rate in the condenser.
- The overheating at the evaporator exhaust by modifying the refrigerant mass flow rate.
- The heat source mass flow rate.

Table 15 displays the extreme values imposed to these parameters during the second set of test.

	Minimum value	Maximum value
Evaporator pressure (bars)	8.79	12.75
Condensing pressure (bars)	1.56	4.186
Overheating (K)	3.9	45.44
Heat source mass flow rate (kg/s)	0.7111	0.9796

Table 15 : extreme values taken by 4 parameters during the second set of tests

5.2 Main results

Table 16 displays the main results of this second set of tests.

	Minimum value	Maximum value
Pressure ratio over the expander	2.42	7.44
Refrigerant mass flow rate	49 g/s	78 g/s
Heat power recovered in the evaporator	13.9 kW	21.2 kW
Shaft power	180.5 W	1851 W
Expander efficiency	16.8 %	70.6 %
Cycle efficiency	-1.4 %	6.64 %
Exergetic efficiency	-4.1 %	19.71 %

Table 16 : main results of the second set of tests

5.3 Analysis

5.3.1 Balances

5.3.1.1 Evaporator

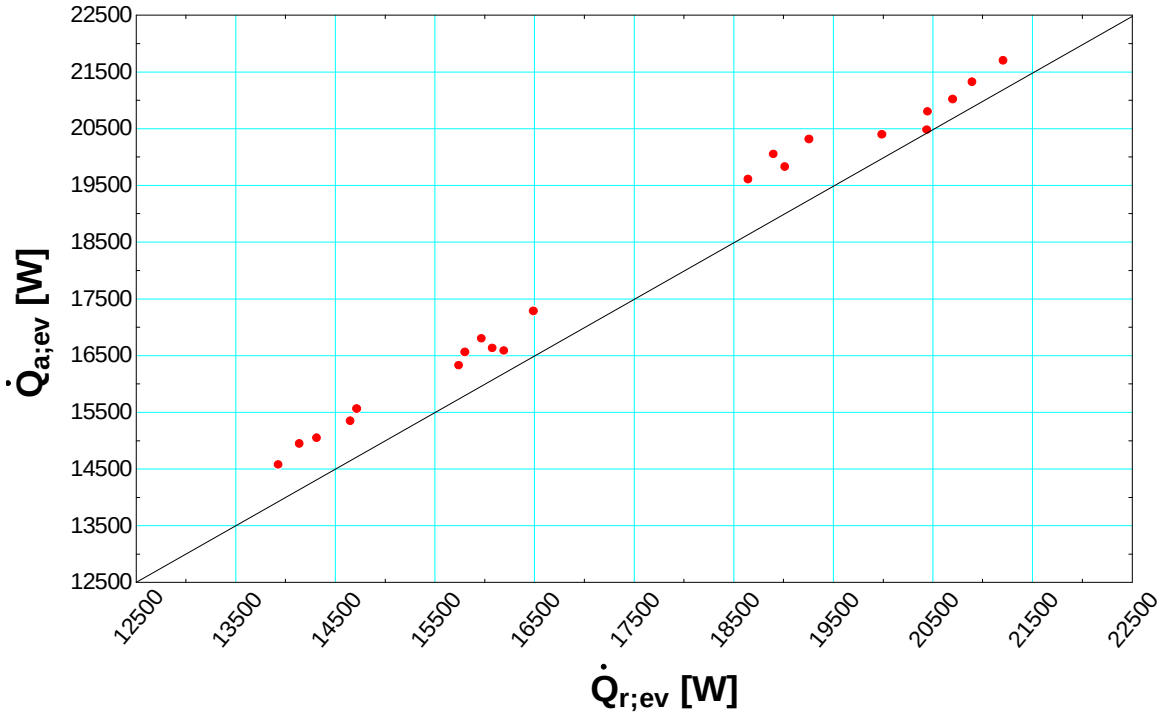

Figure 54 : globa heat balance over the evaporator

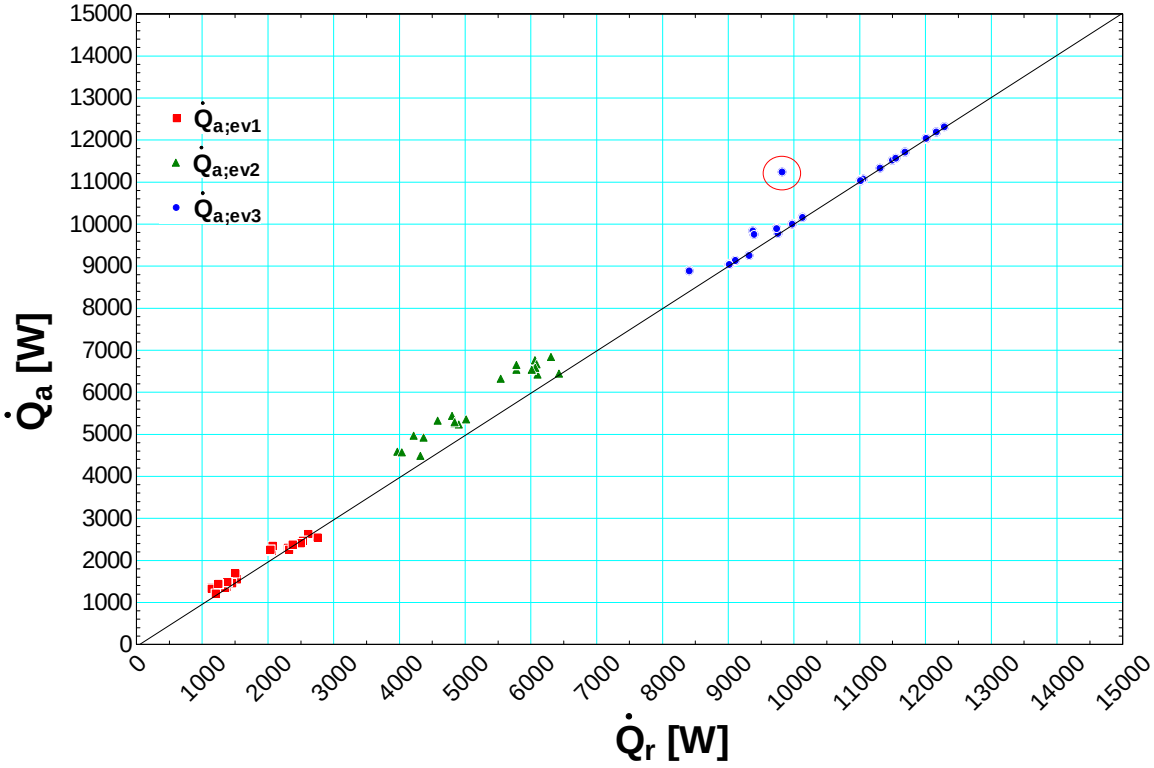

Figure 55 : detailed heat balance over the evaporators

The global heat balance over the evaporator shows a good agreement (see Figure 54). However, the heat power on air side is higher than the one on refrigerant side for all tests. This could be explained by ambient losses on air side.

The detailed balance also shows a good agreement (see Figure 55) except for the point circled in red which correspond to test n°20. During this test, the overheating was relatively low (about 3.9°C) which could explain the heat balance divergence. Indeed, despite of a theoretical overheating, a small fraction of liquid could remain present and distort the temperature measurement.

5.3.1.2 Condenser

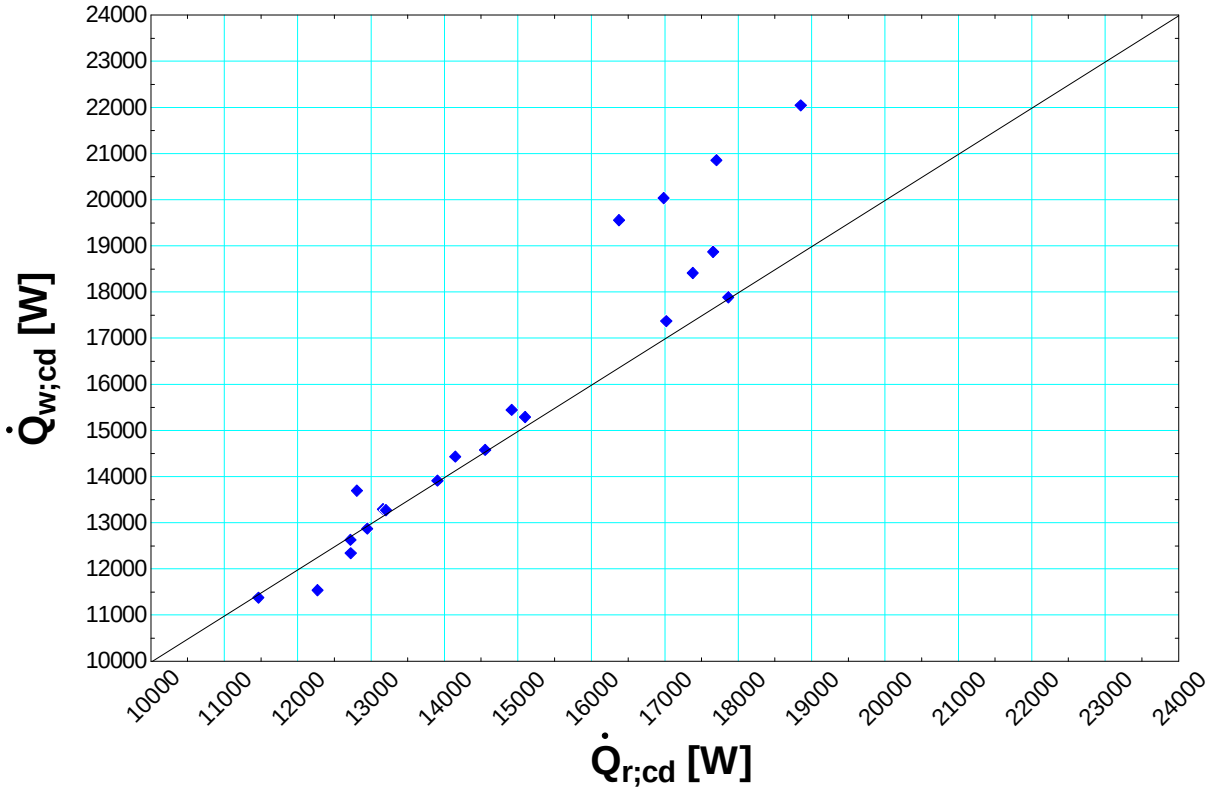

Figure 56 : heat balance over the condenser

The heat balance over the condenser shows a good agreement (see Figure 56) except for 4 points (tests n°1, 2, 18 and 19). For these tests, the water flow rate is maximum (around 0.61kg/s) which leads to a low water temperature difference between inlet and outlet (about 5K). If the uncertainty on both supply and exhaust temperature measurements is set to 0.3K, the error committed on the temperature difference measurement is 8.4%. An additional possible explanation is the two-phase state detected at the subcooler supply for these four tests (huge bubbles during test 1, 2 and small bubbles during test 18 and 19). The refrigerant was thus not completely condensed at the condenser exhaust.

5.3.2 Pressure drops

5.3.2.1 Evaporator

A differential pressure sensor was installed in both refrigerant lines of the evaporator in order to measure pressure drops. The range of both differential pressure sensors was 0-500 mbar while the measured pressure drop is almost zero for all tests. The sensors were thus over-sized and evaporator pressure drops measurements are not reliable.

5.3.2.2 Condenser

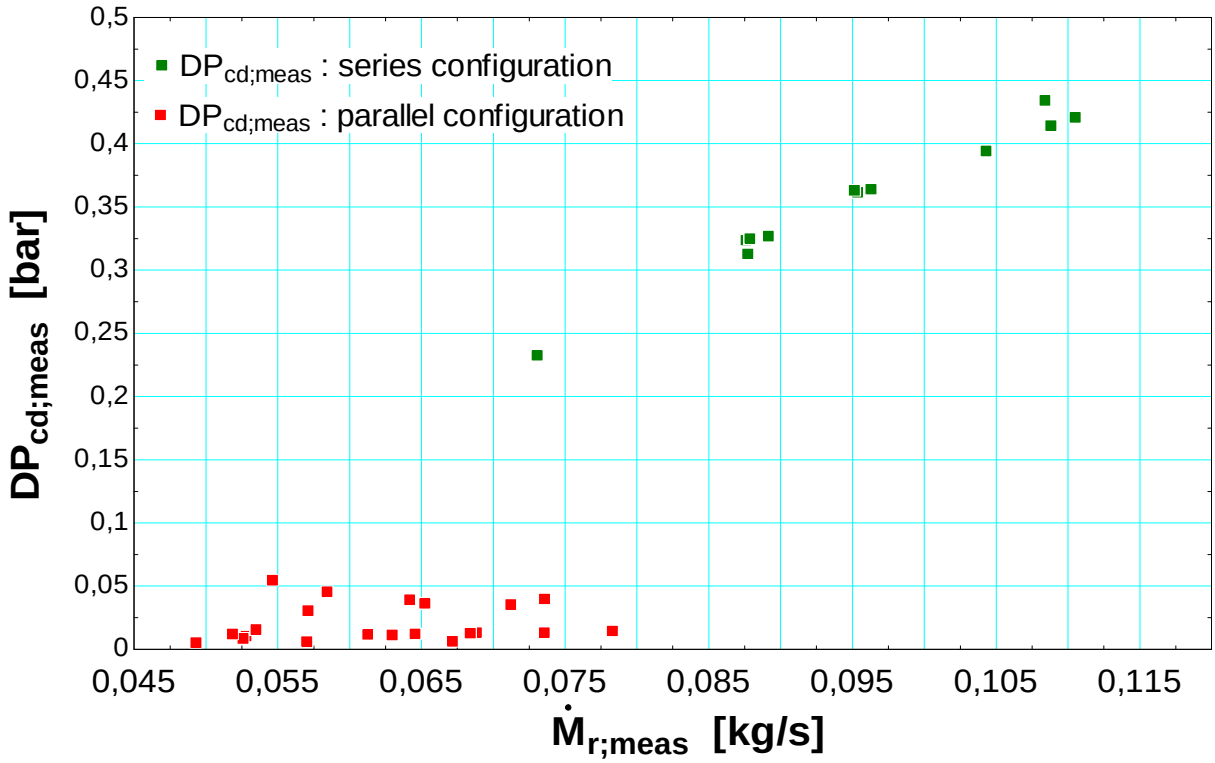

Figure 57 : pressure drop over the condenser vs refrigerant mass flow rate

The remark about the reliability of evaporator pressure drops measurement also applies to the condenser. Indeed, the range of the differential pressure sensor selected to measure pressure drops over the condenser was a 0-1000mbar while the measured values are between 0 and 0.05 bar (see Figure 57). However, Figure 57 shows that the pressure drop over the condenser is much smaller using the parallel configuration on refrigerant side.

5.3.3 Shaft power and expander efficiency

Theoretically, the ideal expansion in volumetric machines can be divided into two steps [9]. The first step is an isentropic expansion from inlet pressure to the adapted

pressure corresponding to the built-in volume ratio. The nature of the second step depends of the adapted pressure compared with outlet pressure:

- If the adapted pressure (P_{ad}) is higher than outlet pressure (under-expansion case, see Figure 58a), the second steps is constituted of an isochoric *expansion*.
- By contrast, if the adapted pressure is lower than outlet pressure (over expansion case, see Figure 58b), the second step consists in an isochoric *compression*.

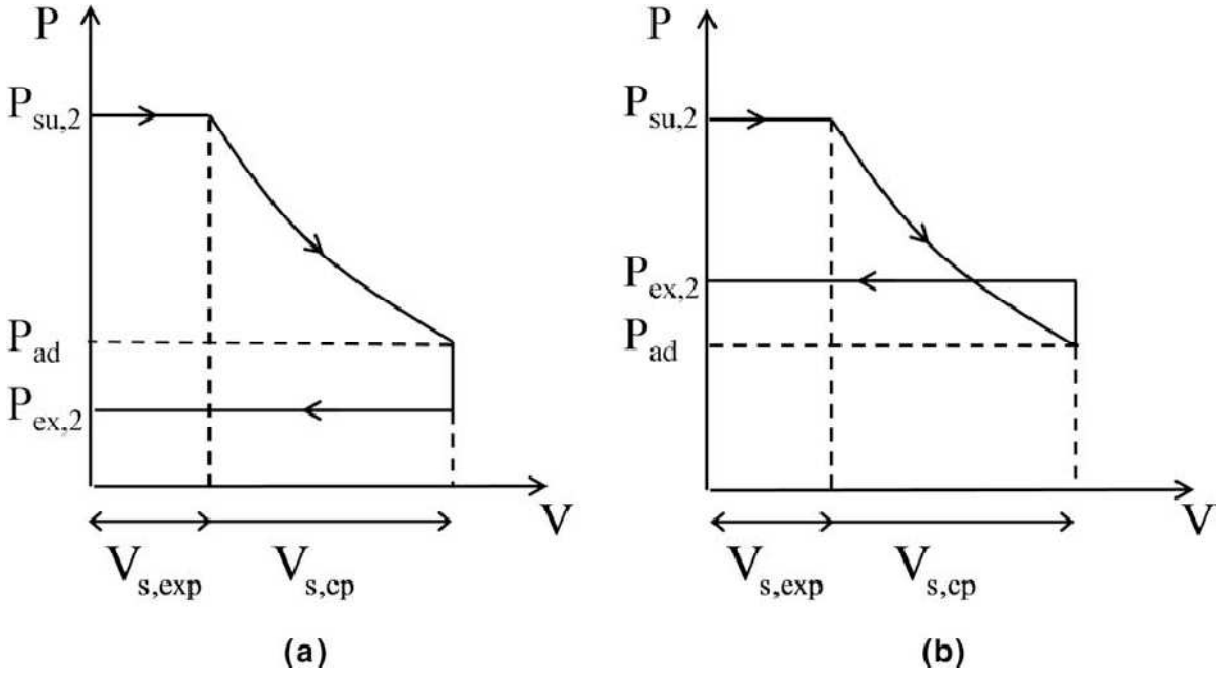

Figure 58 : Representation of the entire expansion process in the pressure-volume [6]

The under expansion case can be illustrated by tests 2, 3 and 6 for which the pressure ratio varies while other conditions are very similar. Table 17 displays pressure ratio, expander isentropic efficiency and shaft power for these three tests.

	Pressure ratio	Expander efficiency	Shaft power (W)
Test n°2	7	62,7 %	1851
Test n°3	6.15	65.6 %	1784
Test n°6	4.9	70 %	1735

Table 17 : pressure ratio, expander efficiency and shaft power for test 1, 2 and 6

From test 2 to 6, the pressure ratio is decreased from 7 to 4.9, which leads to an increased isentropic expander efficiency. This can be explained by a reduction of the isochoric part of the expansion compared with the isentropic one.

As shown in Table 17, the partial compensation of a decreased pressure ratio by an increased isentropic efficiency leads to observe only a slight reduction of the shaft power compared with the reduction of the pressure ratio.

5.3.4 Air flow rate measurement

As explained in section 4.2.5.1, an air flow rate measurement was added between first and second set of tests.

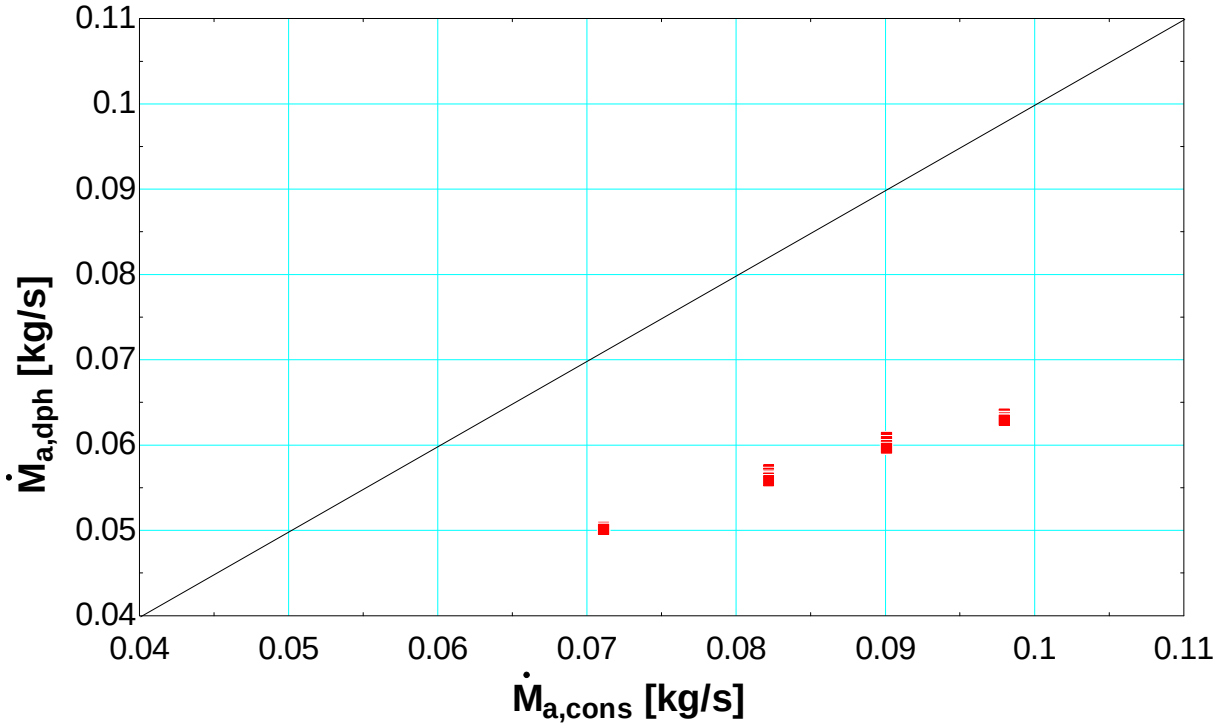

Figure 59 : air flow rate measured vs air flow rate given by the constructor

As shown in Figure 59, the divergence between measured and computed (using the constructor correlation) air flow rate is relatively high and cannot be explained by standard uncertainties on measurements.

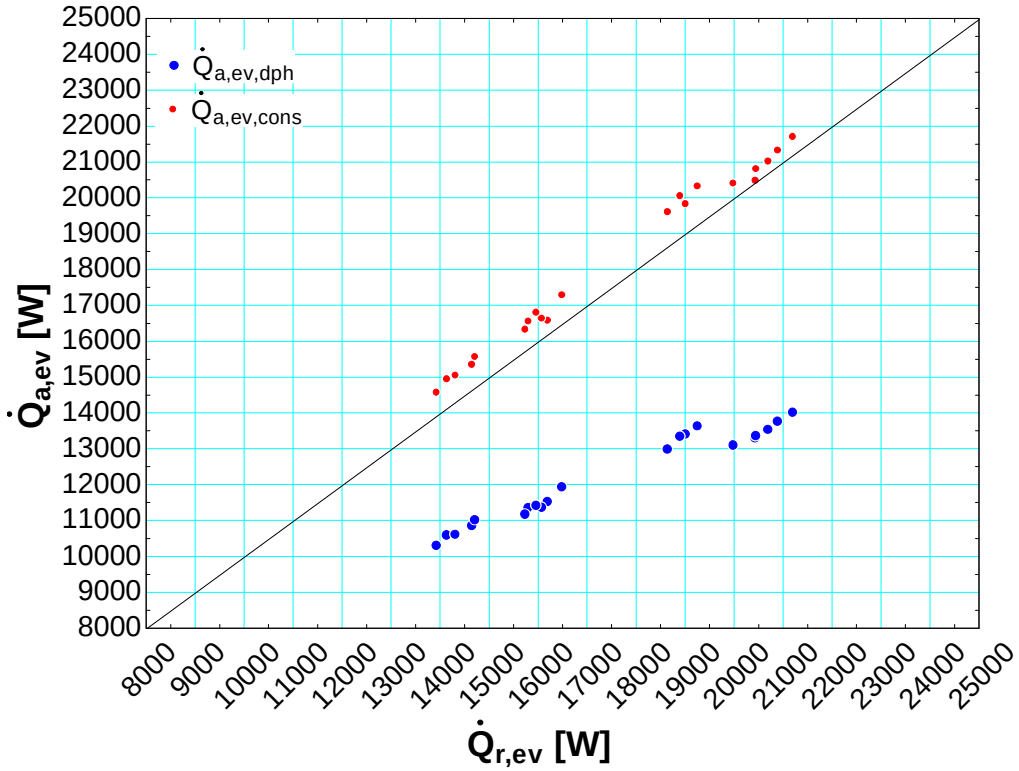

Figure 60 : comparison between evaporator heat balance for measured and correlated air flow rate

Evaporator heat balance shows a much better agreement if the constructor correlation is used in order to compute the air flow rate (see Figure 60). The correlated value seems thus more reliable. A malfunctioning of the differential pressure sensor could explain the divergence between correlated and measured values.

5.3.5 Quality measurement device calibration

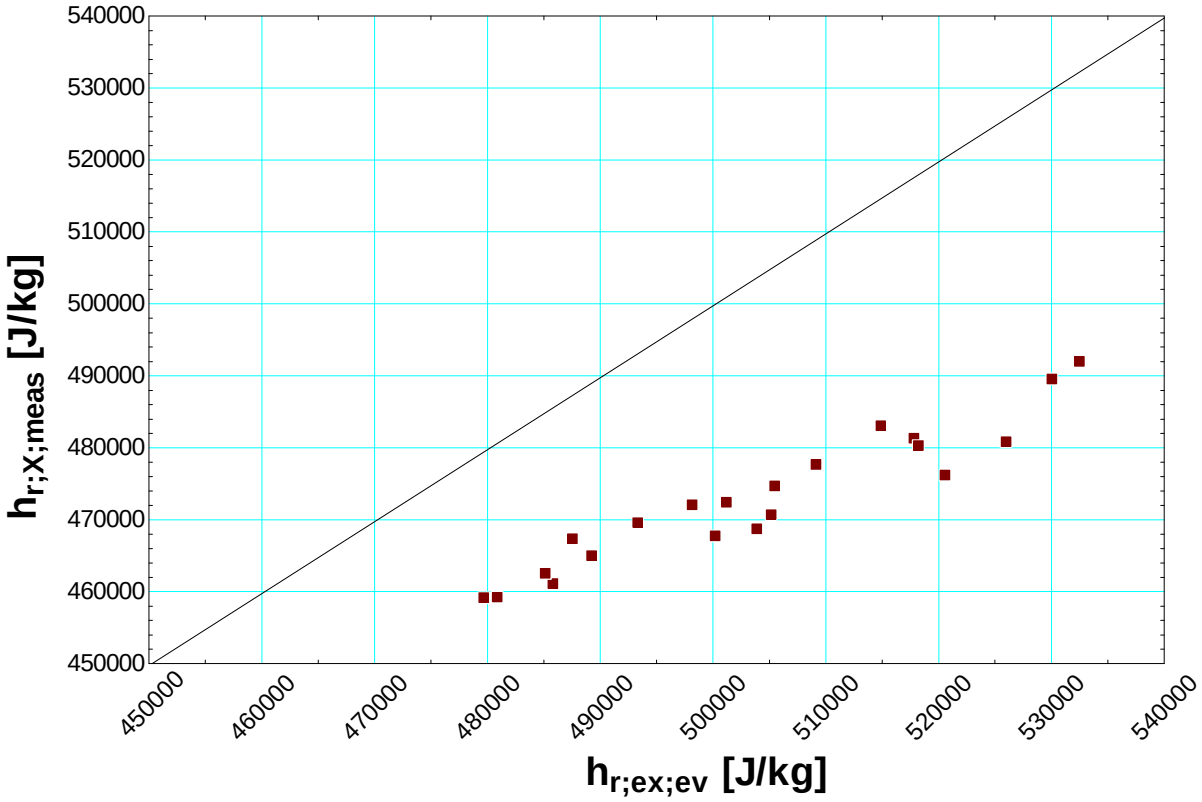

Figure 61: enthalpy measured by the quality measurement device vs enthalpy measured at the evaporator exhaust

As a super heated vapour is produced by the evaporator for all tests, enthalpy measured by the quality measurement device ($h_{r,X,meas}$) can be compared to enthalpy at the evaporator exhaust ($h_{r,ex,ev}$) as in section 4.2.4. Figure 61 shows that $h_{r,X,meas}$ is always smaller than $h_{r,ex,ev}$ which can be explained by ambient losses (see section 4.2.4).

In order to have a reliable measurement of the enthalpy if the evaporator produces a two-phase medium, a correction of $h_{r,X,meas}$ has to be developed. A polynomial law is found:

$$h_{r,ex,ev,pred} = h_{r,X,meas} + a\left(\frac{\dot{M}_r}{\dot{M}_{r,ref}}\right)^{n_1}\left(\frac{\Delta P}{\Delta P_{ref}}\right)^{n_2}\left(\frac{\Delta T}{\Delta T_{ref}}\right)^{n_3}$$

Where $\dot{M}_r$ is the refrigerant flow rate in kg/s, ΔP is the differential pressure between expander inlet and outlet in bar and ΔT is the temperature difference between evaporator exhaust and ambient in °C. $\dot{M}_{r,ref}$, ΔP_{ref} and ΔT_{ref} are respectively set to 0.05 (kg/s), 5 (bar) and 50 (°C).

Values of parameters are determined by means of an optimization algorithm available in EES:

$$a = 14476\ [J/kg],\ \ n_1 = -0.4914,\ n_2 = -0.3431\ and\ n_3 = 1.685$$

As shown in Figure 62, the use of this correction gives a good agreement between measured and predicted values of the evaporator exhaust enthalpy.

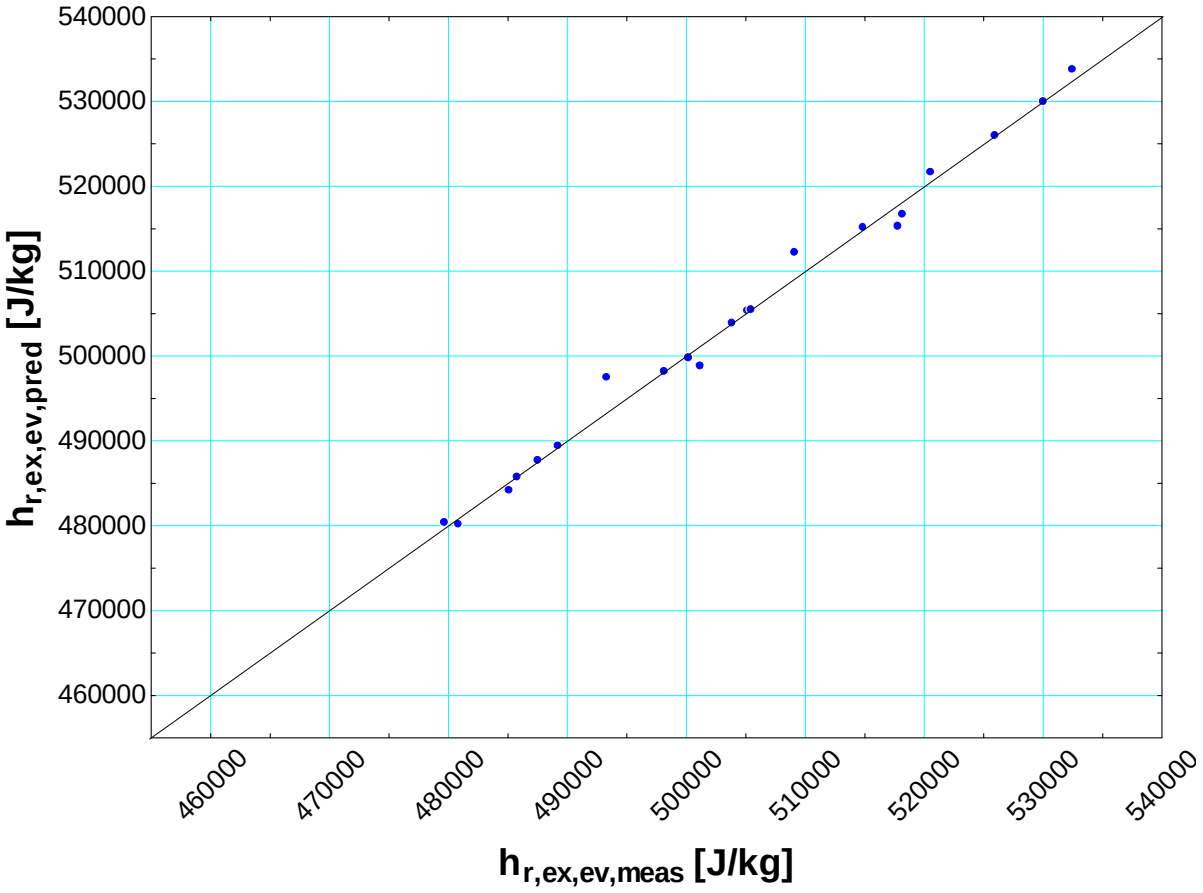

Figure 62

5.4 Exergetic analysis

In this section, an exergetic analysis of the cycle is performed in order to identify the main sources of exergetic losses.

The definition of exergy of a fluid is:

$$E = \dot{M} * [(h - h_0) - (T_0 + 273{,}15) * (s - s_0)]$$

Where s and h are entropy and enthalpy of the fluid at its temperature and pressure while s_0 and h_0 are entropy and enthalpy of the fluid at reference temperature and pressure. $\dot{M}$ is the mass flow rate of the fluid. The supply

temperature of the cold source being around 10°C, this value will be taken as reference (T_0) for exergy calculation. The pressure reference is 1 bar (P_0).

Electrical power is considered as pure exergy.

Exergy of the fluids is calculated for all useful points of the cycle. The variable names used are shown in Figure 63.

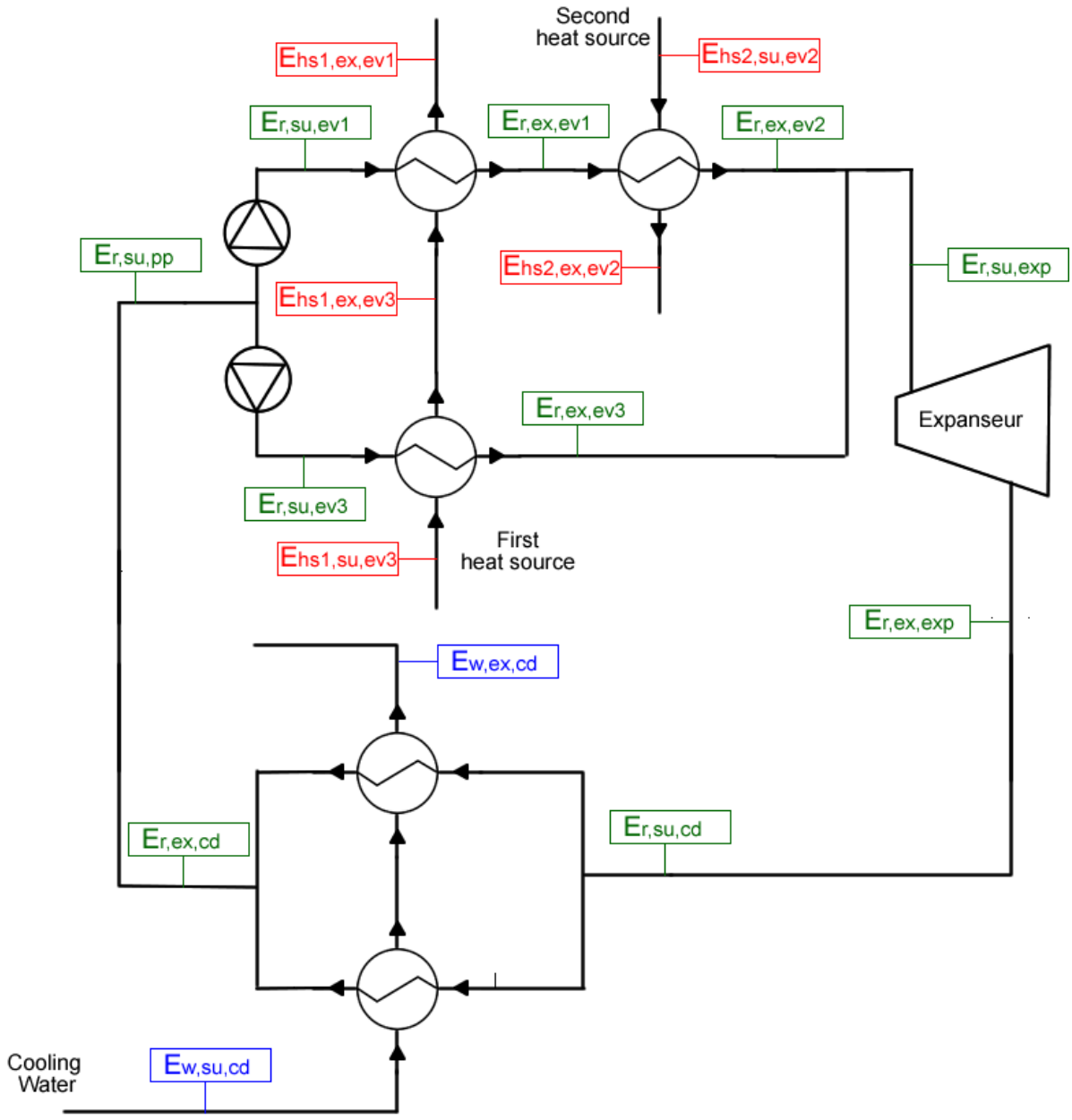

Figure 63

5.4.1 Active

The active part of the exergy balance is composed of three terms:

- Exergy of the first heat source (E_{hs1})
- Exergy of the second heat source (E_{hs2})
- Pumps electrical consumption (E_{pp})

5.4.1.1 Exergy of heat sources

The exergy of both heat sources is given by:

$$E_{hs1} = E_{hs1,su,ev3}$$

$$E_{hs2} = E_{hs2,su,ev2}$$

5.4.1.2 Pumps consumption

$$E_{pp} = \dot{W}_{pp,meas}$$

5.4.2 Passive

The passive part of the exergy balance is composed of ten terms:

- Irreversibility of heat transfer in the first evaporator
- Irreversibility of heat transfer in the second evaporator
- Irreversibility of heat transfer in the third evaporator
- First heat source exhaust
- Second heat source exhaust
- Shaft power
- Expander irreversibility
- Irreversibility of the heat transfer in the condenser
- Condenser water exhaust
- Pump irreversibility

5.4.2.1 Irreversibility of heat transfer in the evaporators

The irreversibility of heat exchanges can be evaluated by the difference between the exergy lost of the hot fluid and the exergy gain of the cold fluid.

Evaporator 1

$$\Delta E_{ev1} = \left(E_{hs1,ex,ev3} - E_{hs1,ex,ev1}\right) - \left(E_{r,ex,ev1} - E_{r,su,ev1}\right)$$

Evaporator 2

$$\Delta E_{ev2} = \left(E_{hs2,su,ev2} - E_{hs2,ex,ev2}\right) - \left(E_{r,ex,ev2} - E_{r,ex,ev1}\right)$$

Evaporator 3 $\Delta E_{ev3} = \left(E_{hs1,su,ev3} - E_{hs1,ex,ev3}\right) - \left(E_{r,ex,ev3} - E_{r,su,ev3}\right)$

5.4.2.2 Heat sources exhaust

A fraction of the exergy of heat sources is not transmitted to the refrigerant in the evaporator:

First heat source $$E_{ex,hs1} = E_{hs1,ex,ev1}$$

Second heat source $$E_{ex,hs2} = E_{hs2,ex,ev2}$$

5.4.2.3 Shaft power and expander irreversibility

The exergy produced by the expander is equal to the shaft power which is given by:

$$E_{shaft} = \dot{W}_{shaft} = 2\pi \frac{N}{60} C$$

Where N is the rotational speed of the expander and C the measured torque.

Expander irreversibility is given by:

$$\Delta E_{exp} = \left(E_{r,su,exp} - E_{r,ex,exp}\right) - \dot{W}_{shaft}$$

5.4.2.4 Irreversibility of heat transfer in the condenser

Irreversibility of heat exchange in the condenser is calculated in the same way than for the evaporators.

$$\Delta E_{cd} = \left(E_{r,su,cd} - E_{r,ex,cd}\right) - \left(E_{w,ex,cd} - E_{w,su,cd}\right)$$

5.4.2.5 Condenser water exhaust

A fraction of exergy is lost in the cold source:

$$E_{w,ex} = E_{w,ex,cd}$$

5.4.2.6 Pumps irreversibility

Pumps irreversibility is given by:

$$\Delta E_{exp} = \dot{W}_{pp} - \left(E_{r,ex,pp} - E_{r,su,pp}\right)$$

5.4.3 Results

Figure 64 shows the results of the exergetic analysis for the second set of tests.

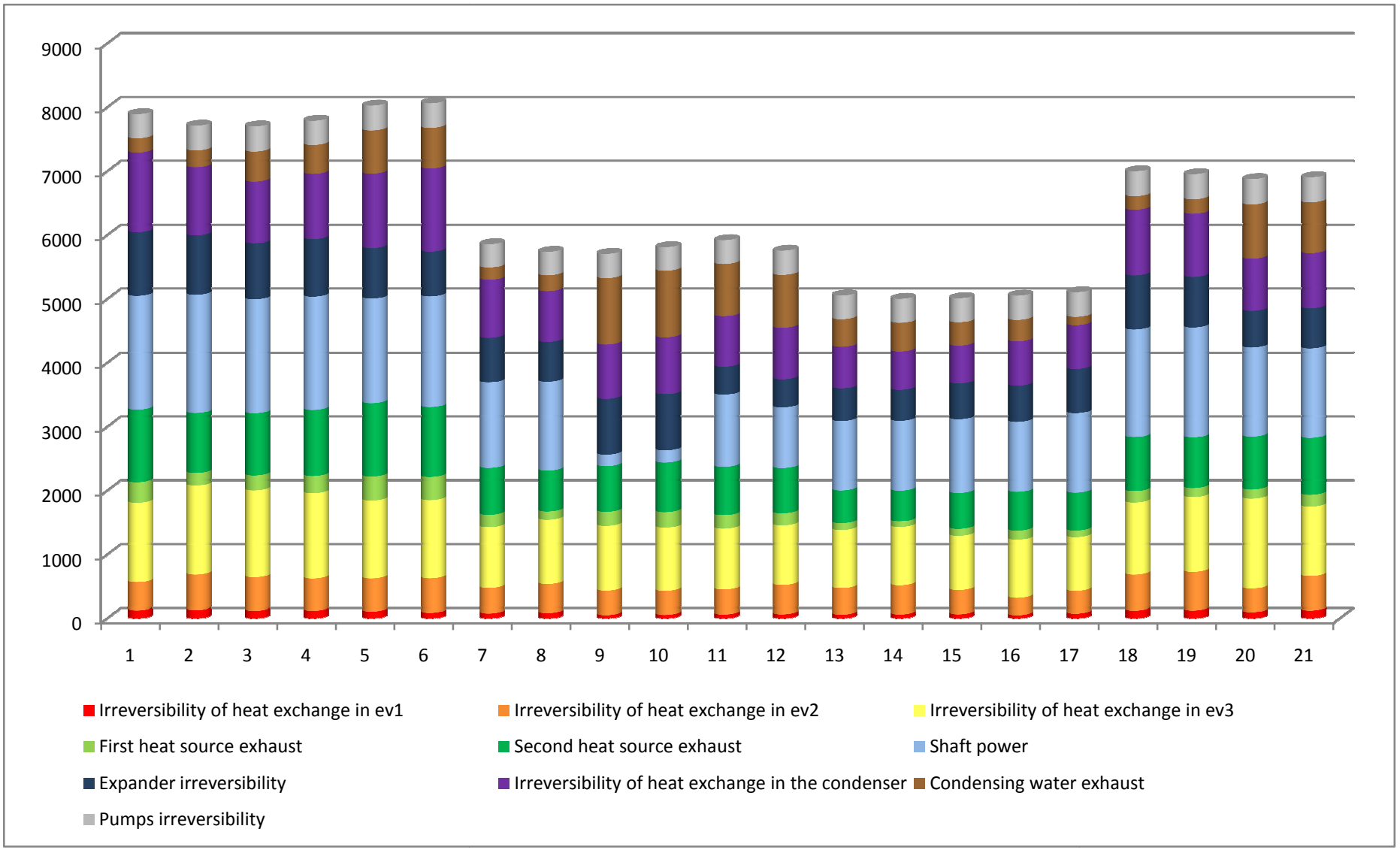

Figure 64 : exergetic analysis

For all tests the sum of the five contributions of exergy losses in the evaporator (Irreversibility of heat transfer and heat sources exhaust) represents more than 30% of the total exergy. This can be explained by the high mean temperature difference between air and R245fa in second and third evaporators (see Figure 65 and Figure 66).

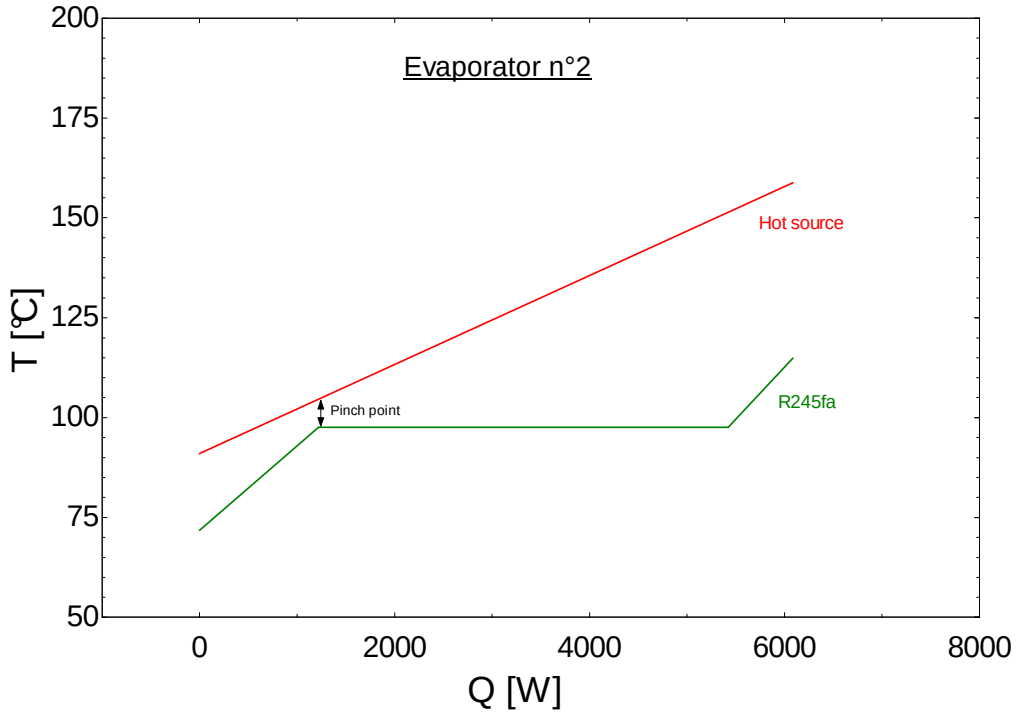

Figure 65 : typical temperature profile in the second evaporator

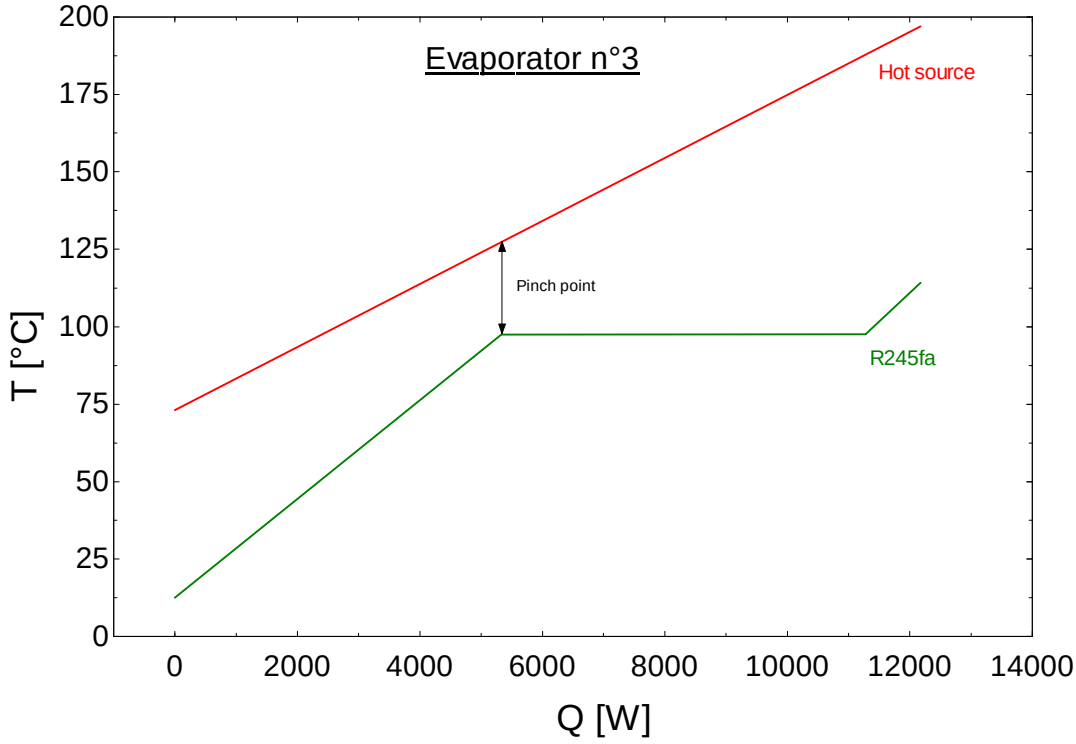

Figure 66 : typical evaporator profile in the third evaporator

Another fraction of exergy (from 16 to 32%) is lost in the condenser. This is mainly due to the high expander exhaust temperature.

The expander efficiency varies from 16.8% to 70.6% which leads to exergy losses varying between 7.3% and 14.8%.

Finally, the pumps inefficiency induces an exergy loss ranging from 4.8% to 7.5%.

6 Third set of tests

While the main goal of the second set of tests was to study the performance of the ORC system over a wide range of conditions, this section focuses on two objectives:

- Produce the maximum shaft power for several hot source flow rates.
- Study the performances of the system if a two-phase medium is supply to the expander.

6.1 Power maximisation

The mass flow rate of hot air is set to 4 different values and other parameters (expander rotational speed and pump capacities) are adjusted in order to produce the maximum shaft power. Table 18 displays the main results obtained

Test	Air mass flow rate (kg/s)	Expander efficiency	Shaft power (W)
C1	0.1264	65.8%	2164
C2	0.1106	64.5%	2028
C3	0.09481	62.6%	1744
C4	0.07901	63.4%	1389

Table 18 : maximum power for several hot air flow rate

The mass flow rate of hot air is decreased by 12.,5% between the first and the second test but power only decrease by 6,2%. This is explained by a very high overheating during the first test. In order to decrease this overheating, the mass flow rate of refrigerant would have to be increased. In the present work, this turned out to be impossible without surpassing the maximum acceptable pressure of the pumps. Indeed, the outlet pressure of the pumps is imposed by the expander and increasing the mass flow rate of fluid leads to an increased pressure.

6.2 Two-phase medium expanding

A few tests are performed in order to evaluate performance of the expander if a two phase medium is supplied. The mass flow rate of hot air is set to two different values. For each one, a first test showing a slight overheating is performed. This overheating is progressively decreased and two tests are performed with a two-phase medium at the expander supply.

The measurement of the vapour quality at evaporator exhaust is corrected by means of the correlation developed in section 5.3.5. Table 19 displays the main results obtained

Test	Air mass flow rate (kg/s)	Overheating or vapour quality	Expander efficiency	Shaft power (W)
C5	0.08217	6.4 K	64.7%	1474
C6		0.938	65.2%	1423
C7		0.886	65.7%	1405
C8	0.09796	8.2K	64.6%	1897
C9		0.9278	64.8%	1836
C10		0.8346	65.6%	1795

Table 19 : two phase medium expanding results

Results show that the power is slightly decreased if the fluid is in two phase state at the expander supply but a slight improvement of the expander efficiency is noticed. However this improvement could be due to measurement error. Indeed, a higher error of about 8% is detected on the evaporator heat balance for all the tests in two-phase state.

7 Modelling

In order to predict the behaviour of the system in a wide range of conditions, a model of the cycle is developed under EES. The model of each component is validated with the second set of tests.

7.1 Evaporator model

7.1.1 First evaporator

The refrigerant being in liquid state in the first evaporator for all tests, the model developed for this heat exchanger is a single zone model. For both refrigerant and air side, the Nusselt number is obtained by means of a non-dimensional correlation:

$$Nu = cRe^m Pr^n$$

Where m is set to 0.5 for laminar regime (Re < 400) and to 0.7 for turbulent regime (Re > 400) while n is equal to 1/3. These values are suggested by Muley [10]. Parameter c is identified from the measurements.

Once the Nusselt number is known, the heat transfer coefficient (α) is deducted by means of:

$$\alpha = \frac{Nu * k}{D_h}$$

Where k is the conductivity of the fluid while D_h is the hydraulic diameter.

7.1.2 Second evaporator

During the second set of tests, the fluid enters the second evaporator in liquid state and leaves it in superheated vapour state. The model of the second evaporator is thus divided into three zones as shown on Figure 67.

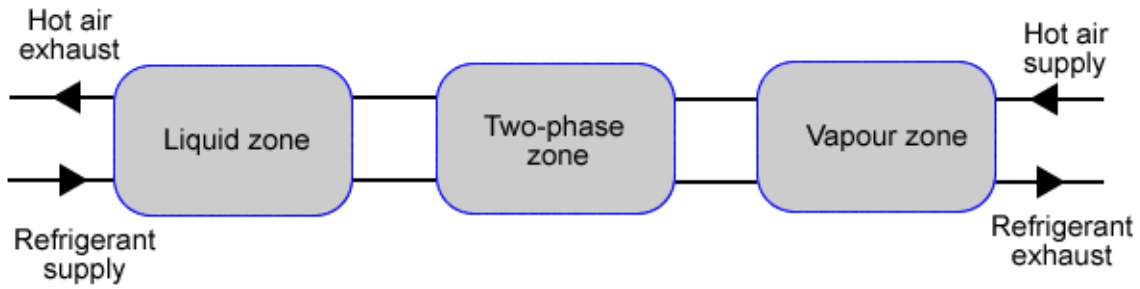

Figure 67 : three zones model

For both side in liquid and vapour zones, heat transfer coefficients are calculated using the method described in section 7.1.1. This method is also use to determine the heat transfer coefficient of air side in the two-phase zone.

The refrigerant side heat transfer coefficient in the two-phase zone (α_{tp}) is obtained by means of Y.Y. Hsieh correlation [11]:

$$\alpha_{tp} = ch_l Bo^{0,5}$$

Where Bo is the boiling number and h_l is liquid heat transfer coefficient. As for single phase heat exchange, the parameter c is identified from measurements.

7.1.3 Third evaporator

The model developed for the third evaporator is similar to the one developed for the second evaporator.

7.1.4 Identified parameters

Table 20 displays a summary of correlations used for each zone in each heat exchanger and the corresponding values of "c" parameters.

		Liquid zone	Two-phase zone	Vapour zone
First evaporator	Air side	$Nu = cRe^m Pr^n$ $c = 0.4849$		
	R245fa side	$Nu = cRe^m Pr^n$ $c = 0.4689$		
Second evaporator	Air side	$Nu = cRe^m Pr^n$ $c = 0.2997$	$Nu = cRe^m Pr^n$ $c = 0.2041$	$Nu = cRe^m Pr^n$ $c = 0.1$
	R245fa side	$Nu = cRe^m Pr^n$ $c = 0.3237$	$\alpha_{tp} = ch_l Bo^{0,5}$ $c = 2.453$	$Nu = cRe^m Pr^n$ $c = 0.117$
Third evaporator	Air side	$Nu = cRe^m Pr^n$ $c = 0.152$	$Nu = cRe^m Pr^n$ $c = 0.1622$	$Nu = cRe^m Pr^n$ $c = 0.1617$
	R245fa side	$Nu = cRe^m Pr^n$ $c = 0.2317$	$\alpha_{tp} = ch_l Bo^{0,5}$ $c = 2.98$	$Nu = cRe^m Pr^n$ $c = 0.1272$

Table 20 : summary of correlations used for each zone in each heat exchanger and the corresponding values of "c" parameters

Figure 68, Figure 69 and Figure 70 shows the comparison between measured and predicted values of the exhaust temperature of the three evaporators.

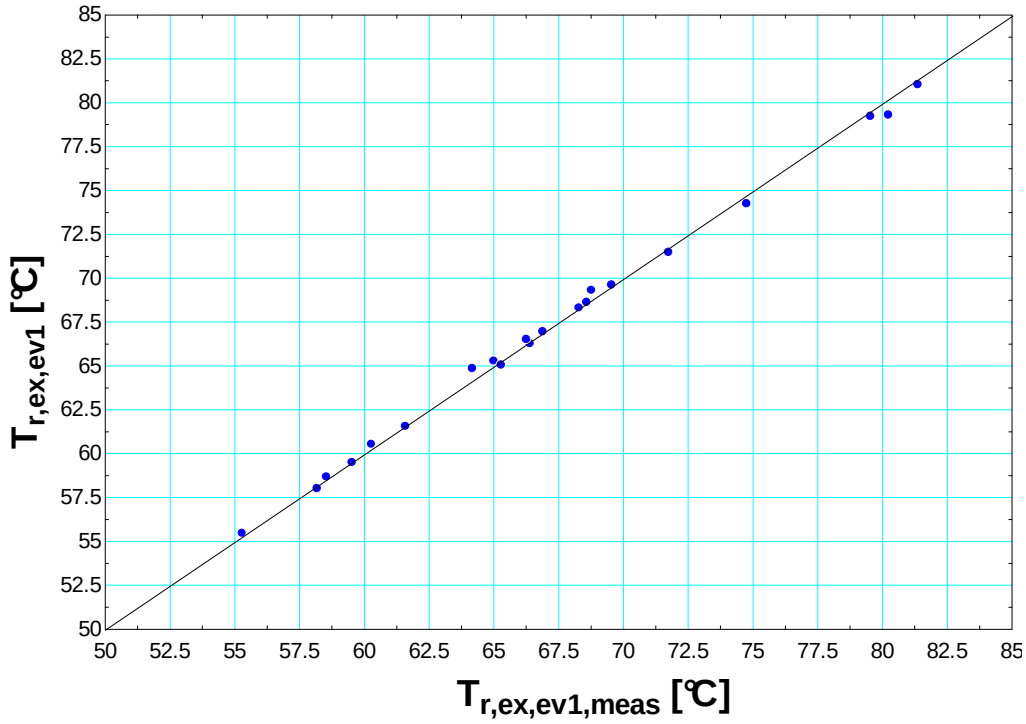

Figure 68 : predicted vs measured first evaporator exhaust temperature

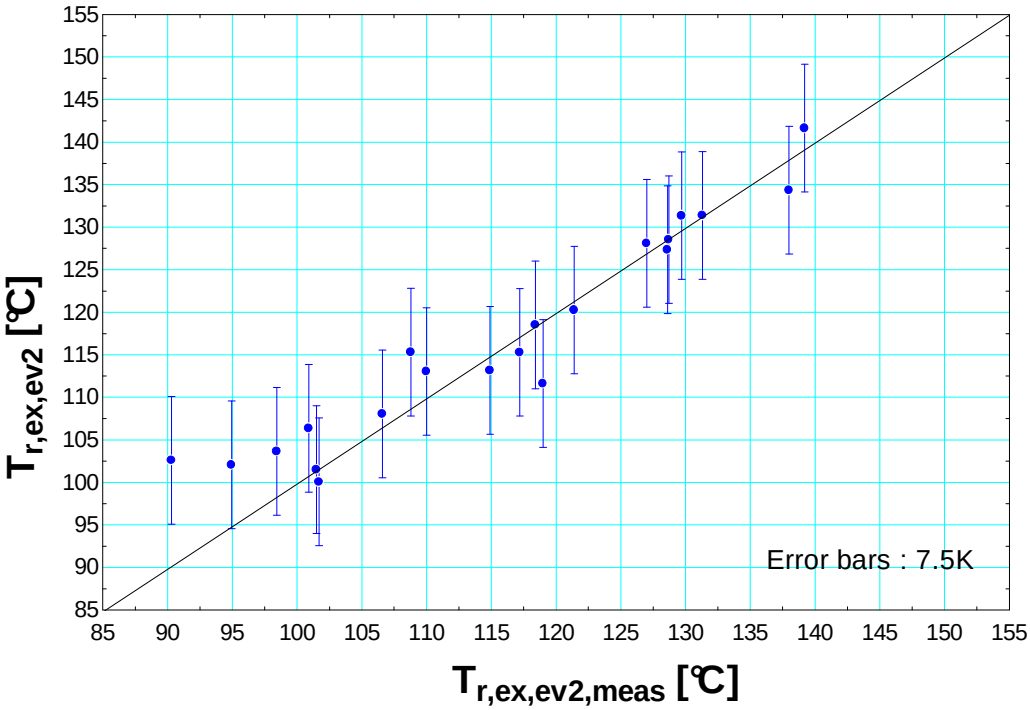

Figure 69 : predicted vs measured second evaporator exhaust temperature

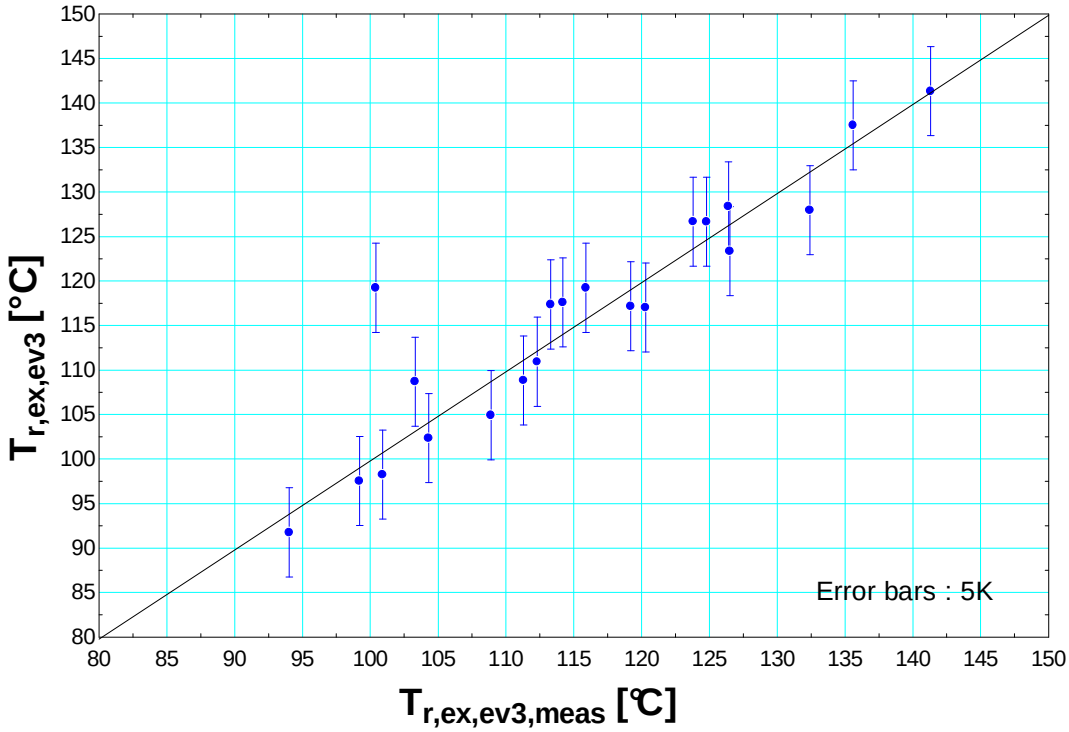

Figure 70 : predicted vs measured third evaporator exhaust temperature

Agreement between predicted and measured values is excellent for the first heat exchanger. For the second one the maximum error is 7.5K except for one point but the model didn't converge for test B20. Finally, the maximum divergence between measured and predicted exhaust temperature of the third heat exchanger is 5K except for the point corresponding to test B20.

7.2 Condenser model

The refrigerant enters the condenser in superheated vapour state and leaves it in liquid state. The model developed for the condenser is thus a three zone model.

The method described in section 7.1.1. is again used for water side in the three zones and for refrigerant side in liquid and vapour zones. The refrigerant side heat transfer coefficient in the two-phase zone (α_{tp}) is obtained by means of W.S. Kuo correlation [12]:

$$\alpha_{tp} = ch_l(0.25Co^{-0.45}{Fr_l}^{0.25} + 75Bo^{0.75})$$

Where Co is the convection number, Fr_l is the froud number of the saturated liquid, Bo is the boiling number and h_l is liquid heat transfer coefficient.

The heat transfer coefficient is not considered as a constant during the evaporation process. An integration is thus required between supply and exhaust quality.

Table 21 displays a summary of correlations used for each zone of the condenser and the corresponding values of "c" parameters.

	Liquid zone	Two-phase zone	Vapour zone
Water side	$Nu = cRe^m Pr^n$ $c = 0.6588$	$Nu = cRe^m Pr^n$ $c = 0.2478$	$Nu = cRe^m Pr^n$ $c = 0.4094$
R245fa side	$Nu = cRe^m Pr^n$ $c = 0.1248$	Kuo correlation $c = 45.08$	$Nu = cRe^m Pr^n$ $c = 0.525$

Table 21

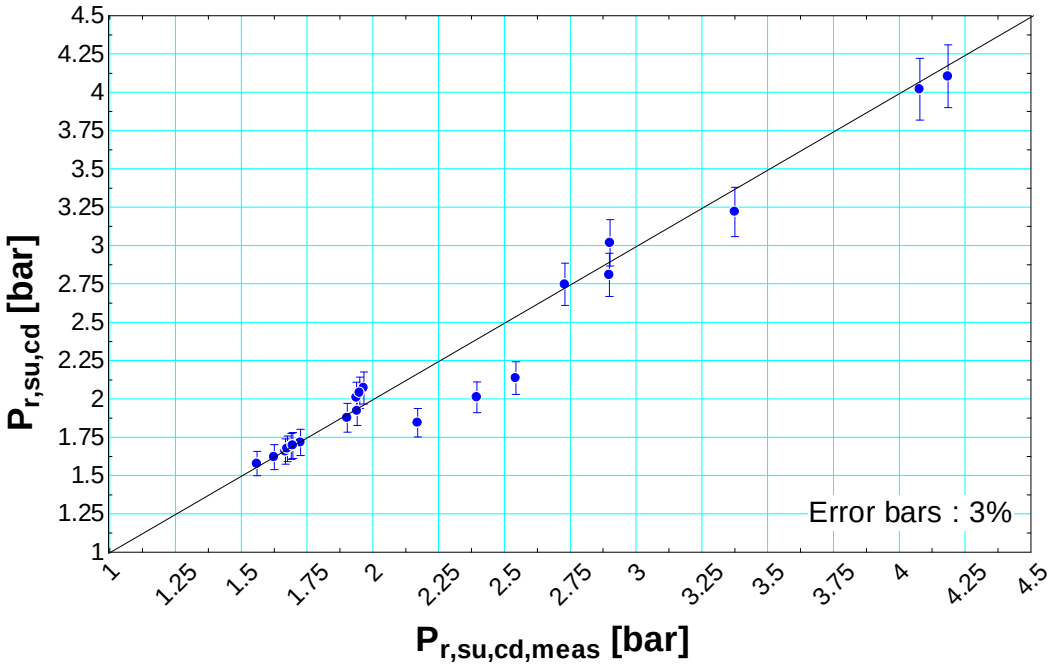

Figure 71: predicted vs measured condenser supply pressure

The maximum error between measured and predicted value of the condenser supply pressure is 3% except for three tests. For these three points, huge bubbles were observed at the subcooler supply and the fluid was therefore not at the thermodynamics equilibrium.

7.3 Expander model

7.3.1 Description of the model

The expander model is based on the model proposed and validated by V.Lemort et al. [6]. The evolution of the fluid in the expander is divided into 7 steps. Figure 72 shows a conceptual scheme of the expander model.

7.3.1.1 First step: supply pressure drop (su => su1)

The supply pressure drop of the expander is modelled by means of an equivalent nozzle. It is calculated by

$$\Delta P_{su} = \frac{C_{thr,su}{}^2}{2 * v_{r,su}}$$

Where $C_{thr,su}$ is the fluid velocity in the nozzle which depends of the cross-sectional area. The cross-sectional ($A_{thr,su}$) of this nozzle is identified from the measurement.

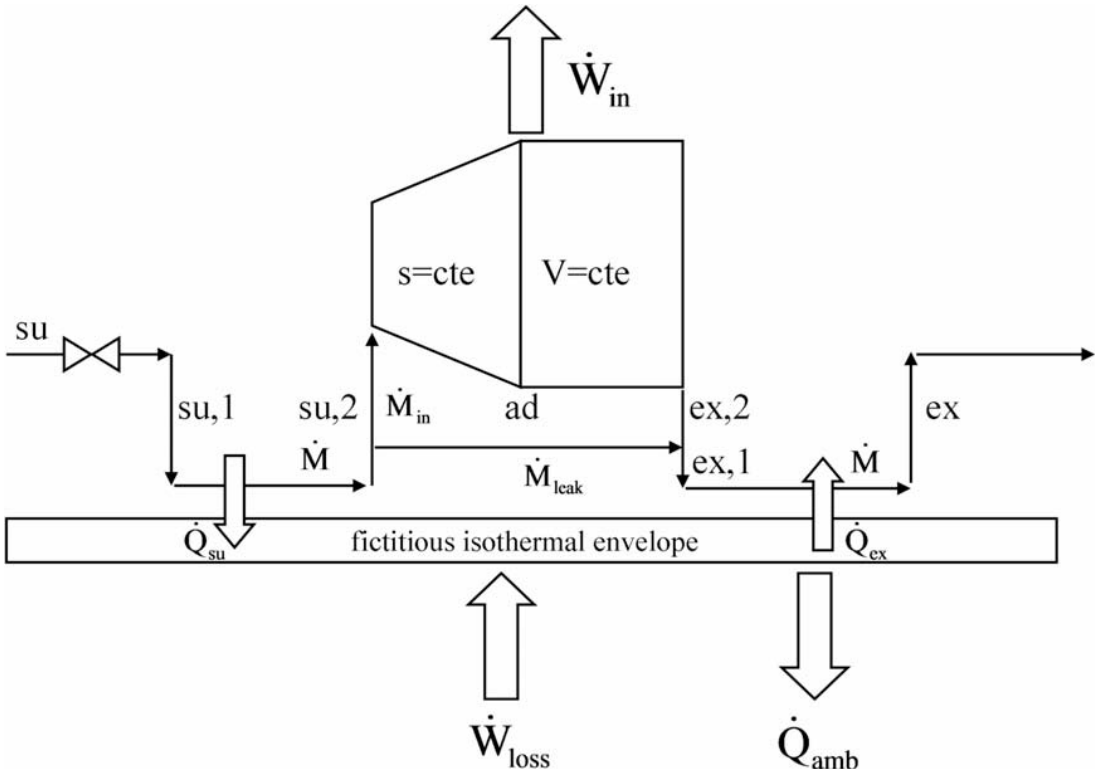

Figure 72 : conceptual scheme of the expander model [6]

7.3.1.2 Second step: Supply cooling down (su1 => su2)

The supply pressure drop is followed by a supply cooling down by contact between the fluid and the expander shell. This heat exchange is supposed to occur between the fluid and a fictitious isothermal surface and is modelled by well-know *log*-mean-temperature-difference (LMTD) method:

$$\dot{Q}_{su} = \dot{M}(h_{su1} - h_{su2}) = AU_{su}\Delta T_{ln}$$

AU_{su} is supposed to vary with the mass flow rate according to:

$$AU_{su} = AU_{su,n}\left(\frac{\dot{M}}{\dot{M}_n}\right)^{0.8}$$

Where $\dot{M}_n$ is the nominal flow rate and $AU_{su,n}$ is the nominal heat transfer coefficient which is identified from the measurement.

7.3.1.3 Third step: leakages

A fraction of the mass flow rate is supposed to leak directly from the inlet to the outlet of the machine without interacting with the scroll and thus without producing mechanical power. The leakage path is modelled by means of a fictitious nozzle whose cross-sectional area is $\mathrm{A_{leak}}$.

$$\dot{M}_{leak} = \frac{A_{leak}}{v_{thr,leak}}\sqrt{2(h_{su2} - h_{thr,leak})}$$

The flow rate that interacts with the scroll is thus given by:

$$\dot{M}_{in} = \dot{M} - \dot{M}_{leak}$$

7.3.1.4 Fourth step: isentropic expansion (su2 => ad)

The first part of the expansion itself is an isentropic expansion from the supply pressure to the adapted pressure corresponding to the built-in volume ratio.

$$\mathrm{P_{ad}} = \frac{\mathrm{P_{su2}}}{\mathrm{r_{p,ad}}}$$

The first contribution to the shaft work is thus given by:

$$w_{exp,1} = h_{su2} - h_{ad}$$

Where h_{ad} is the enthalpy at adapted pressure and supply entropy:

$$h_{ad} = Enthalpy(Fluid, P = P_{ad}, s = s_{su2})$$

7.3.1.5 Fifth step: isochoric expansion (ad => ex2)

The second part of the expansion consists in an isochoric expansion from the adapted pressure to the exhaust pressure (P_{ex}). The second contribution to the shaft work is thus given by:

$$w_{exp,2} = v_{ad}(P_{ad} - P_{ex,2})$$

7.3.1.6 Sixth step: mixing with leakages (ex2 => ex1)

Leakages are mixed with the exhaust of the isochoric expansion. Resulting enthalpy is calculated by energy balance and the process is assumed to be isobaric:

$$\dot{M}h_{ex1} = \dot{M}_{leak}h_{thr,leak} + \dot{M}_{in}h_{ex2}$$

$$P_{ex1} = P_{ex2}$$

7.3.1.7 Seventh step: exhaust cooling down (ex1 => ex)

The model used for the exhaust cooling down is identical to the one used for the supply cooling down. A nominal heat transfer coefficient $AU_{ex,n}$ is identified from the measurements.

7.3.1.8 Mechanical losses and heat balance

The shaft power is calculated by:

$$\dot{W}_{shaft} = \dot{W}_{in} - \dot{W}_{loss}$$

$$\dot{W}_{in} = \dot{M}_{in}(w_{exp1} + w_{exp2})$$

$$\dot{W}_{loss} = 2\pi N T_{loss} - \alpha \dot{W}_{in}$$

Where T_{loss} is a mechanical loss torque that have to be identified from the measurement while N is the rotational speed of the expander. The term $\alpha \dot{W}_{in}$ is absent of the model developed by V.Lemort bus was added in the present work because no satisfactory set of parameters could be identified without it.

Finally, the temperature of the fictitious isothermal surface used to model supply and exhaust cooling down is determined by energy balance:

$$W_{loss} - Q_{ex} + Q_{su} - Q_{amb} = 0$$

$$Q_{amb} = AU_{amb}(T_w - T_{amb})$$

AU_{amb} is identified from the measurement.

7.3.2 Identification of the parameters

The expander parameters are identified from the measurements by minimizing error between predicted and measured values of shaft power, expander supply pressure and expander exhaust temperature.

Table 22 shows the values obtained for all expander parameters.

$A_{thr,su}$	15.03 mm^2
$AU_{su,n}$	2.16 W/K
A_{leak}	1.5 mm^2
$r_{v,in}$	3.789
$V_{s,cp}$	100 cm^3
T_{loss}	0.02 N.m
α	0.181
$AU_{ex,n}$	50.2 W/K
AU_{amb}	8.799 W/K

Table 22 : expander parameters

Figure 73 shows that the expander shaft power is predicted by the model with a maximum error of 5%.

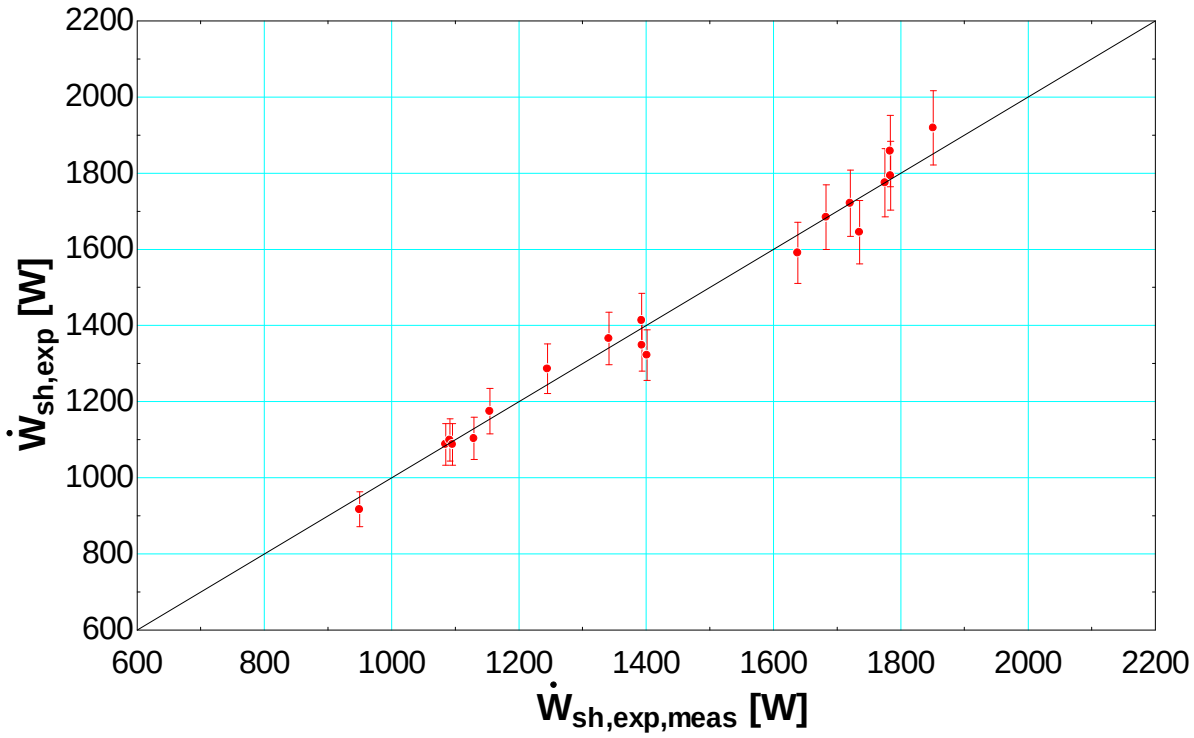

Figure 73 predicted vs measured expander shaft power

The expander supply pressure is predicted with a maximum error of 3% as shown in Figure 74.

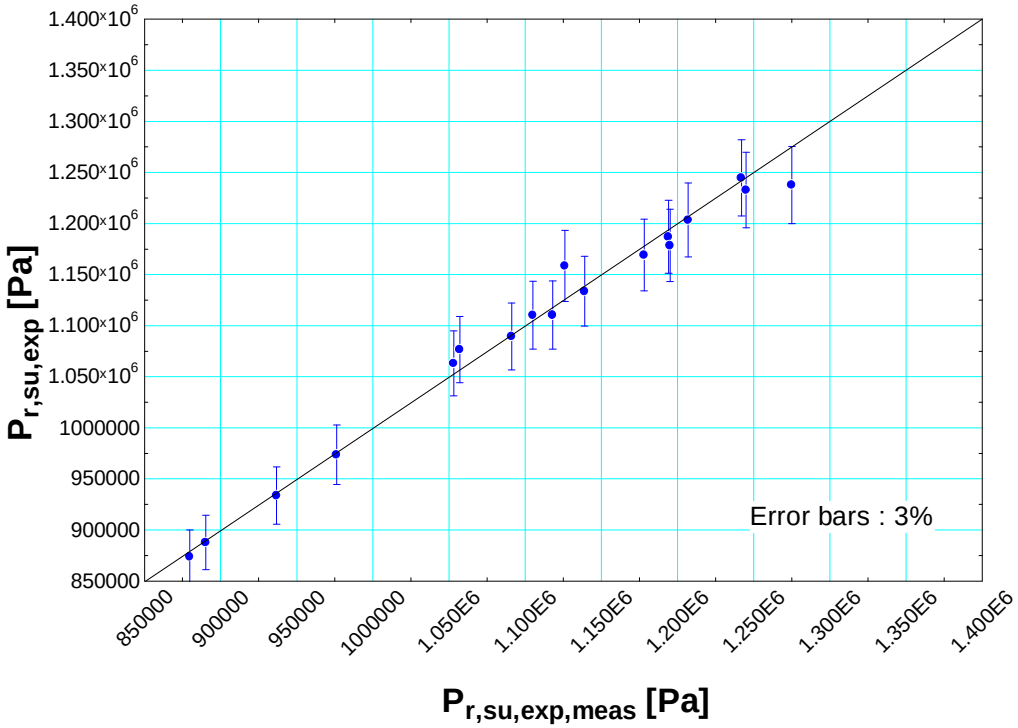

Figure 74 : predicted vs measured expander supply pressure

The maximum divergence between measured and predicted expander exhaust temperature is 6.1K.

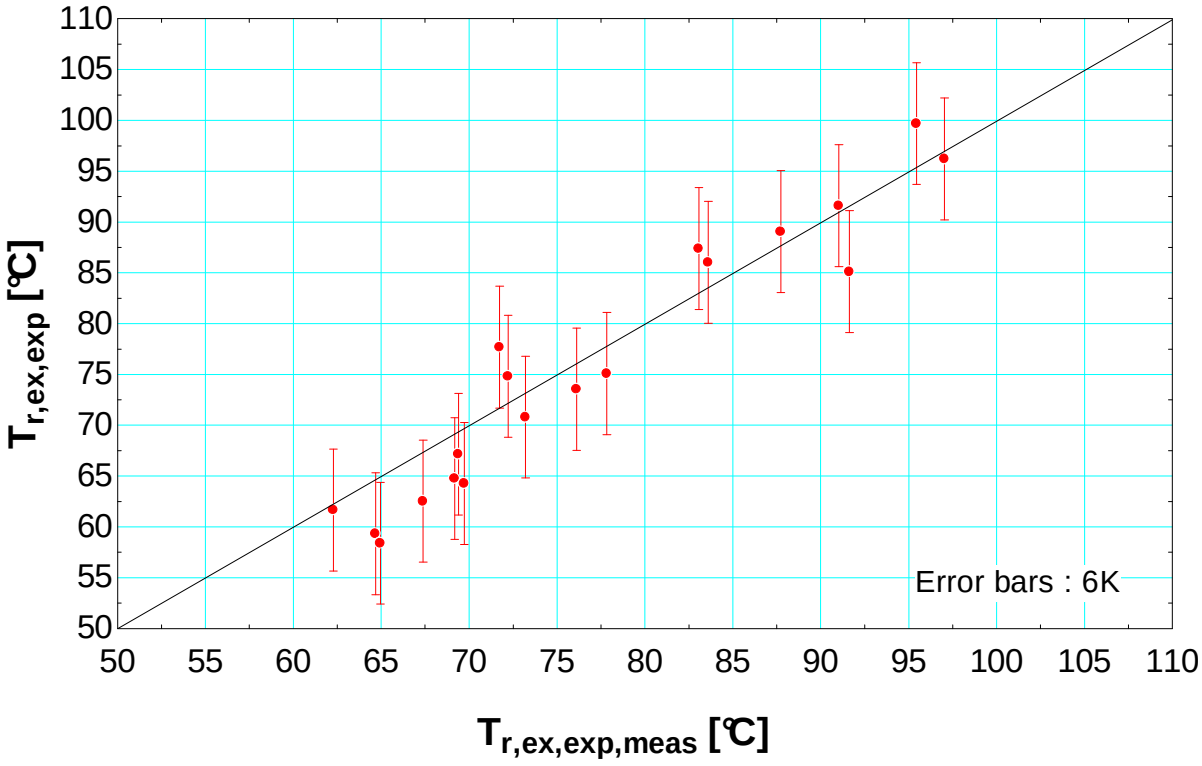

Figure 75 : predicted vs measured expander exhaust temperature

7.4 Pumps model

Pumps are supposed to impose the mass flow rate in each evaporator line:

$$\dot{M}_{pump1} = \frac{\dot{V}_{max,pump1} * X_{pump1}}{v_{su,pump}}$$

$$\dot{M}_{pump2} = \frac{\dot{V}_{max,pump2} * X_{pump2}}{v_{su,pump}}$$

Where $\dot{V}_{max,pump}$ is the swept volume at full capacity is, X_{pump} is the capacity setting and $v_{su,pump}$ is the specific volume at the pump supply.

In order to evaluate pump consumption, an isentropic efficiency of 15% is assumed.

7.5 Global model

The global model is built by connecting models of all single components together as shown in Figure 76.

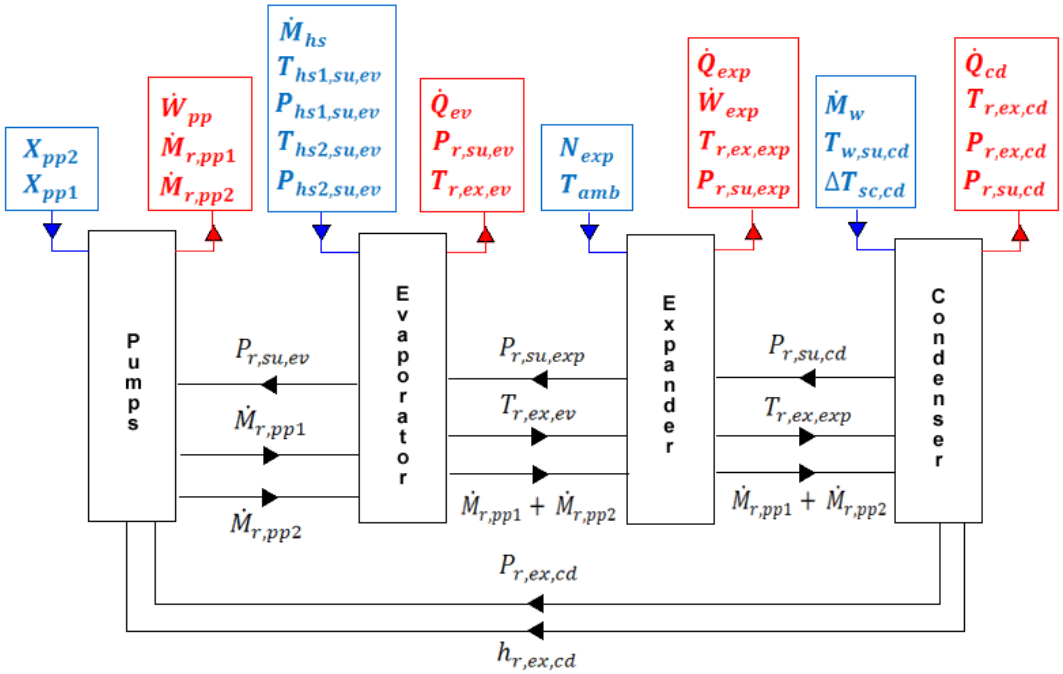

Figure 76 : block diagram of the global model

Figures 77 to 80 show the agreement between measured and predicted values of the expander shaft power, the evaporator exhaust temperature, the expander supply pressure and the condenser supply pressure.

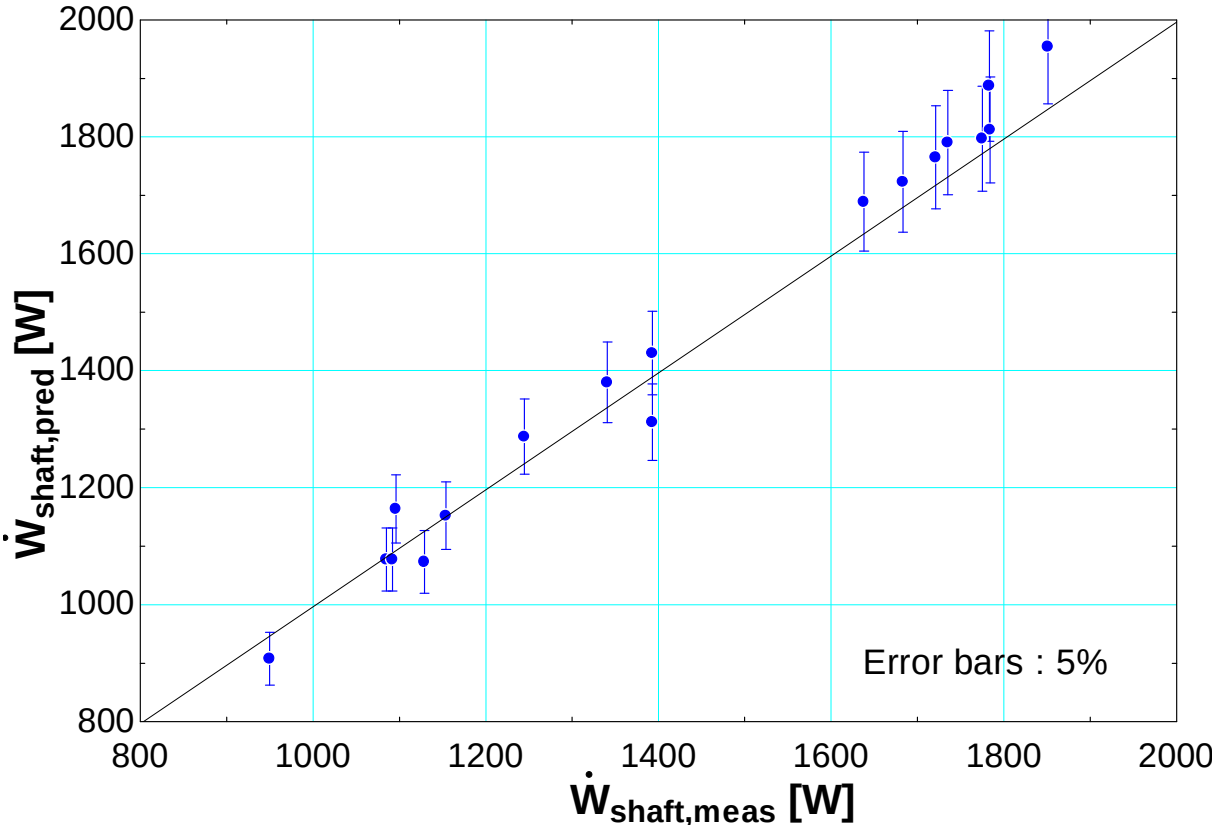

Figure 77 : predicted vs measured expander shaft power

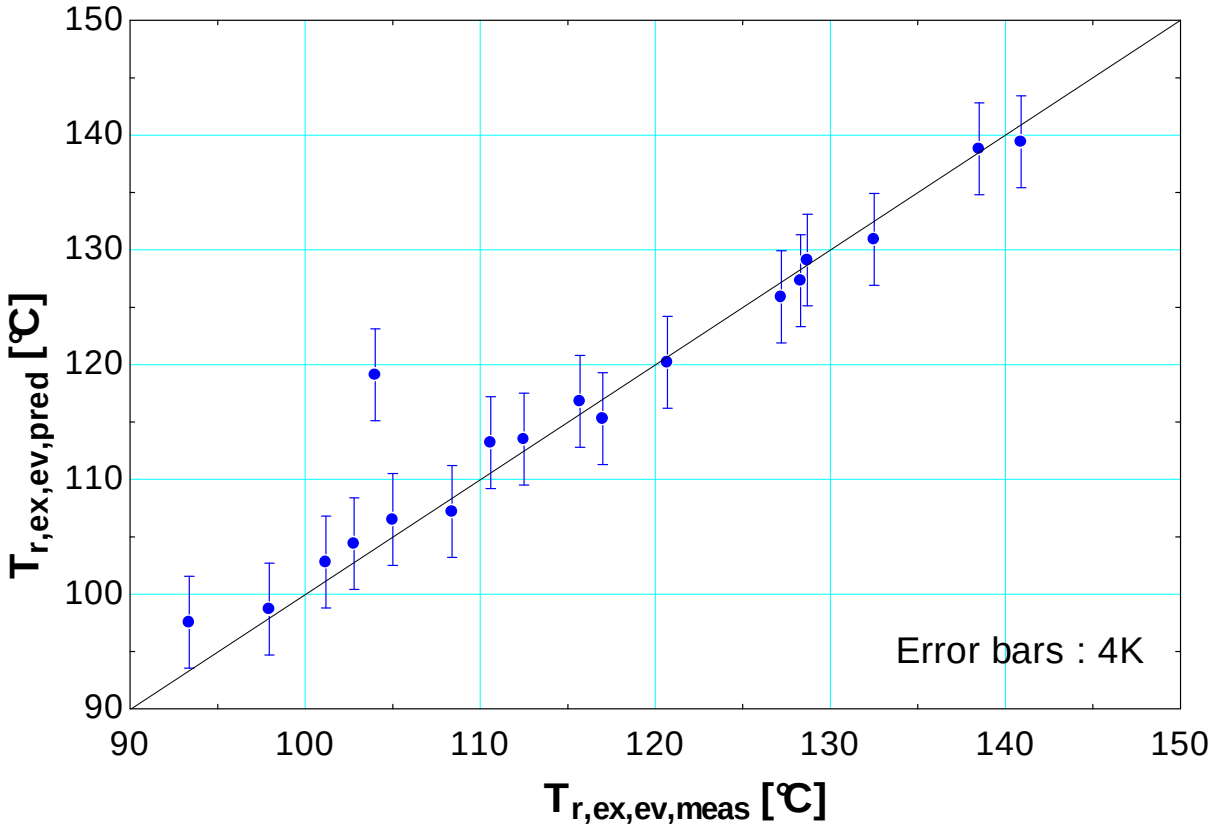

Figure 78 : predicted vs measured evaporator exhaust temperature

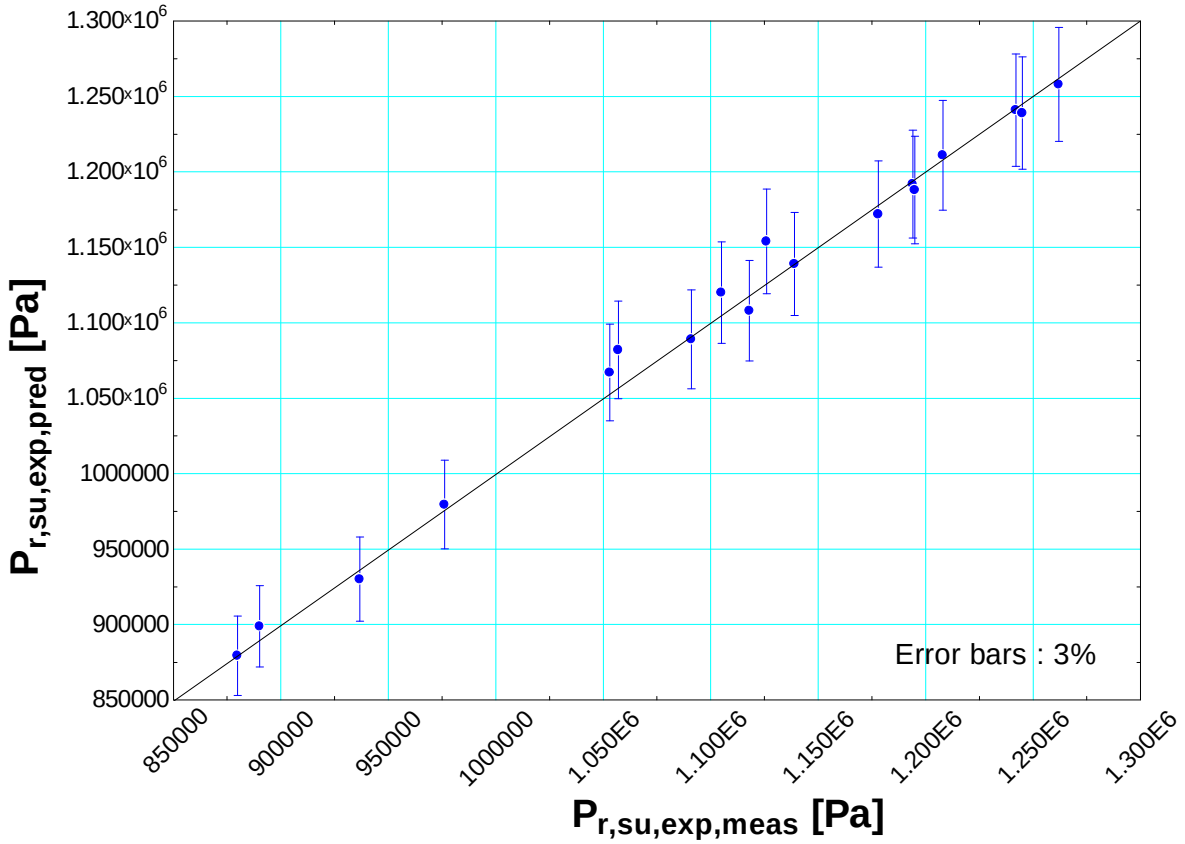

Figure 79 : predicted vs measured expander supply pressure

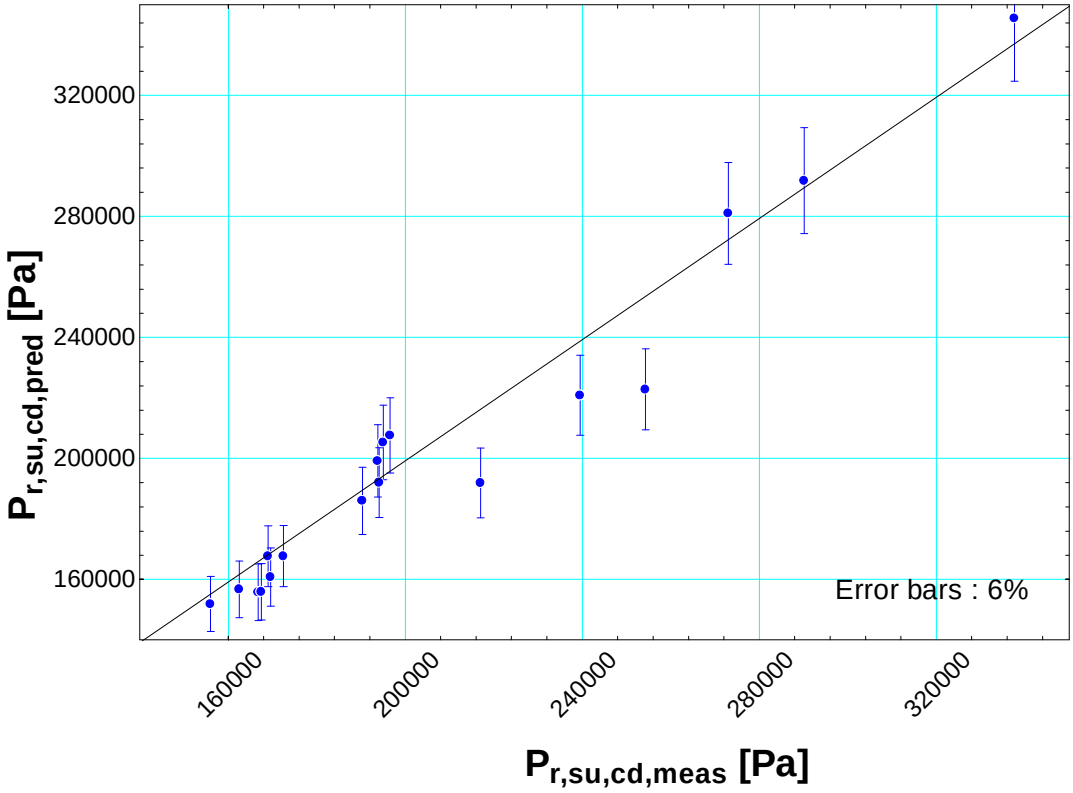

Figure 80 : predicted vs measured condenser supply pressure

The expander shaft power and expander supply pressure are predicted with a maximum error of 5% and 3% respectively. The exhaust temperature is predicted with a maximum error of 4.1K except for test B20. The condenser supply pressure is predicted with a maximum error of 6.1% except for three points. The bad prediction of these three condenser supply pressures was explained in section 7.2.

The global model didn't converge for test B9, B10 and B21.

8 Conclusions and perspectives

8.1 Comparison with result obtained in 2007

Table 23 displays the main maximum results obtained in 2007 and 2009.

	2007	2009
Expander efficiency	68%	70.6%
Expander shaft power (W)	1820	2164
Cycle efficiency (based on NET power)	7.4%	7.1%
Exergetic efficiency (based on NET power)	22.8%	19.8%
Pressure ratio	5.4	7.6
Evaporator power (kW)	22.5	23.9

Table 23 : Main results obtained in 2007 and 2009

Table 23 shows that the expander efficiency is slightly higher in 2009 but it is important to keep in mind that, in 2007, the uncertainty on the efficiency was relatively high due to the use of transmission belts between the expander and the torque meter.

The output power was increased by 18.9%. This is mainly due to the higher pressure ratio achieved in 2009 and also to a slightly higher heat power recovered in the evaporator.

Cycle and exergetic efficiency obtained in 2009 are lower than ones obtained in 2007. This can be partly explained by the less-suited thermodynamics properties of R245fa, with comparison to R123.

8.2 Potential improvement of the system and the measurements

The pump efficiency was around 15% for all tests while their consumption was about 400W. This induces a huge penalty in a system that produces maximum 2.15 kW. Additionally, the maximum acceptable outlet pressure of these diaphragm pumps is 12 bar which limit the pressure ratio over the expander and therefore the output power. Therefore, a first potential improvement consists in replacing the pumps by

another one with a better efficiency and a higher acceptable outlet pressure. A lower NPSH would also be preferable.

Exergetic analysis shows that around 30% of heat sources exergy is lost in the evaporator. In order to reduce this contribution to exergy lost, other fluids including zeotropic ones could be tested. Other possibility would be to use bigger heat exchangers for the evaporator in order to reduce pinch points but actual ones are already oversized.

During all tests, the total refrigerant flow rate was measured but the flow rate in each evaporator line was not measured. Two different calculation methods were developed in order to predict the flow rate in each line from the total flow rate. However, adding a flow rate measurement in one line would be preferable.

The shaft seal of the expander container is only able to handle a positive differential pressure (high pressure inside the container and low pressure outside). The use of fluids for which the saturation pressure is lower than atmospheric pressure at ambient temperature such as pentane or R123 is therefore impossible. The shaft seal should therefore be replaced by another one that can handle positive and negative differential pressures in order to be able to use all type of fluids.

The expander was coupled to an asynchronous machine whose nominal speed was 1450RPM at 50Hz. The inverter could increase the frequency up to 104Hz which allowed the expander to run up to 3125RPM. In order to increase the maximum achievable rotational speed of the expander, an asynchronous machine with a nominal speed of 3000RPM should be selected.

The model developed in section 7 is a steady state model. It could be interesting to develop a dynamic model to predict the evolution of the system between two steady states.

8.3 Conclusion

A new ORC test bench was built at the thermodynamic laboratory in order to improve performance obtained in 2007. The test ring was described and each component was detailed.

A first set of 12 tests was performed without the expander in order to highlight possible issues on the test bench and to solve them. The heat balances over the heat exchangers were checked and modifications were performed on the test bench in order to improve accuracy of the measurements.

A second set of 21 tests was then performed in order to study the performance of the system over a wide range of conditions. The third set of test focused on two objectives:

- Produce the maximum shaft power for several hot source flow rates.
- Study the performances of the system if a two-phase medium is supply to the expander.

A model of each component was developed and these singles models were then connected to each other in order to predict the behaviour of the whole system. The model parameters were identified from the measurement of the second set of tests.

Finally, main results were compared with results obtained in 2007 and several potential improvements were proposed.

9 Bibliography

[1] *X.D. Wang, L. Zhao, 2008. Analysis of zeotropic mixtures used in low-temperature solar Rankine cycles for power generation.*

[2] Pedro J. Mago , Louay M. Chamra, Kalyan Srinivasan, Chandramohan Somayaji, 2007. An examination of regenerative organic Rankine cycles using dry fluids.

[3] Saleh, Bahaa, Koglbauer, Gerald, Wendland, Martin, Fischer, Johann, 2007. Working fluids for low-temperature organic Rankine cycles. Energy 32, 1210-1221.

[4] G. Kosmadakis, D. Manolakos, S. Kyritsis, G. Papadakis, 2008. Comparative thermodynamic study of refrigerants to select the best for use in the high-temperature stage of a two-stage organic Rankine cycle for RO desalination.

[5] Joost J. Brasz, 2008. Assessment of C6F as working fluid for organic Rankine cycle applications.

[6] Vincent Lemort, Sylvain Quoilin, Cristian Cuevas, Jean Lebrun, 2009. Testing and modeling a scroll expander integrated into an Organic Rankine Cycle.

[7] S.Quoilin, *Experimental study and modeling of a low temperature Rankine Cycle for small scale cogeneration*, Master thesis, Université de Liège, June 2007

[8] V. Lemort, Contribution to the characterization of scroll machines in compressor and expander modes, PhD Thesis, Université de Liège, Belgique, 2008.

[9] J. Lebrun, Machines et systèmes thermiques, Université de Liège, Faculté des sciences appliqués, 2007-2008

[10] A. Muley, R.M. Manglik, Experimental study of turbulent flow heat transfer and pressure drop in a plate heat exchanger with chevron plates, Journal of Heat Transfer, ASME 121 (1999) 110-117

[11] Y.Y. Hsieh, T.F. Lin, Saturated flow boiling heat transfer and pressure drop of refrigerant R410a in a vertical plate heat exchanger, International Journal of Heat and Mass Transfer 45 (2002)1033-1044.

[12] W.S. Kuo, Y.M. Lie, Y.Y. Hsieh, T.F. Lin, Condensation heat transfer and pressure drop of refrigerant R410a flow in a vertical plate heat exchanger, International Journal of Heat and Mass transfer 48 (2005) 5205-5220.

[13] P. Ngendakumana, *Echangeurs de chaleur*, Université de Liège, Faculté des sciences appliqués, 2007-2008

[14] O. Leonard, Turbomachines, Université de Liège, Faculté des sciences appliqués, 2007-2008

[15] G. Heyen, *Echangeurs de chaleur*, Université de Liège, Faculté des sciences appliqués, 2007-2008

10 Annexes

10.1 Pumps data

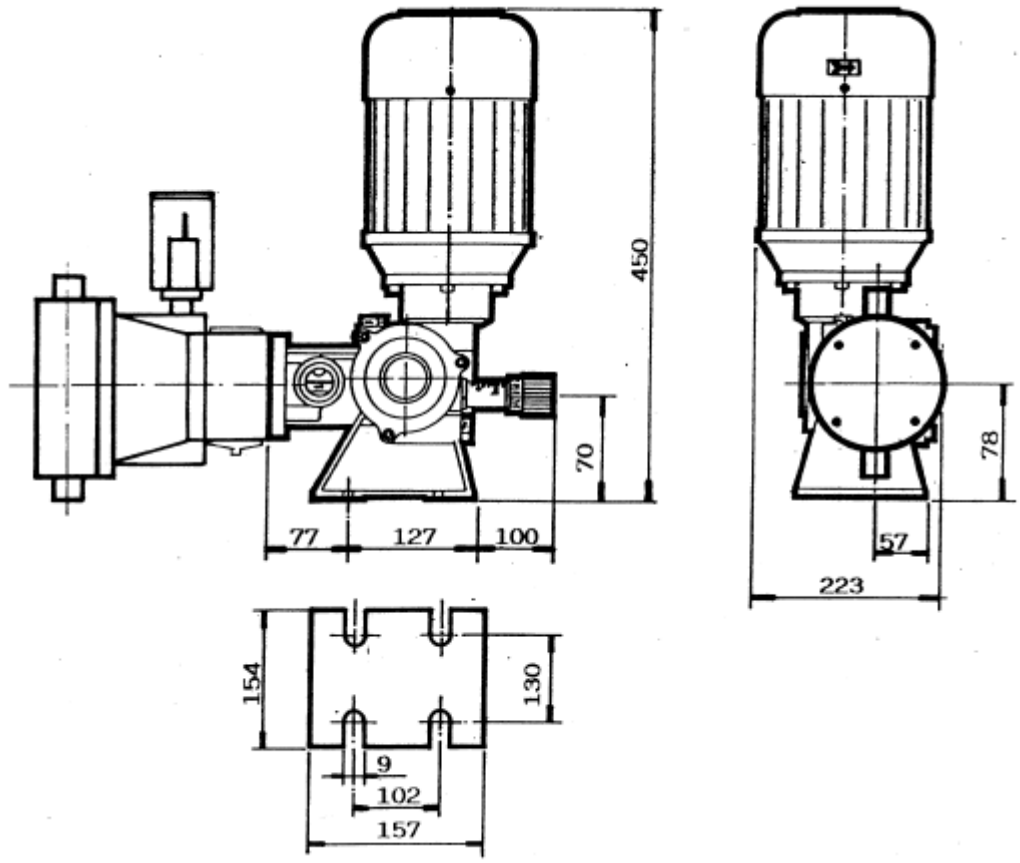

Piston D.	Strokes/min		Maximum load		Maximum pressure	
	50 Hz	60 Hz	50 Hz	60 Hz	Metal material	Plastic material
mm	c/m	c/m	l/h	l/h	bar	Bar
40	56	67	105	126	20 (10)	10 (10)
40	96	116	180	216	20 (10)	10 (10)
40	112	/	210	/	20 (10)	10 (10)
50	56	67	165	198	15 (10)	10 (10)
50	96	116	282	338	15 (10)	10 (10)
50	112	/	330	/	15 (10)	10 (10)
55	56	67	200	240	12.5 (10)	10 (10)
55	96	116	342	410	12.5 (10)	10 (10)
55	112	/	400	/	12.5 (10)	10 (10)
65	56	67	278	333	9 (9)	9 (9)
65	96	116	476	571	9 (9)	9 (9)
65	112	/	556	/	9 (9)	9 (9)
75	56	67	371	445	6.6 (6.5)	6.6 (6.5)
75	96	116	636	763	6.6 (6.5)	6.6 (6.5)
75	112	/	742	/	6.6 (6.5)	6.6 (6.5)
90	56	67	534	641	4.7 (4.5)	4.7 (4.5)
90	96	116	915	1098	4.7 (4.5)	4.7 (4.5)
90	112	/	1068	/	4.7 (4.5)	4.7 (4.5)

10.2 Results of the first set of test

Test	Refrigerant flow rate	Air flow rate	Water flow rate in the condenser	Pump n°1 setting	Pump n°2 setting	Cold source temperature	First hot air source temperature	Second hot air source temperature	Overheating at the evaporator exhaust
	[kg/s]	[kg/s]	[kg/s]			[°C]	[°C]	[°C]	[K]
A1	0.07305	0.1264	0.3765	0.42	0.62	12.81	185.1	148.8	37.54
A2	0.08914	0.1264	0.3894	0.54	0.76	13.52	187.7	157.7	12.92
A3	0.1043	0.1264	0.3894	0.68	0.96	13.44	187.7	153.8	0 (X=0.88)
A4	0.08759	0.1264	0.3457	0.53	0.64	14.54	188.3	155.4	37.06
A5	0.09535	0.1264	0.3455	0.58	0.71	14.69	188.2	153.8	16.72
A6	0.1105	0.1264	0.428	0.73	0.89	13.4	186.8	150.3	0 (X=0.9)
A7	0.08786	0.1264	0.294	0.52	0.65	15.67	189.8	156.2	27.89
A8	0.09629	0.1264	0.2951	0.58	0.71	16.11	189.3	154.2	6.363
A9	0.1088	0.1264	0.4001	0.69	0.85	13.81	188.3	151.6	0 (X=0.85)
A10	0.0877	0.1264	0.2168	0.51	0.66	20.74	190.8	157.8	16.57
A11	0.09513	0.1264	0.2048	0.57	0.69	21.75	190.4	155.3	4.758
A12	0.1084	0.1264	0.2051	0.65	0.79	22.75	189.6	153	0 (X=0.7918)

10.3 Results of the second set of test

Test	Refrigerant flow rate	Air flow rate	Water flow rate in the condenser	Pump n°1 setting	Pump n°2 setting	Cold source temperature	First hot air source temperature	Second hot air source temperature	Subcooling at the subcooler exhaust
	[kg/s]	[kg/s]	[kg/s]			[°C]	[°C]	[°C]	[K]
B1	0.06455	0.09796	0.6392	0.4	0.48	9.127	197.8	163.4	5.76
B2	0.07828	0.09796	0.6392	0.48	0.58	9.283	196.8	158.1	6.89
B3	0.07355	0.09796	0.2853	0.44	0.55	9.403	197	158.8	10.4
B4	0.06883	0.09796	0.284	0.41	0.52	9.477	197.9	160.6	9.74
B5	0.06716	0.09796	0.1732	0.41	0.52	9.662	199.9	165	5.26
B6	0.07356	0.09796	0.1964	0.46	0.57	9.7	200	165.8	4.07
B7	0.05279	0.08217	0.459	0.31	0.4	10.09	185.1	150.2	3.16
B8	0.06125	0.08217	0.4036	0.36	0.46	10.04	184.2	147	3.97
B9	0.05843	0.08217	0.0582	0.33	0.44	10.25	186.2	150.4	26
B10	0.05463	0.08217	0.0554	0.31	0.41	10.3	187.1	152.2	25.94
B11	0.05709	0.08217	0.0936	0.33	0.43	10.26	187.2	151.9	14.06
B12	0.06417	0.08217	0.0837	0.38	0.48	10.18	186.5	149.5	19.92
B13	0.05258	0.07111	0.1507	0.30	0.4	9.783	186.1	147.1	6.97
B14	0.05702	0.07111	0.1571	0.33	0.43	9.894	185.3	145.4	7.47
B15	0.05349	0.07111	0.1476	0.30	0.42	9.98	185.3	145.8	7.57
B16	0.0493	0.07111	0.1571	0.27	0.39	10.09	186.1	147.4	10.95
B17	0.05184	0.07111	0.6148	0.3	0.41	10.06	186.1	147.7	3.93
B18	0.06296	0.09007	0.6167	0.39	0.46	9.287	191.6	160.8	5.34
B19	0.06839	0.09007	0.62	0.43	0.5	9.393	191.7	159.5	5.79
B20	0.07121	0.09007	0.1057	0.44	0.51	9.739	191.5	159	22.28
B21	0.06522	0.09007	0.1034	0.40	0.47	9.797	192.2	160.7	22.74

Test	Overheating at the evaporator exhaust [K]	Refrigerant temperature at the expander supply [°C]	Refrigerant pressure at the expander supply [bar]	Shaft power output [W]	Expander rotational speed [RPM]	Expander isentropic effectiveness	Cycle efficiency	Exergetic efficiency	Pressure ratio over the expander
B1	41.58	140.9	12.42	1783	2708	0.617	0.066	0.182	7.446
B2	6.965	105	12.07	1851	3125	0.627	0.066	0.195	6.997
B3	18.15	115.7	11.94	1784	3125	0.656	0.064	0.184	6.151
B4	31.75	128.7	11.78	1775	3125	0.659	0.065	0.183	6.19
B5	40.91	138.5	11.95	1638	3125	0.682	0.060	0.159	4.99
B6	27.77	127.2	12.45	1735	3125	0.700	0.063	0.170	4.896
B7	45.44	132.5	9.367	1341	3125	0.651	0.058	0.174	5.764
B8	14	102.8	9.762	1393	3125	0.653	0.060	0.185	5.776
B9	25.11	115.4	10.11	180.5	3125	0.168	-0.014	-0.041	2.415
B10	39.36	128.7	9.886	190.9	3125	0.180	-0.013	-0.037	2.424
B11	27.12	120.7	10.91	1129	2550	0.678	0.045	0.129	3.996
B12	3.817	97.95	11.05	949.8	2550	0.657	0.033	0.098	3.273
B13	26.15	110.6	8.798	1085	3125	0.656	0.047	0.147	4.54
B14	8.442	93.38	8.902	1092	3125	0.655	0.047	0.149	4.528
B15	8.997	101.2	10.57	1154	2105	0.655	0.053	0.161	5.421
B16	24.96	117	10.53	1096	2105	0.675	0.049	0.147	4.853
B17	13.44	108.4	11.26	1245	1855	0.610	0.057	0.176	7.218
B18	33.65	128.3	11.18	1683	2975	0.653	0.066	0.191	6.675
B19	17.04	112.5	11.39	1721	2975	0.653	0.066	0.197	6.716
B20	3.962	104	12.62	1393	2406	0.697	0.050	0.146	4.35
B21	19.7	120.2	12.75	1401	2406	0.706	0.051	0.147	4.4

10.4 Result of the third set of test

Test	Refrigerant flow rate	Air flow rate	Water flow rate in the condenser	Pump n°1 setting	Pump n°2 setting	Cold source temperature	First hot air source temperature	Second hot air source temperature	Subcooling at the subcooler exhaust
	[kg/s]	[kg/s]	[kg/s]			[°C]	[°C]	[°C]	[K]
C1	0.07482	0.1264	0.6376	0.47	0.56	10.28	193.1	164.4	6.76
C2	0.08322	0.1106	0.6376	0.52	0.61	10.51	190.4	157.7	7.22
C3	0.07062	0.09481	0.6372	0.40	0.56	10.73	195.1	151.6	5.83
C4	0.05929	0.07901	0.6711	0.34	0.46	11.23	185.7	147.7	4.53
C5	0.06589	0.08217	0.6711	0.40	0.48	11.34	185	153.3	5.03
C6	0.06973	0.08217	0.6711	0.43	0.51	11.36	184.6	152.2	5.23
C7	0.06806	0.08217	0.6711	0.42	0.5	11.45	184.9	152.3	5.07
C8	0.07826	0.09796	0.6711	0.48	0.58	11.46	196.8	160.6	6.42
C9	0.08375	0.09796	0.6711	0.52	0.61	11.5	196.5	160	6.85
C10	0.08576	0.09796	0.6711	0.53	0.62	11.54	196.3	159.3	6.92

Test	Overheating at the evaporator exhaust [K]	Refrigerant temperature at the expander supply [°C]	Refrigerant pressure at the expander supply [bar]	Shaft power output [W]	Expander rotational speed [RPM]	Expander isentropic effectiveness	Cycle efficiency	Exergetic efficiency	Pressure ratio over the expander
C1	44.18	146.6	13.3	2164	3125	0.649	0.071	0.182	7.193
C2	7.333	108.4	12.91	2028	3125	0.645	0.069	0.199	6.963
C3	7.786	109.9	13.21	1744	2260	0.626	0.067	0.192	7.553
C4	7.551	102	11.13	1389	2257	0.634	0.061	0.188	6.721
C5	6.442	97.07	10.19	1474	3125	0.647	0.061	0.191	6.026
C6	0 (X=0.88)	89.28	10.09	1405	3125	0.657	0.058	0.177	5.921
C7	0 (X=0.94)	89.63	10.09	1423	3125	0.652	0.060	0.183	5.953
C8	8.238	106.9	12.24	1897	3125	0.646	0.068	0.198	6.846
C9	0 (X=0.93)	97.37	12.15	1836	3125	0.642	0.066	0.189	6.691
C10	0 (X=0.83)	97.22	12.2	1795	3125	0.657	0.066	0.184	6.692